Cranfield University

Andrea Calonghi

Alternative design of front door side impact beam for Nissan Navara

School of Engineering

MSc by Research Thesis

Cranfield University

School of Engineering
Crashworthiness Impact and Structural Mechanics Group

MSc by Research Thesis

Academic Year 2005 – 2006

Andrea Calonghi

Alternative design of front door side impact beam for Nissan Navara

Supervisor: Mr J. Brown

Academic Year 2005 – 2006

This thesis is submitted in partial fulfilment of the requirements for the
degree of Master of Science

Vanità delle vanità, dice Qoèlet,
vanità delle vanità, tutto è vanità.
Quale utilità ricava l'uomo da tutto l'affanno
per cui fatica sotto il sole?
[…]
Per ogni cosa c'è il suo momento, il suo tempo per ogni faccenda sotto il cielo.
C'è un tempo per nascere e un tempo per morire,
un tempo per piantare e un tempo per sradicare le piante.
Un tempo per uccidere e un tempo per guarire,
un tempo per demolire e un tempo per costruire.
Un tempo per piangere e un tempo per ridere,
un tempo per gemere e un tempo per ballare.
Un tempo per gettare sassi e un tempo per raccoglierli,
un tempo per abbracciare e un tempo per astenersi dagli abbracci.
Un tempo per cercare e un tempo per perdere,
un tempo per serbare e un tempo per buttar via.
Un tempo per stracciare e un tempo per cucire,
un tempo per tacere e un tempo per parlare.
Un tempo per amare e un tempo per odiare,
un tempo per la guerra e un tempo per la pace.

(dal libro del **Qoèlet, cap I, 1 - 2; cap III, 1 - 8**)

Alla mia "Famiglia allargata",
perché tutti gli eventi di questo biennio 2005 – 2006
rendano "questa roccia" ancora più "roccia".

28 Settembre 2005…..strano ed inaspettato modo per
festeggiare il XXV…
non lo dimentichero' mai

Acknowledgements

Abstract

In this thesis the aim is to assess the performances of the circular side-impact beam of Nissan Navara / Pathfinder considered in isolation and subjected to a bending test.

Established the performances of the actual design in term of Force – displacement, comparing also the results with a bending test on the isolated beam, the following step is to start with the initial design of new open section beams to identify which of the beams designed could substitute the actual circular one.

For the new design the evaluation is not only based on the comparison with the Force – displacement graph obtained with test and simulations for the actual circular design, but also on the comparison between the weight of the new designs and of the current side impact beam.

Even if the cost is an other parameter of choice, in this thesis it has not been really considered, because the study for the new design is only at the initial phase.

List of contents

List of figures

List of tables

1. Introduction

1.1 Nissan's area of interest

The motivation for the work developed in this thesis is given by an area of interest for two current Nissan models: the pick-up Navara and the associated Sport Utility Vehicle Pathfinder.

Fig. 1.1: Nissan Navara (left) and Nissan Pathfinder (right)

As a careful reader can see from the pictures above, the two cars are basically derived from the same baseline, so the main features between the two models are the same; in particular it is easy to recognize that the front door is in common.
In these currently produced models the side door side-impact-beam mounted inside of the front door is made with a tubular section attached through two quite complicated brackets to the door structure, as shown in Fig.1.2, provided by Nissan.
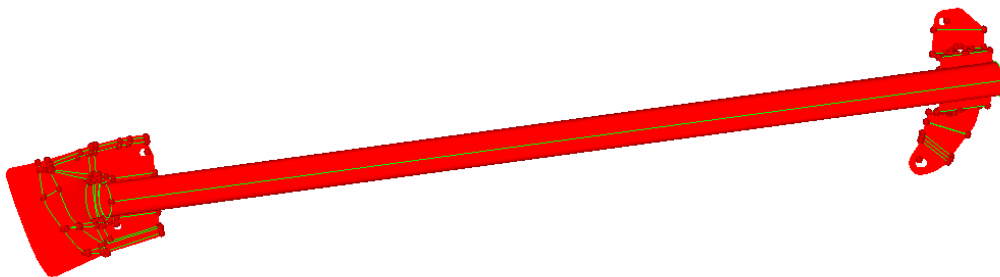
Fig. 1.2: Existing tubular side-impact-beam.

The intention manifested by Nissan's engineers At the European Technical Centre is to design a press formed open-section-beam in place of the tubular one, for vehicles manufactured in its European plants.

1.1.1 Advantages

The new open section could have some advantages, as explained by Nissan's engineers:

- reduction of the complexity of the actual beam
- quicker manufacturing process, including:
    - elimination of the brackets, this implies two less pieces
    - press forming technique which allows production of the whole beam in one step
- less expensive manufacturing process for a car produced in UK:
    - while in Japan it is less expensive to buy a steel pipe, as on the original beam
    - in Britain it is less expensive to use the press forming technique on sheet steel to manufacture this type of component

Further Observations

This intended change is not unreasonable because research by the author (see *Appendix A*) showed that the press-formed technique is used by most other manufacturers for their European vehicles. Other examples are shown in Fig.1.3 (Fiat Punto) and Fig.1.4 (Skoda).

Images of other side-impact-beams from other manufacturers are shown in *Appendix A*.

Fig.1.3: Fiat Punto first series (left), Fiat Punto second series(right).

Fig. 1.4 : Skoda side- impact-beam (left); Mini side-impact-beam (right).

1.2   Objectives of the thesis

- To assess the performance of the existing tubular beam in isolation
- Preliminary study for a new design of an open section press-formed beam.

1.3   Intended approach

The intention is to develop a press-formed beam with collapse and energy absorbing properties as similar as possible to those of the original tubular beam.
Since in this project it will not be possible to test a complete vehicle, most of the work will concentrate on the door beam in isolation.

Existing side-impact-beam.

- Simulate a bending test on the beam in isolation
- Perform a bending-test on the isolated beam
- Comparison of the results between laboratory test and computer simulations in terms of:
    - Force-displacement graph
    - Mechanism of collapse of the beam.

The reason for considering the beam in isolation are explained in *section 1.4*

New Press-formed design.

- Preliminary analysis of Nissan requirements and restrictions relative at the new design.
- "Tear down approach" to know some of Nissan's competitors actually designing their side-impact-beams.
- Choice of possible candidate shapes for the new design.

10

- Simulation of a bending test of the side-impact-beam in isolation.
- Comparison between new designs and the old side-impact-beam (test and best simulation) in terms of:
  - Force - displacement graph
  - Weight of the side-impact-beam

1.4 Comments on methods adopted

Reasons for using quasi-static tests on an isolated beam in this thesis:
- It is not possible to perform a dynamic test because the University has not the resources to perform it.

Reasons for treating the side-impact-beam in isolation:
- The test machines available do not allow for incompatibility of the dimensions to test the compete door of the car.
- A complete vehicle body was not available for test.

Final choice:
- To extract the complete side-impact-beam from the door of the car.
- To perform a bending-test on the isolated side-impact-beam.
- To use the properties of the isolated beam as a benchmark for the design of the new beam.

1.5 Thesis outline

1. General background study about Side-impact, *Chapter 2*

Reasons:
- To introduce the reader to the problem of crashworthiness
- To understand the importance of passive safety in relation of side impact
- To gain a better understanding of the structural requirements for side impact protection.

2. General background about Side – impact regulations, *Chapter 3*

Reasons:
- The beam is a part of the protection system involved during a side impact in a car.
- It looks reasonable to contextualise the problem having a minimum knowledge about regulations, because the beam has to contribute within the complete car-structure to pass the compulsory tests.
- The two Nissan vehicles in the analysis have to pass the certification rules for side impact.

3. Collapse mechanism of a simple car-model made with beam-elements, *Chapter 4*

Reasons:
- To understand the role played by the side-impact-beam in the whole structure of the car.
- To understand that during the side impact the whole structure is involved in the collapse mechanism
- To try to find the preferable collapse sequence of the car structure.

4. Basic phenomena of the collapse sequence of an isolated beam, *Chapter 5*

Reasons:
- The Nissan beam is treated in isolation in this thesis
- To understand the collapse sequence of a beam in isolation
- To show the presence of the tension force in the collapse sequence, which leads to the Catenary effect

5. Software used for non-linear Finite Element models, *Chapter 6*

Reasons:
- To give a brief explanation of the software packages used in the Thesis.

6. Introduction to Finite Element Modelling, *Chapter 7*

Reasons:
- To explain which software was used to build and analyse the models
- To have an essential and general background about non-linear Finite Element Modelling
- To understand the main features of the code used in the thesis, Ls-Dyna in particular.

7. Properties of the isolated beam, *Chapter 8*

Reasons:
- To explain the geometrical property of the tubular beam actually used by Nissan.
- To show how the tubular beam is attached at the car-door.
- To give information about the material of the beam.

8. Bending test on the existing side-impact-beam in isolation, *Chapter 9*

Reasons:
- To provide an experimental benchmark to check the validity of the FE models.
- To provide phenomenological information on the collapse of the tubular beam.

9. Computer models description, *Chapter 10*

Reasons:
- Explanation of aims of detailed Ls-Dyna FE models.
- Modelling and meshing decisions.

10. Computer simulations of existing tubular side-impact-beam, *Chapter 11*:

Reasons:
- Initial modelling to develop confidence in Ls-Dyna models, using experimental results as a benchmark.
- FE based study of the performance of the new press formed beam.
- Parametric study to improve weight efficiency of the new beam.

Intended approach:
- Simulation of a bending test on the beam in isolation:
    - Modelling problems:
        - Mesh effects on the models, in term of:
            - Force – displacement graph

        - Sensitivity analysis on type of shell elements formulation used, in term of:
            - Force – displacement graph

        - Evaluation of the Computational time in relation at:
            - Mesh density
            - Shell element formulation adopted

    Deliverables:
    - Selection of the most reliable meshes from a "numerical point of view"

    - Simulations behaviour:
        - Evaluation of the collapse mechanism in relation at different types of constraints used, in term of:
            - Force – displacement graph

11. Comparison between bending test and simulation, *Chapter 12*:

Methodology adopted:
- Comparison between experimental and FE results based on:
    - Mechanism of collapse
    - Force – displacement graph
    - Selection of FE model with best fidelity.

12. Initial study for press-formed side-impact beams, ***Chapter 13***:

Intended approach:
- Preliminary analysis of Nissan requirements and restrictions relative to the new design.
- "Tear down approach" to know how some of Nissan's competitors are actually designing their side-impact-beams.
- Choice of possible candidate shapes for the new design.
- Simulation of a bending test of the new side-impact-beam in isolation.
- Comparison between new designs and the old side-impact-beam (test and best simulation) in terms of:
  - Force - displacement graph
  - Weight of the side-impact-beam
.

13. Main conclusions achieved from the work developed in this Thesis, ***Chapter 14***

2 Introduction to side impact crashworthiness

Nowadays the problem of passive safety has become more and more significant: the percentage of people who showed high interest in vehicle safety increased from 64% in 1981 to 84% in 1999 in the U.S.A.[1]   In Germany, companies such as Audi and Volkswagen have published figures that state that 85% of people who were asked mentioned safety as the top issue.[2]   Because of consumer interest, one of the most common questions asked is why the tests for the certification of a car are performed at lower speed than the average velocity of a common driver, or lower than the maximum limits prescribed on the roads.   The answer to this question is not so simple: first of all is important to underline that the aim of passive safety is not to "save all lives", but to reduce the number of fatalities and injuries during what are defined survivable accidents.

2.1 General background on side – impact regulations

Reasons:
- Introduce the reader to problem of crashworthiness
- Understand the importance of passive safety in relation to the side impact.

Methodology adopted:
- Literature survey and analysis of different papers, journals, books about crashworthiness and safety, and other publications and statistics.

Deliveries:
- Basic general knowledge about safety and prevention of injuries.

In the last 10 years on European roads, car accidents account for approximately 40,000 fatalities and more than 3 million injuries per year. This represents an enormous societal and economical loss, so the European Commission aims to reduce road casualties by least 50% within the next 10 years.[3] See Fig. 2.1.
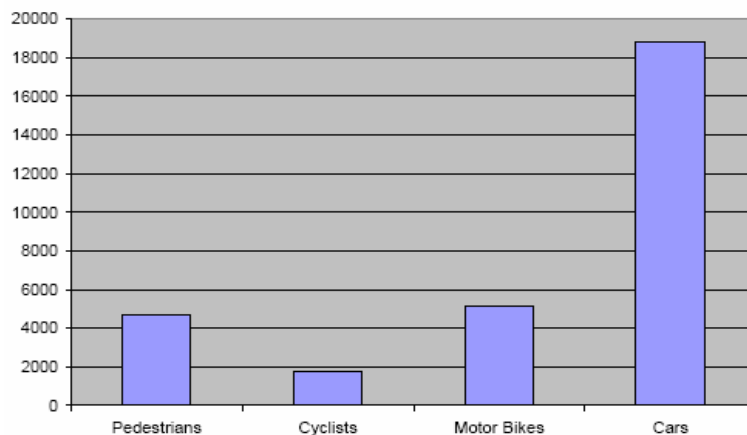
Fig. 2.1: Road Fatalities by Traffic Participation in all EU Countries 2001 [IRTAD 2002] [4]

In this huge number of automobile accidents, side impacts are the second most important type of crash causing serious injury and death.[3]
As we can see from the Fig.2.2, around 40% of the fatalities of car occupants occur in front impacts, while in side impacts the rate of people killed is about 35% of the total.
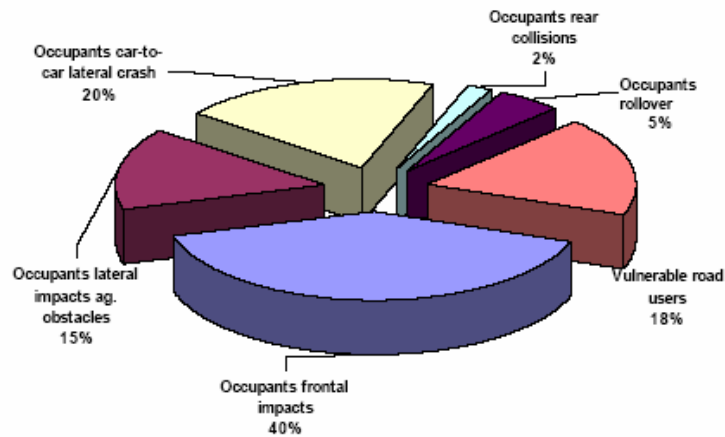
Fig. 2.2: Fatality rates for individual collision categories involving cars [Klanner, 2001] [3]

More than a half of side impacts are between cars, typically travelling on paths perpendicular one to another and in which the speed of the struck (target) car is less than of the striking (bullet) car.[2]

.

3 General background on side – impact regulations

Reasons:
- The beam is a part of the protection system involved during a side impact on a car.
- To contextualise the problem having a minimum knowledge about regulations, because the beam has to contribute within the complete car – structure to pass the compulsory tests.
- The two Nissan vehicles in analysis have to pass the certification rules for side impact.

Methodology adopted:
- Literature survey to gather information relative to:
  - European side – impact regulations.
  - EuroNCAP side – impact assessment.
  - US side – impact regulations.

Deliverables:
- Procedures adopted for the different rules
- Injury criteria limits to pass the compulsory tests
- Other requirements and prescriptions for side – impact.

3.1 European side impact

The European side impact regulations are specified in the directive 96/27/EC, which was adopted on the 20th of May 1996. This directive specifies how a side impact test has to be developed to certify a mass production car in the European Community.
The test consists of a moveable deformable barrier(MDB), driven at a speed of 50 km/h, hitting the side of a stationary car, in which is seated a EuroSID dummy.

To pass the test it is necessary to satysfy all the specified prescriptions:

- Dummy injury criteria below limits (see paragraph *2.5 Injury criteria*)
- No doors opening during the impact
- After the impact the dummy has to be easily removed from the car, without the use of particular tools.
- The rate of liquid leakage from the fuel-feed has not to exceed 30g/min
- No increased injury risk from sharp edges or detached devices

The movable deformable barrier has to be a trolley with a mass of 950 kg, with a deformable impact zone 1500 mm wide, 500 mm high and with a ground clearance of 260 mm.
The material of the impactor must be an aluminium honeycomb or other materials with specified characteristics.[6]
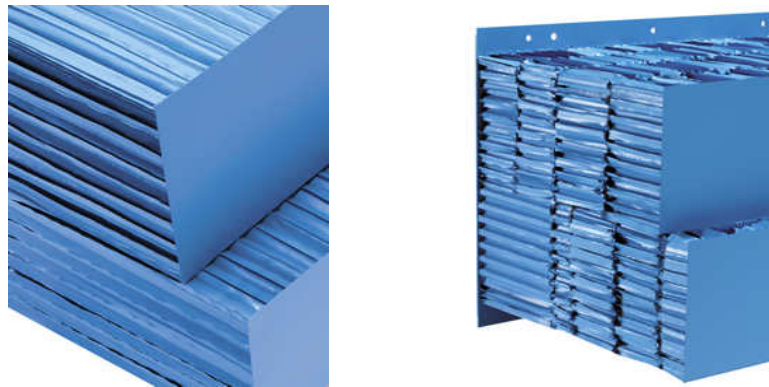
Fig. 3.1: Honeycomb aluminium for impactor.

Finally it is important to underline that the impact has to occur at an angle of 90° to the driver's side, if the car is symmetric, otherwise special conditions may be applied.

3.2 Euro-NCAP side impact

The Euro New Car Assessment Programme (Euro-NCAP) publishes test results that provide consumers with accurate information based on in-depth research about the safety performance of individual car models in frontal and side collisions.

In the Euro-NCAP side impact test, a stationary vehicle with dummies seated in the driver's and front passenger's seat is rammed by a moving trolley (with a crushable aluminium face and a mass of 950 kg) going 50 km/h directly centered on the driver's seating position.[7] [8]

As can be seen, the Euro-NCAP reproduces totally the requirements and the prescriptions provided by European side impact, with the addition of a dummy in the passenger seat.
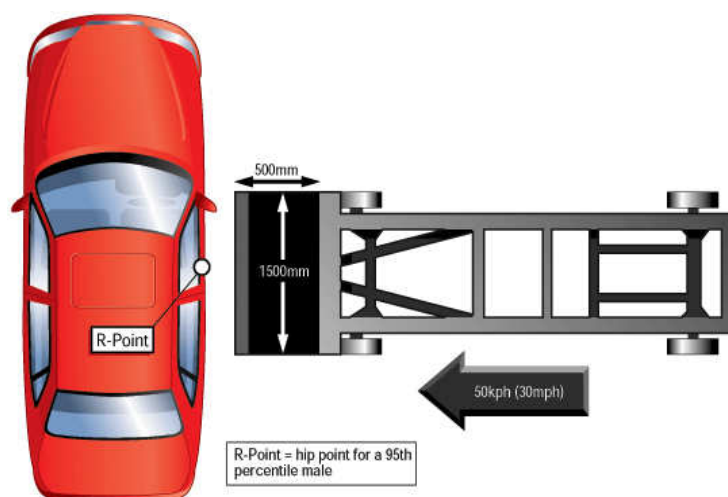
Fig. 3.2: Euro-NCAP side impact.[7]

18

3.3 US side impact

The US regulations about side impact are specified in the directive FMVSS (Federal Motor Vehicle Standard) No. 214, amended in 1990 to assure occupant protection in a dynamic test that simulates a severe angle collision and phased into new passengers cars during 1994-1997. The impact trolley's wheels are crabbed to simulate the effect of a moving target car as well as a moving bullet car.

It prescribes two different types of tests:

- Quasi-static: intended to measure the intrusion of the door panel into the passenger compartment
- Dynamic: intended to measure the forces acting on the occupant's body.[8] [9]

1. Quasi static test

The quasi-static test in the U.S. regulation is performed pushing the door of the car with a (very low) constant velocity of 0.03 m/s, using a rigid steel cylinder with a diameter of 300 m, to reach the maximum displacement of 450 mm.

To pass the test is necessary to calculate and respect the following prescriptions :

- the initial average crash resistance $P_{initial}$ is the average force required to deform the door over 150mm. [9]

$$P_{initial} = \frac{\int_{0}^{150\,mm} P * d\Delta}{\Delta_{150}} > 1250 \text{ pounds force (with seats not installed in the vehicle)}$$

(pounds force units are specified in the regulation)

or:

$$P_{initial} = \frac{\int_{0}^{150\,mm} P * d\Delta}{\Delta_{150}} > 2250 \text{ pounds force (with seats installed in the vehicle)}$$

Where P is the applied load at the door beam and Δ is the maximum deflection imposed.

- the intermediate average crush resistance $P_{int\,ermediate}$, is the average force required to deform the door over 300mm [9]

$$P_{int\,ermediate} = \frac{\int_{0}^{300\,mm} P * d\Delta}{\Delta_{300}} > 3500 \text{ pounds force (without seats)}$$

or:

$$P_{\text{int }ermediate} = \frac{\int_0^{300\,mm} P * d\Delta}{\Delta_{300}} > 4375 \text{ pounds force (with seats installed)}$$

Where P is the applied load at the door beam and Δ is the maximum deflection imposed.

- the peak crush resistance P_{crush}, that is the average force required to deform the door over 350mm. [9]

$P_{crush} > 7000$ pounds force (without seats in the car) within 450mm of deflection

or:

$P_{crush} > 12000$ pounds force (with seats mounted in the car) within 450mm of deflection

Where P is the applied load at the door beam and Δ is the maximum deflection imposed, in the test. (which is 450mm)

2. Dynamic test

The dynamic side impact test simulates in the U.S. regulation, a 90-degree intersection impact of a striking vehicle traveling 48 km/h into the tested vehicle traveling 24 km/h. This is achieved by running a moving deformable barrier (MDB), which has all wheels rotated 27 degrees (crab angle) from the longitudinal axis, into the side of a stationary vehicle at a 90-degree contact angle with a speed of 54 km/h.
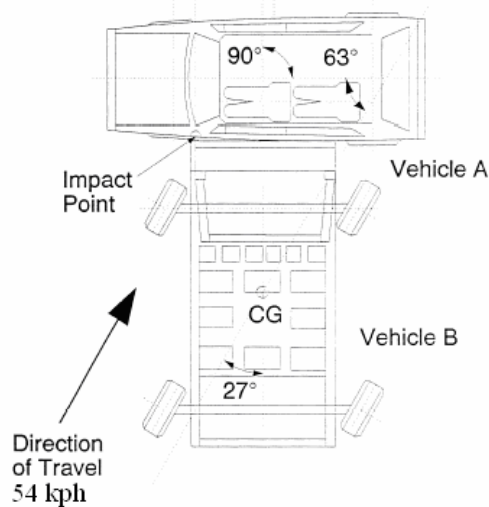
Fig. 3.3: US side impact configuration [9]

At the initial contact, the longitudinal axes of the MDB and the test vehicle are perpendicular to each other. Two side impact dummies (SIDs) are used in the target vehicle. They are positioned on the struck side of the vehicle, one in the front seat with the other directly behind in the rear seat.

The MDB, which simulates the striking vehicle, has a mass of 1361 kg, and dimensions of 1676 mm of wide, 560 mm of height, 280 mm of clearance from the ground.

To pass the test is necessary to respect these requirements:

- Chest and pelvis deceleration within the prescribed limits (see paragraph *2.5 Injury criteria*)
- Doors on struck side must not separate
- Other doors must not open or separate

See Ref. [8] [9]

3.4 Injury Criteria

In a side impact, injuries in the struck car arise mainly from 3 reasons:

- The side of the car is deformed inward, so the occupants could be hit by intrusion, causing injury to the body and to the legs.
- The head of the occupant on the struck side could hit the unpadded zones of the car.
- The passenger, on the near side seat, could move across the car, impacting with interior parts.[16]

As seen in the previous regulations, to successfully pass the side impact test, is necessary to satisfy some important injury criteria, developed to relate the behaviour of human body, with some characteristic parameters measured during a crash phenomenon in the used dummies. For a side impact the most common injury risks are:

- HPC (head performance criterion)

$$\max\left(\left(t_2 - t_1\right) * \left[\frac{1}{\left(t_2 - t_1\right)} \right] * \int_{t_1}^{t_2} a \cdot dt \right)^{2.5}$$

where t_2 and t_1 are any two times between the initial and final contact times
a is the head acceleration in g. t_1 and t_2 are chosen to maximise this function.

This parameter is compulsory for the European Test which specifies that it shall be less than 1000.[6] [10]

- TPC (thorax performance criterion)

    o Chest deflection

        The maximum deflection for any ribs of the crash dummy must be less than 42 mm for the European Rules[6] [10]

    o Viscous criterion

        $$VC = \max\left(\frac{D}{0.14} \cdot \frac{dD}{dt}\right)$$

        where D is the rib deflection

    This parameter shall be less than 1 m/s for the European Side Impact.[4]

- APF (abdominal peak force)

    This is a measure of the maximum abdominal force and it must be less than 2.5kN as underlined in the European regulations.[6]

- PSPF (pubic symphysis peak force)

    The maximum pelvis force must be less than 10kN for the European regulations.[4]

- TTI (thoracic trauma index)

    $$TTI = \frac{1}{2}\left(G_r + G_{ls}\right)$$

    where G_{ls} is the peak acceleration of the spine while G_r is the peak acceleration of the ribs, both expressed in g. For the American FMVSS 214 the TTI value shall be less than 90g for a 2-door car and of 85g for a 4-door car.[9]

- PELVIC LATERAL ACCELERATION

    This value shall be less than 130g for the American dynamic test.[9]

3.5 Considerations with respect to this Thesis

All the injury criteria and the prescriptions indicated as compulsory to pass the side-impact-tests refer to the complete car-structure. It has not been found in the described rules any limitations or obligatory design-requirements relative to one single component in isolation, which is the case analysed in this thesis. The solution adopted in this thesis, as stated in *paragraph 1.3 and 1.4*, is to compare side-impact-beams in isolation,

in terms of Force-displacement graphs, maximum peak of Force and weight, based loosely on the static provisions of US regulation FMVSS214.

The assumption implicit in this approach is that if the behaviour of the new beam in isolation in a quasi-static test is similar to that of the old one then the overall behaviour of the side impact system is likely to be similar.
It would be necessary to check this assumption on complete vehicles at some stage in the future, but this was outside the capability of test facilities available for this Thesis.

4 Collapse mechanism of a simple car made of beam elements.

Reasons:
- To understand the role played by the side–impact-beam within collapse behaviour of the whole structure of the car
- To understand that during a side impact the whole car body structure is involved in the collapse mechanism
- To try to find the preferable collapse sequence of the car structure.

Methodology adopted:
- Reproducing in a simplified way the quasi-static test of the American FMVSS214 on a simple model of a car, made of beam elements, provided by Prof. Brown [45]. The model used is an illustrative one only.
- Using the software CrashD, developed in Cranfield University and suited to treat and predict the collapse mechanism of beam made structures, using a quasi static large deflection calculation.
- Literature survey relative at what should be the best mechanism of collapse of the complete car.

Deliverables:
- The beam is only a part of the whole structure that has to resist at the lateral force of the side-impact.
- The main function of the beam is to guide and promote the correct collapse sequence
- Catenary effect: birth in the side-impact-beam of a tension force that pulls forward and inward the B-pillar of the car, backward and inward the A-pillar of the vehicle.
- Catenary effects are noticeable in almost all the beams that constitute the frame of the car.

4.1 Description of the vehicle.

A simplified CrashD model of the structure of a car was provided by Prof. Brown see Fig 4.1.
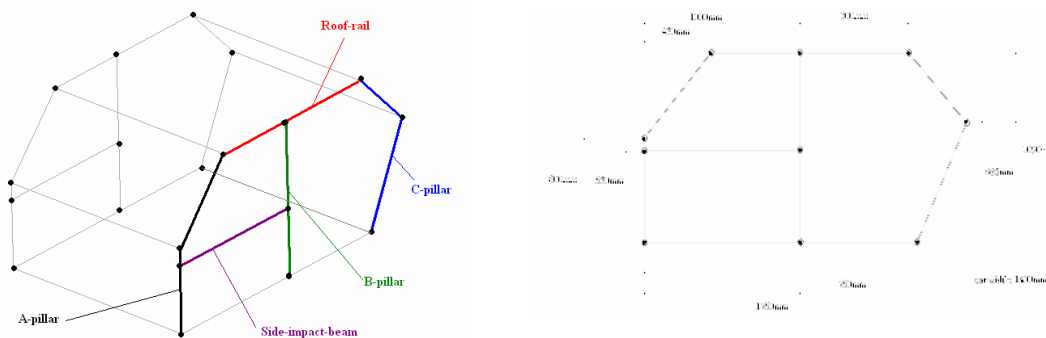
Fig. 4.1: Model of the car provided and dimensions.

The car body dimensions are specified in Fig.4.1. The model is made with 24 non-linear beam elements of assigned geometrical properties, as described by Ref [45].
To understand how the various parameters and properties are assigned, the reader has to refer to the CrashD user's manual.[12]

4.2 Simulation description

The simulation is performed using the software CrashD and it tries to reproduce in a simplified way the quasi-static test of the American rule FMVSS 214 (see paragraph NN).
At the car structure is applied a constant displacement in the middle of the side-impact-beam, as illustrated by Fig. 4.2.
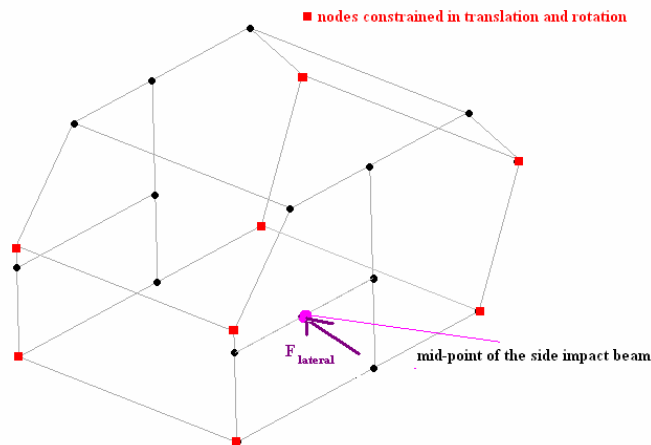
Fig. 4.2: Externally loaded point on the car model and constraints.

The aim is to obtain the Force–displacement graph of the externally loaded point, see Fig. 4.2, to analyse how the car collapses.
The intention is to reproduce the test procedure prescribed in the static provisions of FMVSS214.
The non-linear capabilities of the CrashD program include:
- Modelling the appearance of plastic hinges (local bending failures)
- Modelling the effect of large changes in the structure geometry during collapse.
- Modelling the effect of catenary effects
- Analysis of structural behaviour well into the deep collapse range.

4.3 Mechanism of collapse of the complete car

The collapse is due to a consecutive formation of plastic hinges at the ends of the beam elements, as shown by the black dots in the Fig. 4.3.
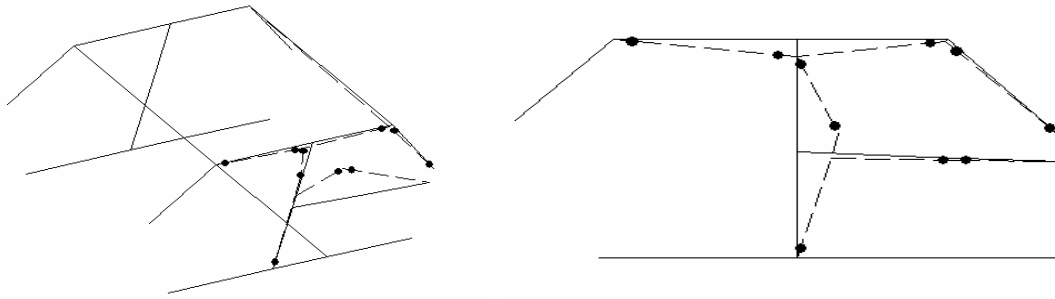
Fig. 4.3 : Rear oblique view and side view of the car, showing the collapse mechanism predicted by CrashD.

The car follows a sequence of collapse. This emerges from an analysis of the Force-displacement graphs, Fig 4.4, Fig. 4.5.

In these plots, the Force measured refers to the lateral reaction acting on the centre of the door of car, while the displacement is the one applied at the mid-point of the side-impact-beam, as previously shown. In Fig. 4.4 vertical lines are traced to indicate when the formation of plastic hinges occur. The sequence of formation of the plastic hinges is given in CrashD outputs [12].
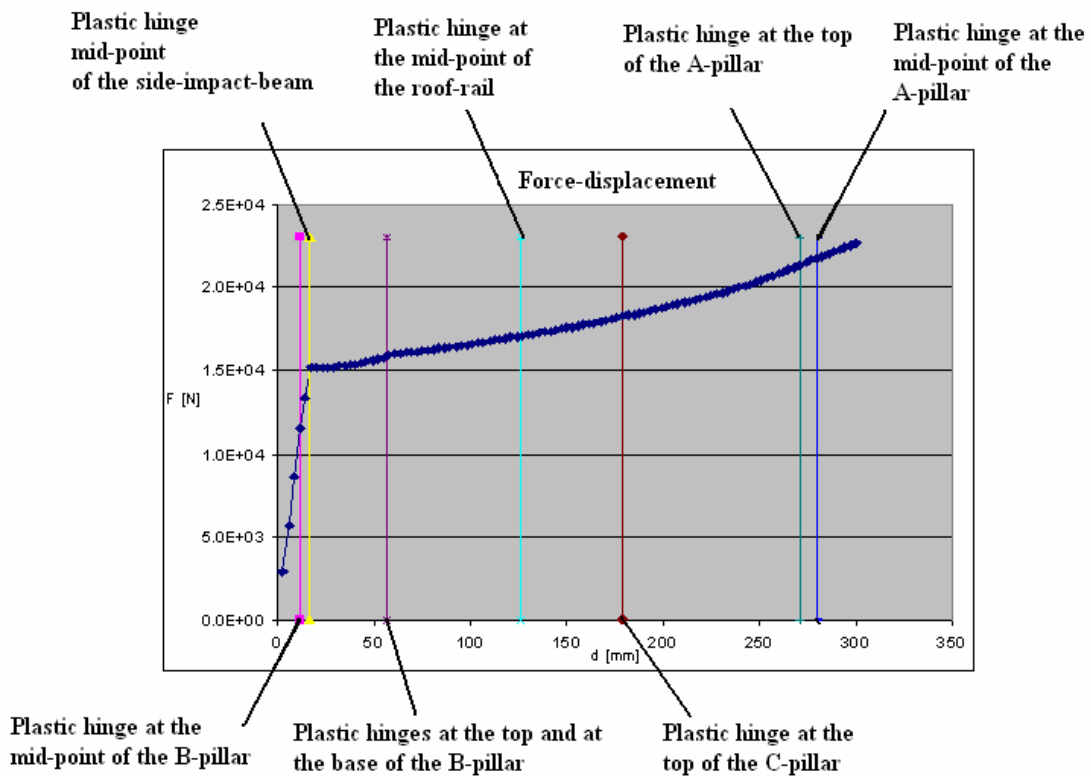
Fig. 4.4 Force-displacement graph and formation of plastic hinges in the structure

Every change in the slope of the Force-displacement graph means that the apparent stiffness of the whole car structure has varied. The stiffness change is due to the collapse of parts of the car-structure; in this case, as shown by Fig 4.5, a sudden change in slope is evident when one of the beams that constitute the car-frame collapses. This collapse occurs when all the plastic hinges that make the beam in question a mechanism are formed.
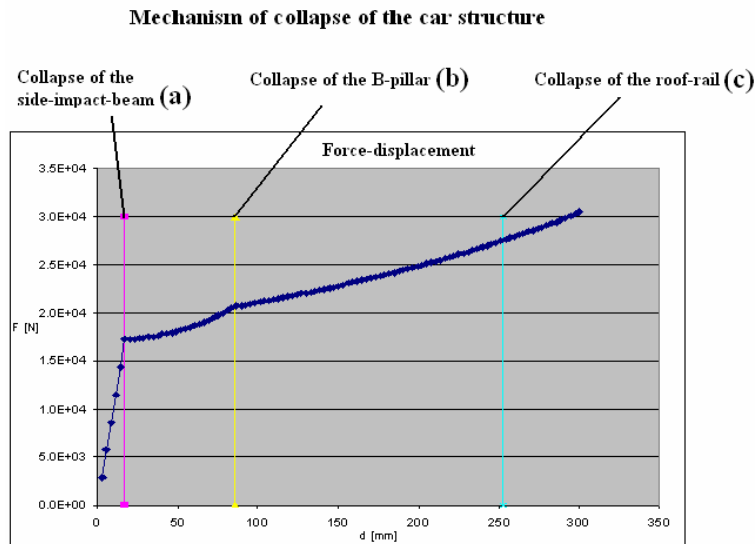
Fig. 4.5 Force-displacement graph and progressive collapse of the car-frame.

Referring to Figs 4.3, 4.4, 4.5 the sequence of collapse may be summarised as follows:

I. Formation of plastic hinge at the centre of door beam, causing it to collapse (see discontinuity (a) in Fig.4.5). The ends of the door beam were modelled as free pin joints.
II. Development of catenary (tension) force in door beam as collapse deflection becomes large. This is manifested as rising resistance in Fig.4.5
III. Catenary force in the door beam pulls against the B-pillar at the latch, causing the B-pillar to collapse with 3 plastic hinges (see (b) in Fig.4.5).
IV. As lateral deflection of the B-pillar at the latch becomes large, catenary force develops in the B-pillar.
V. The B-pillar catenary force pulls downward on the roof rail causing the latter to collapse downwards.

4.4 Best mechanism of collapse

Theoretically, it is possible to obtain different mechanisms of collapse by strengthening differently the various constituting parts of the car but what is the preferable?
A suggested answer to this question is in the work developed by Ming Loo on Ford AUII Falcon, in which is shown that the best mechanism of collapse should direct large deformation away from beltline and roof, promoting a pivot effect of the B-pillar from the roofline and eliminating high plasticity at the hinge point at beltline. [14]   The clear aim is to reduce the deceleration that the occupants have to sustain in case of

accident, but also to guarantee enough survival space to avoid that the passengers can be crushed by dangerous mechanism of collapse of the structure.

This collapse mechanism could be obtained by adjusting appropriately the plastic hinge moments of the beams and making up the passenger cell structure.

Fig 4.6: B-pillar deflection [14]

4.5 Conclusions on overall vehicle collapse.

- It is possible to obtain different mechanisms of collapse of the car by the variation of the strength of the structural parts.
- The beam is only a part of the car-frame, it has the function of promoting the correct collapse of the car during a side-impact.
- It is meaningless to evaluate the side-impact-beam in terms of Energy absorbed, in fact, the Energy absorbed is a parameter that refers to the complete structure.
- The catenary effects play an important role in the collapse sequence of the car-structure.

5 Simple hand calculation model of the collapse sequence of an isolated beam

Reasons:
- The Nissan beam is treated in isolation in this thesis
- To understand the collapse sequence of a beam in isolation
- To show the presence of the tension force in the collapse sequence, which leads to the catenary effect.

Methodology adopted:
- Simple hand calculations on an isolated beam

Deliverables:
- Collapse sequence on an isolated beam.

5.1 Main assumptions
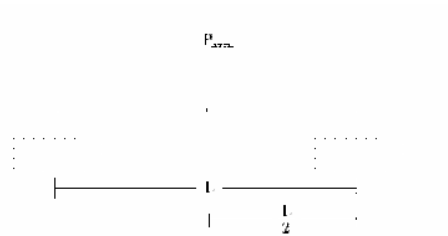
Fig.5.1 beam subjected to a lateral Force.

The beam-ends are fixed in translation but not in rotations, which are allowed, see Fig.5.2. On the car, in fact, a rotation of the side-impact-beam extremities is allowed.
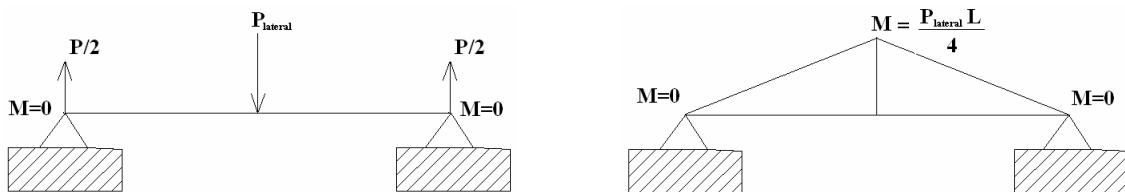
Fig.5.2 Free body diagram (on the left) and trend of the internal bending-moment (on the right).

The plastic moment M_p is assumed constant with the rotation θ, see Fig.5.3 and Fig.5.4.
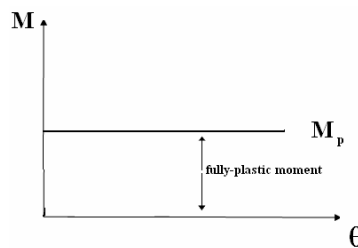
Fig.5.3 idealized relation between plastic moment and rotation.
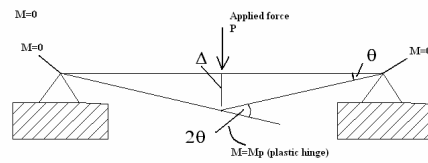
Fig.5.4: rotation and displacement on the isolated beam.

The beam is made with mild steel, characterised by a stress-strain curve which can be approximate as a bilinear-elastic-plastic curve, see Fig.5.5
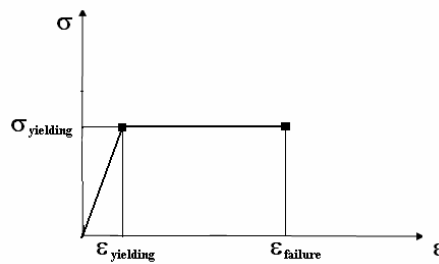
Fig.5.5 bilinear elastic-plastic curve for stress and strain.

5.2 Collapse sequence

Small deflections
   1. elastic behaviour
   2. bending-moment collapse at centre
   (plastic collapse mechanism entailing plastic hinge at centre and pin joints at ends).

Large deflections
   3. catenary effects
   4. axial yielding collapse
   5. failure

5.2.1 Collapse mechanism for small deflections

- Elastic stage

In the elastic range, the relation between the applied lateral force and the deflection at the centre of the beam is:

$$1) \quad P_{elastic} = \frac{48EJ}{L^3} \Delta_{elastic}$$

see Ref [11] and Ref [38].

The elastic range ends when the stress in the extreme fibres at the centre of the beam teaches the yield stress σ_y of the material. However the beam does not collapse at this stage(see Fig. 5.6).

If the applied force P continues to increase, additional yielding at the centre of the beam moves in toward the neutral axis until a "plastic hinge" forms at this point. This, with pin joints at the ends of the beam, causes a "plastic collapse mechanism". At this stage the force "levels off" to a constant value (the beam collapses).

For simplified theory the transitional region (Fig.5.6) is simplified to a sharp transition
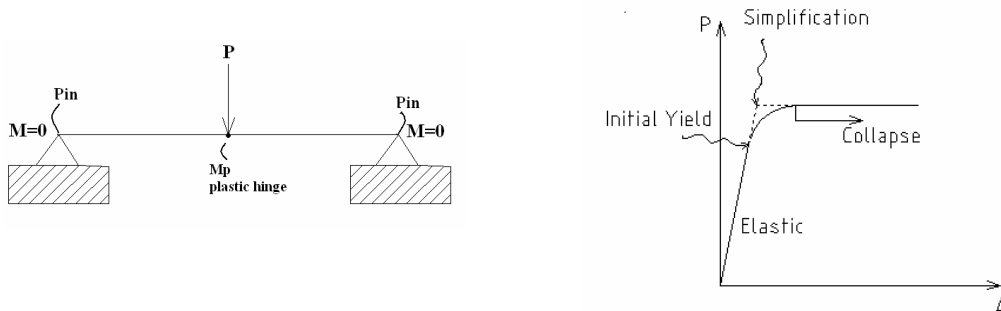
Fig.5.6: transition from initial yield to collapse mechanism

- Bending-moment collapse

If the lateral Force ($P_{lateral}$) is increased over $P_{elastic}$, the yield spreads to all the mid-section of the beam until it is fully plastic. At this stage the bending-moment at the mid-span of the beam is equal to the plastic hinge moment M_p, see Fig.5.7.
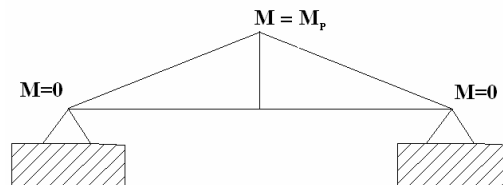
Fig.5.7: trend of the bending-moment within the beam.

When M_p is reached there is a formation of a plastic hinge in the middle of the beam, see Fig.5.8, and the beam becomes a mechanism, see the assumption made in *paragraph 5.1 point 1.*
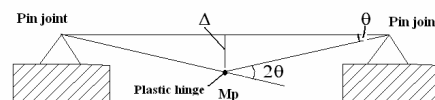
Fig.5.8: formation of a plastic-hinge.

On applying (small) deflection Δ to the beam centre causes the plastic hinge to rotate through angle 2θ (see Fig.5.8).

31

Internal plastic strain energy $= M_P \cdot (2\theta)$ (M_p assumed constant with θ; θ in radians)

Corresponding external work done $= P_\text{collapse} \cdot \Delta$ (P_collapse is constant for small deflections)
Energy balance:
External work done = Internal plastic strain energy

$$2)\ M_P \cdot (2\theta) = P_{lateral-bending} \cdot \Delta$$

Considering the geometry in Fig. 5.8 it can be seen that:

$$d)\quad \Delta = \frac{L}{2} \cdot \theta\ \text{ (for small } \theta \text{ in radians)}$$

and substituting d) in equation 2), we can express the lateral Force due to bending-effects ($P_\text{lateral-bending}$) in function of the plastic moment M_p, 3), by cancelling θ.

$$3)\ P_{lateral-bending} = \frac{M_P \cdot 4}{L}$$

For small displacements, according to the idealized relation of point 2 of *paragraph 5.1*, the rotation at the plastic hinge and hence the deflection (Δ) increases at a constant load ($P_\text{lateral-bending}$), see Fig.5.9.
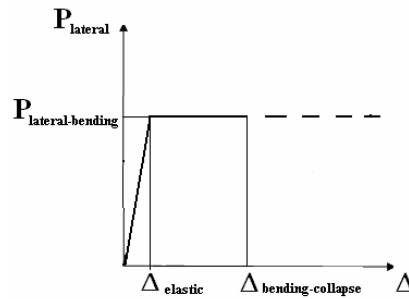
Fig.5.9: bending-moment collapse

The increase in deflection during the collapse is caused by the rotation at the central hinge without a concurrent change in curvature of the two halves of the beam; as shown in Fig.5.8, each half of length $\frac{L}{2}$ of the beam can be considered a straight line.

In this phase the bending moment at sections other than mid-span is less than M_p, see Fig.5.7, and the beam remains elastic away from the plastic hinge

5.2.2 Collapse mechanism for large deflections

- Catenary effect

I. Elastic phase of catenary effect.

When the plastic moment is reached at the mid-span section of the beam, if the load is increased further axial (catenary) forces develop in the two halves of the beam.
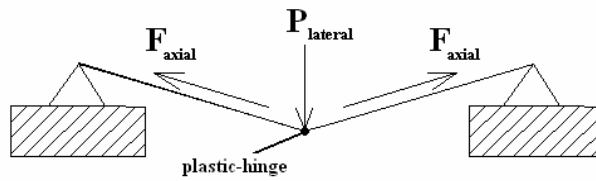
Fig.5.10: birth of axial Forces within the beam (catenary effect).

This is because at large deflections, the collapsed beam is longer than its original undeformed length, so that the beam becomes stretched. (support points assumed un-moveable)

While the stretched half-beams remain elastic, the axial Forces can be calculated using relation 4)

$F_{axial} = \varepsilon \cdot E \cdot A$ (this assumes elastic behaviour)

Extra force due to catenary effect
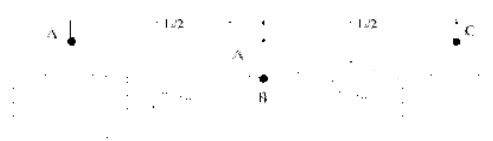
Fig.5.11: plastic hinges.

Strain $\varepsilon = \dfrac{change\ of\ length}{original\ length}$ (in half beam) $\varepsilon = \dfrac{\sqrt{\left(\dfrac{L}{2}\right)^2 + \Delta^2} - \dfrac{L}{2}}{\dfrac{L}{2}}$

Although there are plastic hinges at A-B-C, see Fig.5.11, initially the remainder of the beams remain elastic at large deflections.

In the elastic range in the 2 beam halves.

$$\text{Stress} = \sigma = E \cdot \varepsilon = E \cdot \frac{\sqrt{\left(\dfrac{L}{2}\right)^2 + \Delta^2} - \dfrac{L}{2}}{\dfrac{L}{2}}$$

Hence tension force (elastic catenary force) $F = \sigma \cdot A$ in beam halves

$$5)\ F_{axial} = E \cdot A \cdot \left(\frac{\sqrt{\left(\dfrac{L}{2}\right)^2 + \Delta^2} - \dfrac{L}{2}}{\dfrac{L}{2}} \right)$$

This is the axial force in each of the beam halves, see Fig.5.12.
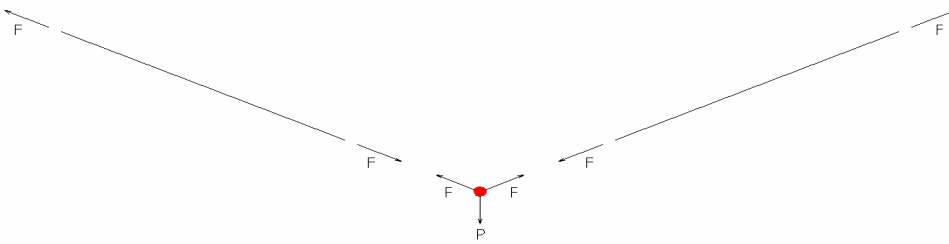
Fig.5.12: axial force along the beam halves.
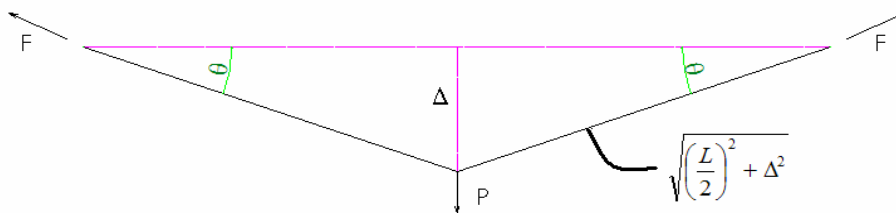
Fig.5.13: lateral and axial forces acting on the beam

This axial Force is related to the external beam force as follows:

Resolve vertically

$$6)\ P\ =2\cdot F_{axial}\cdot\cos(90°-\theta)=2\cdot F_{axial}\cdot\sin(\theta)=2\cdot F_{axial}\cdot\left(\frac{\Delta}{\sqrt{\left(\frac{L}{2}\right)^2+\Delta^2}}\right)$$

and substituting equation 5) in equation 6):

$$P=\frac{2\cdot E\cdot A\left(\sqrt{\left(\frac{L}{2}\right)^2+\Delta^2}-\left(\frac{L}{2}\right)\right)}{\frac{L}{2}}\cdot\frac{\Delta}{\sqrt{\left(\frac{L}{2}\right)^2+\Delta^2}}=\frac{2\cdot E\cdot A}{\frac{L}{2}}\left\{1-\frac{\frac{L}{2}}{\sqrt{\left(\frac{L}{2}\right)^2+\Delta^2}}\right\}\cdot\Delta$$

Simplifying further

$$8)\ P=2\cdot E\cdot A\left\{\frac{2}{L}-\frac{1}{\sqrt{\left(\frac{L}{2}\right)^2+\Delta^2}}\right\}\cdot\Delta$$

This is in addition to the reaction force $P_{collapse}$ for the bending collapse mechanism.

II. Axial yield of beam halves

For steel, the stress - strain graph eventually enters the yield range when the stress becomes limited to σ_y, the (constant) yield stress
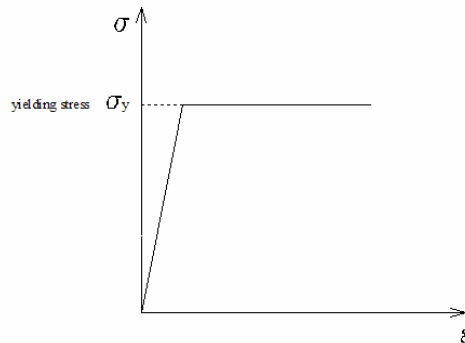
Fig.5.14. stress – strain graph with constant yield stress.

In the yield range the tension in the beam halves is equal to F_y, where

$F_y = A \cdot \sigma_y$ (constant value)

The lateral force P, becomes P_y, see Fig.5.15
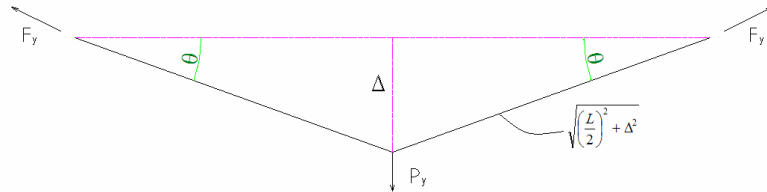
Fig.5.15 lateral force P_y acting on the beam

$$P_y = 2 \cdot F_y \cdot \sin(\theta)$$

$$9)\ P_y = 2 \cdot A \cdot \sigma_y \cdot \frac{\Delta}{\sqrt{\left(\dfrac{L}{2}\right)^2 + \Delta^2}}$$

These lateral Forces due to catenary effects have to be added to the lateral Forces due to bending-effects to obtain the lateral Forces ($P_{lateral}$) acting on the beam.

$P_{lateral} = P_{lateral-bending} + P_{lateral-catenary}$

- **Summary**

In the catenary range:

If half beams are elastic

$$P_e = 2 \cdot E \cdot A \left\{ \frac{2}{L} - \frac{1}{\sqrt{\left(\frac{L}{2}\right)^2 + \Delta^2}} \right\} \cdot \Delta$$

If half beams have yielded in tension

$$P_y = 2 \cdot A \cdot \sigma_y \cdot \frac{\Delta}{\sqrt{\left(\frac{L}{2}\right)^2 + \Delta^2}}$$

Either of these forces could reach a limit if the half-beam axial forces exceed the strength of the end connections F_{break}.

The limiting lateral force $P_{break} = 2 \cdot F_{break} \cdot \sin(\theta)$
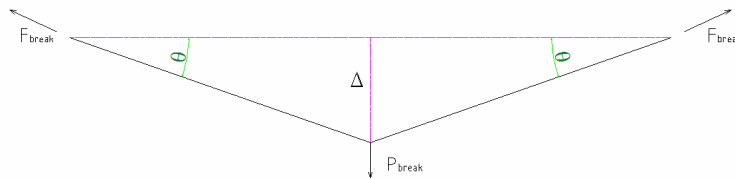
Fig.5.16: limiting lateral force (P_{break}) acting on the beam.

$$10) \; P_{break} = 2 \cdot F_{break} \cdot \frac{\Delta}{\sqrt{\left(\frac{L}{2}\right)^2 + \Delta^2}}$$

Final failure

The beam-failure can occur for two main reasons:

Axial-failure of the beam: the axial Forces along the beam induce a strain that is higher than the ultimate strain of the material, see assumption 3 of *paragraph 5.2*:

$\varepsilon_{axial} > \varepsilon_{ultimate}$

Failure in supports(brackets)-zone: the axial Forces along the beam are higher that the ones sustainable by the supports (brackets):

$F_{axial} > F_{break}$

A comparison between the results achieved with hand calculations and with a Ls-Dyna computer model is collected in the *Appendix D*.
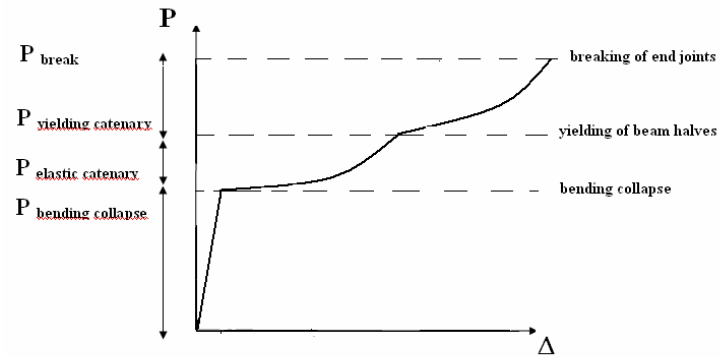
Fig.5.17: sequence of collapse for a pin-jointed beam.

6 Software used for non-linear finite element models

In this chapter the software packages used for the development of the present project will be briefly presented.

6.1 Hypermesh

Hypermesh is a high performance finite element pre and post-processor that allows to build finite element and finite difference models for engineering simulations and analysis. [32]
Hypermesh provides a variety of data import options to facilitate the treatment of models built with different software as well as several input cards, organised in different template options to realize models for a specific solver.
In the case of this thesis, Hypermesh was chosen because it is able to support input cards for Ls-Dyna, facilitating the definition of the models by the use of a graphical interface.
The analyst, in fact, has only to chose the correct template and once the input is complete, he exports the file in question in the desired format, .k, for Ls-Dyna.
Hypermesh is supplied by Altair Engineering Ltd.

6.2 Ls-Dyna 970

Ls-Dyna is a general purpose finite element code for analyzing the large deformation dynamic response of structures including structures coupled to fluids. The main solution methodology is based on explicit time integration. An implicit solver is currently available with somewhat limited capabilities including structural analysis and heat transfer. [23]
The origin of Ls-Dyna dates back to the public domain software, DYNA3D, which was developed in the mid-seventies at the Lawrence National Laboratory.
The first version of DYNA3D was released by Hallquist in 1976 and since then considerable progress has been made to improve the code.
Ls-Dyna is supplied by the Livermore Software Technology corporation.

6.3 Ls-Post

Ls-Post is the post processor and can except data output from Ls-Dyna and display it graphically. The program also contains a multitude of tools that allows the user to plot curves of the model response and to visualise the response of the structure to the applied load.

7 Introduction to non-linear dynamic Finite Element Method

Reasons:
- To explain which software was used to build and analyse the models
- To have an essential and general background about no-linear Finite Element Modelling
- To understand the main features of the code used in the thesis, Ls-Dyna in particular.

The finite element method is a numerical technique used for solving system of equations over the domain of a continuous physical system.

The whole domain of the body in analysis is divided in small parts, elements, connected each other through punctual entities called nodes to form what in technical language is called mesh. Every element of the domain is subjected to the physical equations that govern the problem, which are expressed in function of unknown values of the same specific solution at the nodes. Through the subdivision of the entire domain into little domains, the general solution of the problem becomes a system that expresses the global solution as a combination of these elemental equations. As stated above, because all the equations are function of nodal values, eventually loads applied or even the boundary conditions must be referred to the nodes.[15]

Ls-Dyna is capable of transient dynamic analysis of structures using the explicit time integration. It has powerful non-linear capabilities for application to crash problems.

7.1 Finite element procedure

- Divide the structure into finite elements (mesh generation) with the help of the pre processor (e.g. Hypermesh)
- Apply boundary conditions to the mesh
- Define any initial conditions
- Assign material properties to the elements
- Assign physical properties to the elements
- Analyse the model
- Post process the results

It is finally important to underline that this procedure has to be reiterated several times to verify the assumptions made in the modelling and in the meshing approach, with a careful analysis of the output obtained during the Post processing phase.[30]

7.2 Finite element mathematical techniques

From a mathematical point of view the dynamic finite element technique is a solution of a system of differential equations, that express the behaviour of each single element in which is divided the domain. This problem implies an appropriate techniques for the integration of these equation and for the solution of a system. Two popular direct integration methods are the implicit and the explicit, each of these methods has its own applicability depending on the problem to solve.[10]

In a dynamic phenomenon the equilibrium is expressed trough the equation

$$M \cdot \vec{a} = \sum P$$

Where M is the mass, a is the acceleration and P are the loads applied to the body.
In the case of direct integration method the above equation is mathematically expressed as

$$[M] \left\{ \ddot{D} \right\}_n + [C] \left\{ \dot{D} \right\}_n + [K] \left\{ D \right\}_n = \{R^{\text{external}}\}_n$$

Where n indicates the time $n\Delta t$ with Δt the time step, $\{R^{\text{external}}\}$ represents the external forces applied and [M], [C], [D] are respectively the matrices of mass, damping and stiffness. In crash phenomenon we are generally in presence of great displacements, which usually lead also a material non-linearity, translated into a matrix of stiffness time and displacement dependent.
That is why the equation of motion assumes another aspect:

$$[M] \left\{ \ddot{D} \right\}_n + [C] \left\{ \dot{D} \right\}_n + \{R^{\text{internal}}\}_n = \{R^{\text{external}}\}_n$$

where $\{R^{\text{internal}}\}_n$ are the internal forces at the time $n\Delta t$.

The characteristic of a direct explicit integration method is that the displacement at a time $n\Delta t$ is independent from the acceleration at the same time $n\Delta t$, so to express it in a mathematical form [44]:

$$\{D\}_{n+1} = f\left(\left\{ D \right\}_n, \left\{ \dot{D} \right\}_n, \left\{ \ddot{D} \right\}_n, \left\{ D \right\}_{n-1} \ldots\ldots\right)$$

This means that the displacements at the actual step are expressed in terms of accelerations and displacements at the previous steps, so the method does not require a complete solution of the system variables, but only pure historical data.

In the implicit method ,instead, displacements have the form [44]:

$$\{D\}_{n+1} = f\left(\left\{ \dot{D} \right\}_{n+1}, \left\{ \ddot{D} \right\}_{n+1}, \left\{ D \right\}_n \ldots\ldots\right)$$

and hence computation of the displacements at a time step $n\Delta t$ requires knowledge of the unknown time derivatives of the entire system.

7.3 Implicit method

The equation of motion that governs this method is at time t_{n+1}:

$$[\text{M}]\left\{\ddot{D}\right\}_{n+1} + [\text{C}]\left\{\dot{D}\right\}_{n+1} + [\text{K}]\left\{D\right\}_{n+1} = \left\{R^{external}\right\}_{n+1}$$

The Newmark technique is used as an example to understand the main features of this mathematical. This method begins with the definition of displacement and velocity[10] [44]:

$$\left\{D\right\}_{n+1} = \left\{D\right\}_{n+1} + \left\{\dot{D}\right\}_{n+1}\Delta t + \left[\left(\frac{1}{2}-\alpha\right)\left\{\ddot{D}\right\}_n + \alpha\left\{\ddot{D}\right\}_{n+1}\right]\Delta t$$

$$\left\{\dot{D}\right\}_{n+1} = \left\{\dot{D}\right\}_n + \left[(1-\delta)\left\{\ddot{D}\right\}_n + \delta\left\{\ddot{D}\right\}_{n+1}\right]\Delta t$$

where α and δ are Newmark's parameters of integration [10] [44].
If now we substitute these two developments into the previous equation of motion, what we obtain is:

$$\left(c_0[M]+c_1[C]+c_2[K]\right)\left\{D\right\}_{n+1} = \left\{R^{ext}\right\}_{n+1} + [M]\left(c_0\left\{D\right\}_n + c_2\left\{\dot{D}\right\}_n + c_3\left\{\ddot{D}\right\}_n\right) + [C]\left(c_1\left\{D\right\}_n + c_4\left\{\dot{D}\right\}_n + c_5\left\{\ddot{D}\right\}_n\right)$$

here the matrix $\left(c_0[M]+c_1[C]+c_2[K]\right)$ has to be inverted for each time step and the stiffness matrix K recalculated, because of its dependence on the displacements; these aspects imply a high computational cost.

7.4 Explicit method

For the explicit scheme of integration the equation of motion is written at the time at which acceleration and velocity are known:

$$[\text{M}]\left\{\ddot{D}\right\}_n + [\text{C}]\left\{\dot{D}\right\}_n + [\text{K}]\left\{D\right\}_n = \left\{R^{external}\right\}_n$$

The main assumption for this method is that displacement can be approximated as linear within time-steps, as show in Fig.7.1:
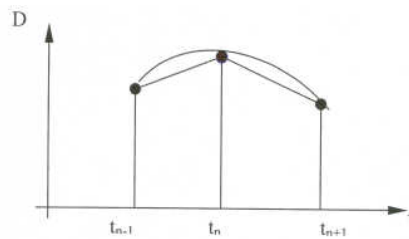
Fig. 7.1: linear approximation for displacements.

With this consideration accelerations and velocities are calculated as follow:

$$\left\{\ddot{D}\right\}_n = \frac{1}{\Delta t^2}\left(\left\{D\right\}_{n+1} - 2\left\{D\right\}_n + \left\{D\right\}_{n-1}\right)$$

$$\left\{\dot{D}\right\}_n = \frac{1}{2\Delta t}\left(\left\{D\right\}_{n+1} - \left\{D\right\}_{n-1}\right)$$

If we substitute these two expressions into the equation of motion we obtain:

$$\left(\frac{1}{\Delta t^2}[M]+\frac{2}{\Delta t}[C]\right)\left\{D\right\}_{n+1} = \left\{R^{ext}\right\}_n - \left([K]-\frac{2}{\Delta t^2}[M]\right)\left\{D\right\}_n - \left(\frac{1}{\Delta t^2}[M]-\frac{1}{2\Delta t}[C]\right)\left\{D\right\}_{n-1}$$

In this equation it is clear that all the terms on the right side are historical, therefore known at the time (n+1) Δt.

The advantage of this method is that the matrix [K] does not have to be inverted in order to obtain the displacement $\left\{D\right\}_{n+1}$, so compared to an implicit one, it requires less computer storage and computational operations.

But on the other hand, the explicit method is not like the implicit method because it is not unconditionally stable numerically; its stability, in fact, is strongly related to the time step. In the Ls-Dyna models in the thesis, the explicit scheme was used.

7.5 Time step

As stated above, one essential feature of an explicit method is the dependence of its stability to the time step.

This means that the step of integration has to be smaller than what we can define a critical step, defined as:

$$\Delta t = \frac{2}{\omega_{max}}$$

where ω_{max} is the highest frequency of vibration within the whole system.

In a structural problem the frequency ω can be determined through the stiffness and density of the element, using the following relationships:

$$\omega = \left(\frac{2}{d}\right)\cdot c$$

and

$$c = \sqrt{\frac{E}{\rho}}$$

where c is the wave speed in the material, E is the stiffness, ρ the density and d the characteristic dimension of the element.[10] [23]

In a beam element, for example, with a length L, using the previous equations, the critical time step is defined as:

$$\Delta t = \left(\frac{L}{c}\right)$$

Moreover in Ls-Dyna for stability reasons the calculated time step Δt is reduced with a scale factor of 0.9[23]:

$$\Delta t = 0.9 \cdot \left(\frac{L}{c}\right)$$

In conclusion it is important to underline that the characteristic dimension and the propagation velocity c, used for the calculation of the time step, are different in relation to the type of element considered; in fact, for a shell element, we have:

$$d = \frac{A}{\max\left(l_1, l_2, l_3, l_4\right)}$$ for a quadrilateral shell with edges equal to l_1, l_2, l_3, l_4 and area A

and

$$d = \frac{2A}{\max\left(l_1, l_2, l_3\right)}$$ for a triangular shell with edges equal to l_1, l_2, l_3 and area A

with

$$c = \sqrt{\frac{E}{\rho\left(1 - \upsilon^2\right)}}$$

7.6 Material models

Ls-Dyna version 970 can model a wide range of materials; in fact, from a simple analysis of its Keyword manual, it is evident that more than 100 different types of material models are available.

In this thesis the material used is steel, so its behaviour is an isotropic one, for which it is possible to identify five main different idealised representations based on the stress strain diagram:
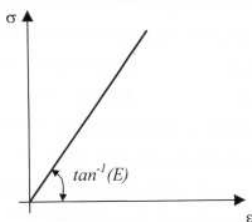
Perfectly elastic   *Perfectly plastic*
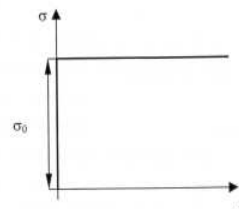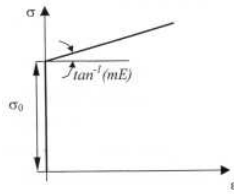
Plastic with linear strain hardening   *Elastic perfectly plastic*
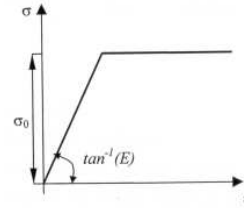
Elastic plastic with linear strain hardening
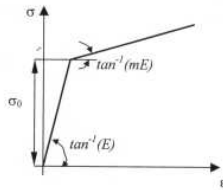
In the simulations performed this work, for all the deformable materials were used the elastic plastic with linear strain hardening model, indicated as plastic kinematic(type 3) in Ls-Dyna.

7.7 Contact algorithm

As state by reference [23]: "the treatment of sliding and impact along interfaces has always been an important capability in the DYNA 3D codes. Three distinct methods for handling this have been implemented: the kinematic constraint method, the penalty method and the distributed parameter method.
Interfaces can be defined in three dimensions by listing in arbitrary order all triangular and quadrilateral segments that comprise each side of the interface. One side of the interface is designed as the slave side and the other one is designed as the master side.
In the symmetric penalty method this distinction is irrelevant, but in the other methods the slave nodes are constrained to slide on the master surface after impact and must remain on the master surface until a tensile force develops between the node and the surface".
For this thesis automatic contact definitions have been used, which are one of the most common types of contact exploited. In this approach the slave and master surfaces are generated internally by Ls-Dyna from the ID's given for each surface.

7.7.1 Penalty method

In this paragraph the penalty method will be described because in the present work all the contacts used are based on it.   In case of penetration, once verified the contact between the generic node and the contact surface, the method tries to replace the node and the surface in the position it had (at the time) before the contact and it places normal

forces, whose values depends on the depth of the penetration between the node and the contact surface.

The method acts as if springs were placed between node and surface, whose stiffness is approximately of the same order of magnitude as the stiffness of the element at which the contact segment belong, see Fig.7.2.

7.7.2 Contact search

In all the methods cited above, as stated by reference [10], the contact algorithm is based on a procedure which follows some important steps. For all slave nodes is necessary to:

- Localise the closest node on the master surface
- Determine the master segment attached to that node
- Localise the contact point
- Verify the penetration.
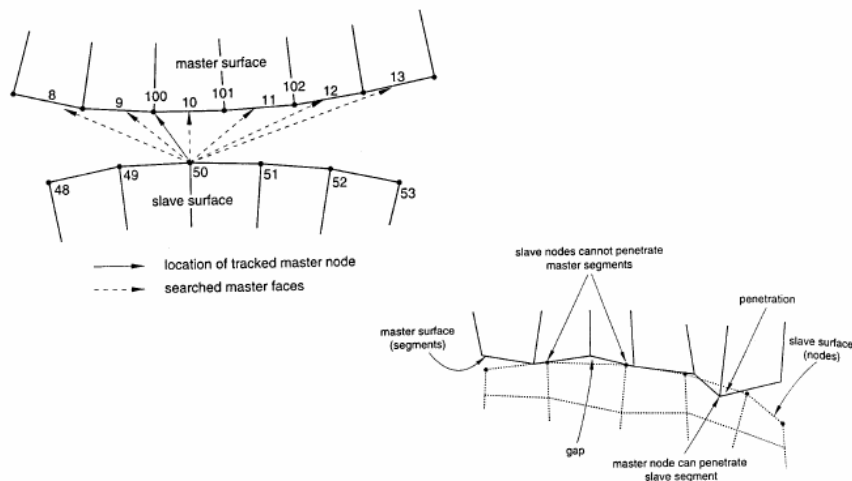
Fig. 7.2: contact search, from Ref [10].

If the slave segment has penetrated the master segment, it is necessary to:

- Determine the contact force: if the penetration distance is positive, a force F, proportional to the penetration, is applied to the slave node, in a normal direction to the surface on which the segment previously identified lies.
- Impose the conservation of the momentum.

It is important to underline that the first stage of this procedure is common to the algorithms mentioned above, while the second step is what really characterizes them.

46

7.8 Properties

All the models implemented in the simulations are made with shell elements.
As stated by Rao [36] many different formulations have been developed for this kind of element, in particular, in the Ls-Dyna *SECTION_SHELL card makes available more than 20 different types of shell, including quadrilateral and triangular elements.
In the simulations a sensitivity analysis was performed varying the type of shell, from a Belytschko-Lin-Tsay to a Belytschko-Wong-Chang, using also a Hughes-Liu fully integrated element for some coarser meshes.
The Belytschko-Lin-Tsay, default shell element for Ls-Dyna, has a formulation based on a flat geometry which is not capable of considering warpage, which is instead included in the Belytschko-Wong-Chang formulation.
The Hughes-Liu shell however, is derived from the eight-nodes-brick element formulation, as described by the Ls-Dyna theoretical manual [23] at which the reader can refer to a deeper mathematical explanation of the subject.

```
*SECTION_SHELL    FORM                 NIP
         1           2                    2
        1.4         1.4        1.4       1.4
```

In the second field of the first row of the card is possible to chose the desired formulation for the shell element, 2 for a Belytschko-Lin-Tsay shell, 10 for a Belytschko-Wong-Chang and 16 for a Hughes-Liu fully integrated element.
In the second row it is possible to specify the thicknesses of the element in question and for the existing tubular side-impact-beam the values provided by Nissan are the following:

- 2.6 mm pipe thickness
- 1.6 mm small bracket thickness
- 1.4 mm big bracket thickness

An other parameter that can be set in the *SECTION_SHELL card is the number of integration points through the thickness of the element, fourth card field (NIP) of the first row.
In this work the number of integration points were set equal to 2, default value, and later to 4, to understand if they could have a great influence on the models.
In fact, with an increased number of integration points in the thickness, the stress (through the element thickness) is better calculated, but the computational cost is higher.

7.9 Hourglass

To determine the stiffness, damping and mass matrices and the external force vector, it is necessary to integrate with respect to the volume all of the different terms that are present in the equation of motion which characterize the problem in question. The method typically used to integrate is the Gauss quadrature rule.

In particular in Ls-Dyna the integration is conducted with a low order Gauss method, that in the case of shell elements uses only one integration point, located at the centre of the element. This "under integrated" approximation is beneficial in terms of CPU time saved, but leads also to a phenomenon called Hourglass.

If we use an under integrated procedure we have some modes of deformation, known as Hourglass modes that show zero strain at the Gauss point, determining a zero internal energy. These zero-energy-modes have no stiffness and can propagate quickly giving a typical uneven ("zigzag") appearance to the mesh.

The presence of this phenomenon can cause numerical errors, a decrease of time-step and also an interruption of the calculations when the length of an element edge reaches a value equal to zero.

Some images are collected here to explain as an example the meaning of the hourglass modes.

Fig. 7.3: deformable and rigid modes for a membrane element, from Ref [10].
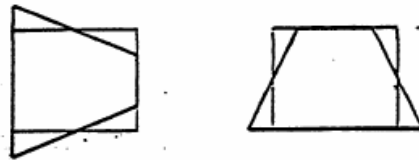
Fig. 7.4: hourglass modes for a membrane element, from Ref [10].

Hourglass modes are controlled by the addition of artificial forces that resist this mode of deformation.

In this thesis, in particular, it was decided not to use the default value which is present in Ls-Dyna, but it was decided to introduce an Hourglass control based on a stiffness coefficient, using the Ls-Dyna *CONTROL HOURGLASS card.

This coefficient was chosen to be equal to 0.05, a typical value set by many users in case of automotive crashworthiness, as indicated by the Ls-Dyna Users' Manual.[23]

```
*CONTROL_HOURGLASS
$$      IHQ        QH
         5       0.05
```

48

8 Properties of the isolated beam

IGES files containing the geometry, in terms of surfaces, of the actual circular beam and its two supports was provided by Nissan. Fig. 8.1, obtained from IGES files provided by Nissan, shows the complete side-impact-beam mounted within the front door of Nissan Pathfinder / Navara.
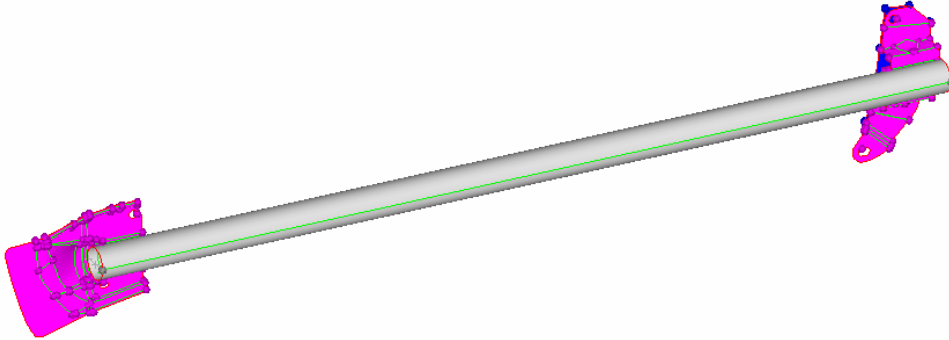
Fig. 8.1: complete beam from Nissan CAD file.

- Beam total length: 977mm.

8.1 Geometry of the pipe

- Pipe length: 878mm.
- Pipe external diameter: 31.8mm
- Pipe thickness: 2.6mm

8.2 Geometry of the small bracket

- Small bracket thickness: 1.6 mm
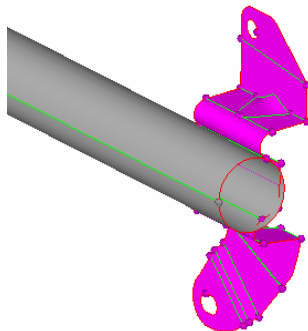
Fig. 8.2: small bracket from Nissan IGES files.
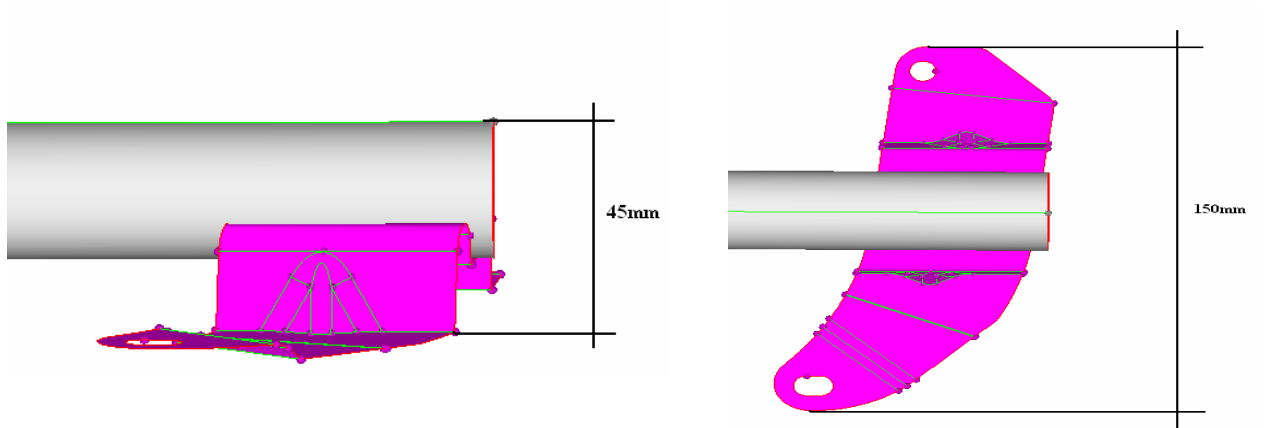
Fig. 8.3: useful geometrical references of the small bracket.

8.3 Geometry of the big bracket

- Big bracket thickness: 1.4 mm
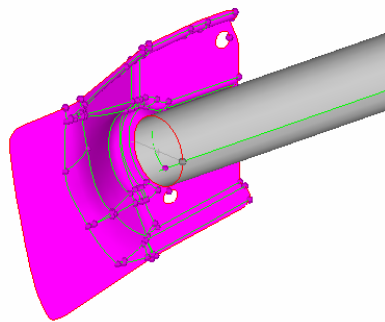
Fig. 8.4: big bracket from Nissan IGES files.
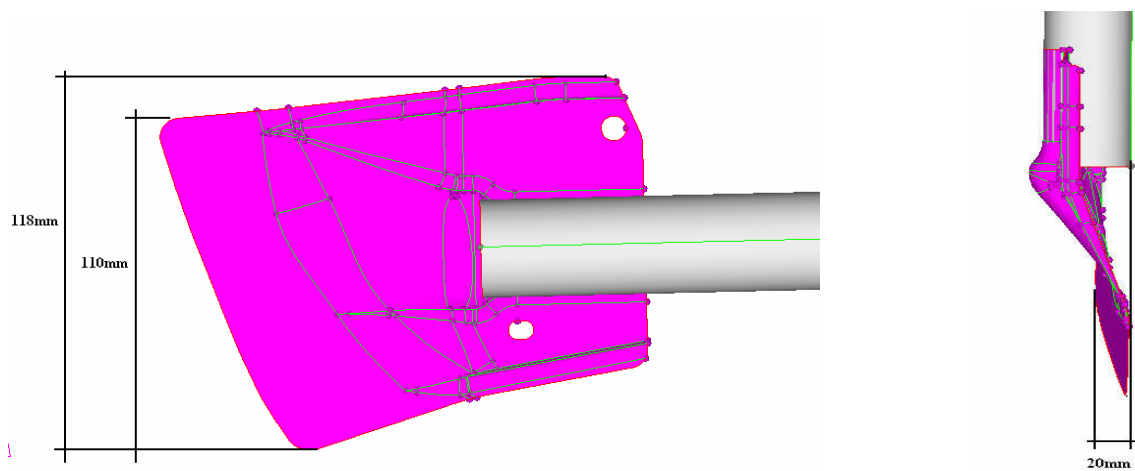
Fig. 8.5: useful geometrical references of the big bracket.

8.4 Welds between pipe and support brackets

- Weld length: 25mm (see Fig.8.6, Fig.8.7)

The following pictures (Fig. 8.6, Fig. 8.7) are taken from the isolated side-impact-beam provided by Nissan: in the left images it is possible to notice the presence of the inner skin of the door at which the beam brackets are attached.

Fig. 8.6: welds between pipe and small bracket

Fig. 8.7: welds between pipe and small bracket

8.5 Side-impact-beam within the door.

The following pictures show the position of the side-impact-beam within the front door of the Nissan Pathfinder / Navara.

Fig. 8.8 side-impact-beam within the front door of Nissan Pathfinder / Navara.

Fig. 8.9: big bracket (left) and small bracket (right) within the door.

8.5.1 Spot-welds between inner-skin of the door and side-impact-beam-brackets

The support brackets of the side-impact-beam are spot-welded to the inner-skin of the
door as described in Fig 8.11 for the big bracket and Fig. 8.12 for the small bracket.

Fig. 8.10: position of the spot-welds between the big bracket and the inner-skin of the door.

Fig. 8.11: position of spot-welds between the small bracket and the inner-skin of the door.

8.5.2 Absorbers between outer-skin of the door and side-impact-beam.

Between the outer-skin of the door and along the side-impact-beam it is possible to notice some absorbers, whose function is to avoid vibrations of the door skin.

The five black spots evident on the pipe in Fig.8.13 indicate that absorbers of the type shown in Fig.8.14 are collocated in those positions.

Fig. 8.12: position of the absorbers between the pipe of the side-impact-beam and the outer -skin of the door.
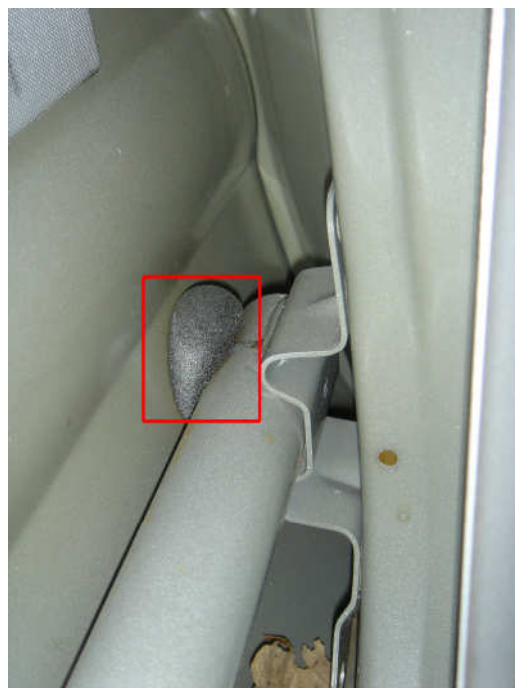
Fig. 8.13: type of absorber used by Nissan to prevent vibrations of the door skin.

8.6 Material data from Nissan

8.6.1 Pipe

The pipe of the side-impact-beam is made with an high strength steel, as indicated in Nissan's papers (see *Appendix E*).
Unfortunately, a characterisation curve is not available and the only available data are here summarized:

- $\sigma_{ultimate}$ = 1470 MPa (minimum value required by Nissan)
- E = 205000 MPa
- Density = 7.860E-9 tons/mm^3
- Elongation at break = 10,8% (minimum value required by Nissan)

There is a completely leak of information about the material behaviour at the yielding point; a research has been undertaken on Web-materials [35] to find a material with properties similar to the ones indicated in Nissan's papers (see *Appendix E*).
A material that has an elongation at break similar is the AISI 1080 tempered at 480°C:

- $\sigma_{ultimate}$ = 1280 MPa (AISI 1080)
- E = 205000 MPa
- E$_{tangential}$ = 3805 MPa
- Density = 7.860E-9 tons/mm^3
- Elongation at break = 11% (AISI 1080)

The Fig. 8.15 shows the bilinear-elastic-plastic approximation of the stress and strain curve for the AISI 1080.
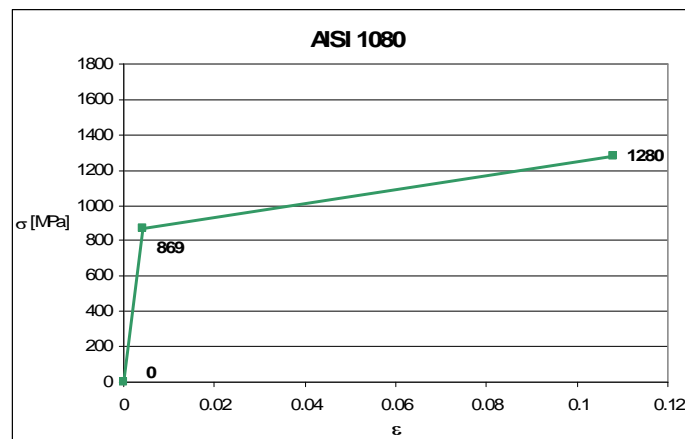
Fig. 8.14: bilinear approximation of the stress-strain curve of the AISI 1080.

As we can see the AISI 1080 is not able to guarantee, in term of ultimate stress, the minimum performances of the steel indicated by Nissan. At this stage we decided to use the bilinear stress and strain curve of Fig. 8.16 to represent the steel of the pipe:
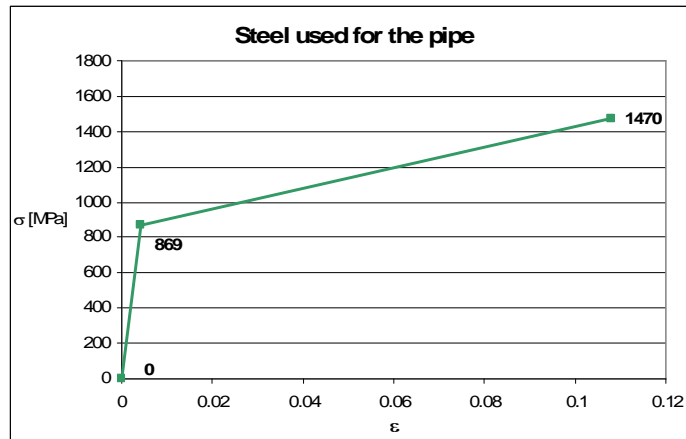
Fig. 8.15: bilinear approximation of the stress-strain curve of the material chosen to represent the steel of the pipe.

In the stress and strain curve of Fig.8.15 the values of $\sigma_{ultimate}$ and $\varepsilon_{ultimate}$ are the minimum prescribed by Nissan, while the values corresponding to the yield point are assumed equal to the ones found on Web-materials [35] for the AISI 1080.

Approximation of the high strength steel of the pipe of the side-impact-beam:

- $\sigma_{ultimate}$ = 1470 MPa (minimum value required by Nissan)
- E = 205000 MPa
- Density = 7.860E-9 tons/mm^3
- Elongation at break = 10,8% (minimum value required by Nissan)
- $\sigma_{yielding}$ = 869 MPa (as AISI 1080)
- E $_{tangential}$ = 5669 MPa.

8.6.2 Brackets

For the two brackets the data available on the papers(see *Appendix E*) given by Nissan are more precise:

- 360MPa $<$ $\sigma_{yielding}$ $<$ 430 MPa
- 600MPa $<$ $\sigma_{ultimate}$ $<$ 750MPa
- $\varepsilon_{ultimate}$ $\geq$ 21%

After a research on Web-Materials [35] it was found that a steel with characteristics between the range indicated by Nissan is the AISI 1060 annealed at 790°C:

- $\sigma_{yielding}$ = 370 MPa
- E $_{tangential}$ = 1169MPa.
- $\sigma_{ultimate}$ = 625 MPa
- E = 205000 MPa.
- Elongation at break = 22%.
- Density = 7.860E-9 tons/mm^3
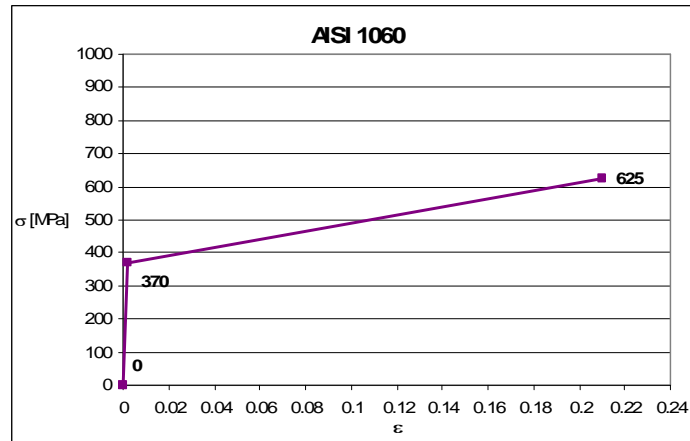
Fig. 8.16: bilinear elastic-plastic stress-strain curve for the AISI 1060.

Although the AISI 1060 respects the minimum characteristics required by Nissan, it has been decided at this stage to consider the maximum values of the stress range indicated at the beginning of the paragraph and also in *Appendix E*. This choice leads to the stress-strain curve of Fig. 8.17, that was used to represent the steel of the brackets.
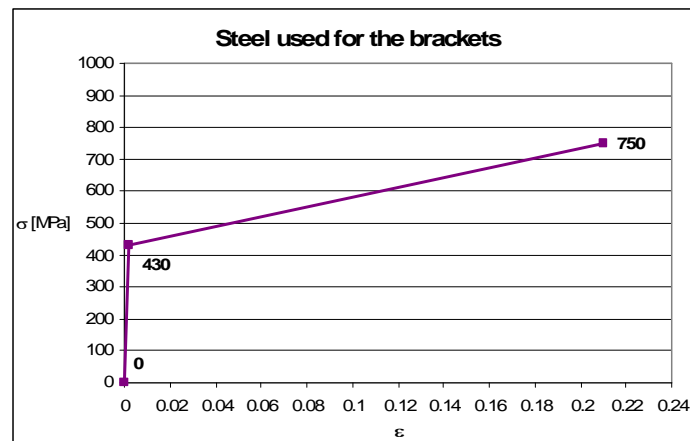
Fig. 8.17: bilinear elastic-plastic stress-strain curve for the material chosen to represent the steel of the brackets.

- $\sigma_{yielding}$ = 430 MPa
- $E_{tangential}$ = 1468MPa.
- $\sigma_{ultimate}$ = 750 MPa
- E = 205000 MPa.
- Elongation at break = 22%.
- Density = 7.860E-9 tons/mm^3

9 Bending Test on the isolated side-impact-beam.

This chapter is about test rigs and the procedure followed to realize a quasi-static laboratory bending test on the complete Nissan Navara / Pathfinder front door side-impact beam, and the test setup used for this.

Reasons:
- It was not possible to perform a dynamic test on the complete door provided by Nissan because the University has not the necessary resources.
- It was not possible to perform a quasi-static bending test on the complete door because of its excessive dimensions, incompatible with the University test machines available.
- The only choice was to extract the side-impact-beam from the door and test it in isolation.

Deliverables:
- Force – displacement graph of the isolate side-impact-beam.
- Mechanism of collapse of the isolated side-impact-beam.

These will be used as a benchmark against which finite element models can be checked.

9.1 Test Rigs

The test rigs used to support the beam during the test consist of one C-channel used as a base; two C-channels necessary to raise the beam brackets from the base; two plates 12mm thick, on which the beam brackets are welded along their edges; a cylinder with a diameter of 75mm to load the beam in the middle of the pipe.(see *Appendix C*)
The resulting structure was built in Cranfield University workshop under the supervision of Mr A. Hutchings is shown in Figs 9.1, 9.2, 9.3.

Fig. 9.1: complete test rig
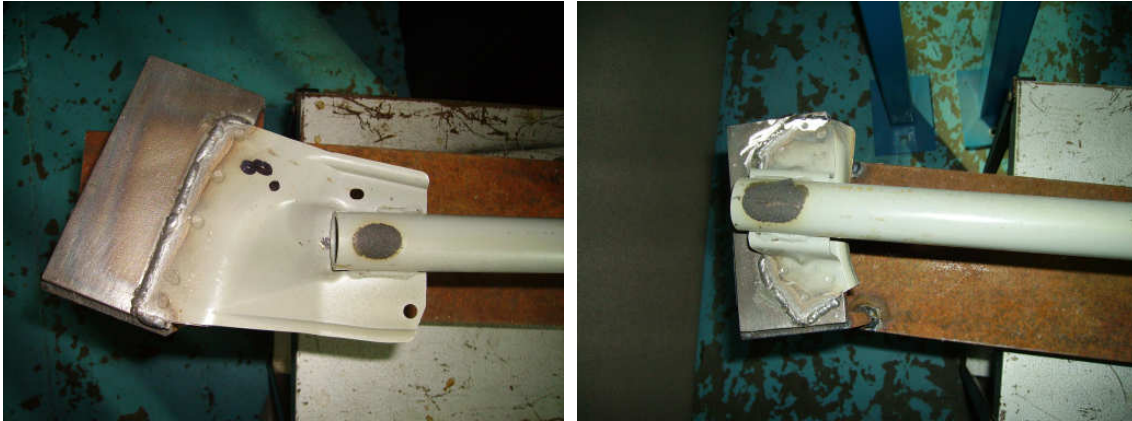
Fig. 9.2: big bracket (left) and small bracket (right) welded along their edges on two plates 12mm thick.
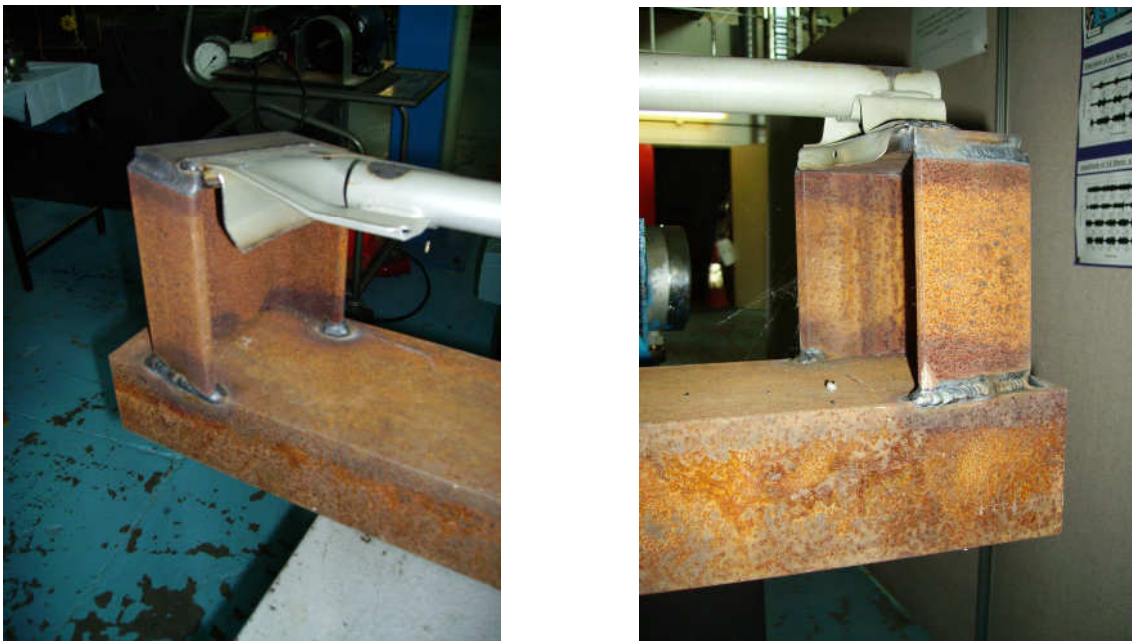
Fig. 9.3: big bracket (left) and small bracket (right) s sustained by two C-channels.

9.1.1 Loading and boundary conditions.

a. As a careful reader can notice, between the side-impact-beam brackets and the two 12mm thick plates on the C-channels, the skin of the inner-door at which the beam-ends are spot-welded is still present.

   The decision of keeping this thin sheet of metal was made to preserve the real welds existing on the car and it was possible because Nissan supplied a complete door.

   It was believed that this arrangement would give support moments at the ends of the beam which were similar to those in the real door.

b. Longitudinal support

   The ends of the sheet metal door beam brackets were welded to the 12mm plates on the support rig. This support was much stronger and more rigid than that in the vehicle door. The catenary effect can be expected to be more pronounced

than in the real vehicle. This effect is somewhat mitigated by the inclusion of the sheet metal brackets.

c. The diameter of the loading cylinder was smaller than that specified in the FMVSS214 test. This was due to non availability of a 12inches (inches are specified in the US regulation) diameter cylinder. Since the door tube is thick walled, this was not expected to have a major influence.

9.2 Test Equipment

The equipment used to perform the bending test is constituted by an Instron 8032 servo-hydraulic tensile\compressive test machine, with a capacity of ±100kN, fitted with an Instron 8500 digital controller.

Fig. 9.4: servo-hydraulic test machine.

The support rig with attached door beam was clamped onto the lower platen of the test machine . It was positioned so that the load cylinder (mounted in the upper taws of the machine) would load the door beam midway between the supports.

9.3 Test procedure

The load cylinder was lowered till it just touched the centre of the door beam.
Then, a constant velocity of 3mm/s was applied at the middle point of the tubular part of the door beam, using a steel cylinder with a diameter of 75mm, as showed by the following pictures of Fig. 9.5.
The test was stopped when the applied displacement was 134mm, to avoid the entire collapse of the side-impact-beam, due to a material failure in the small bracket zone.

Fig. 9.5: bending test procedure
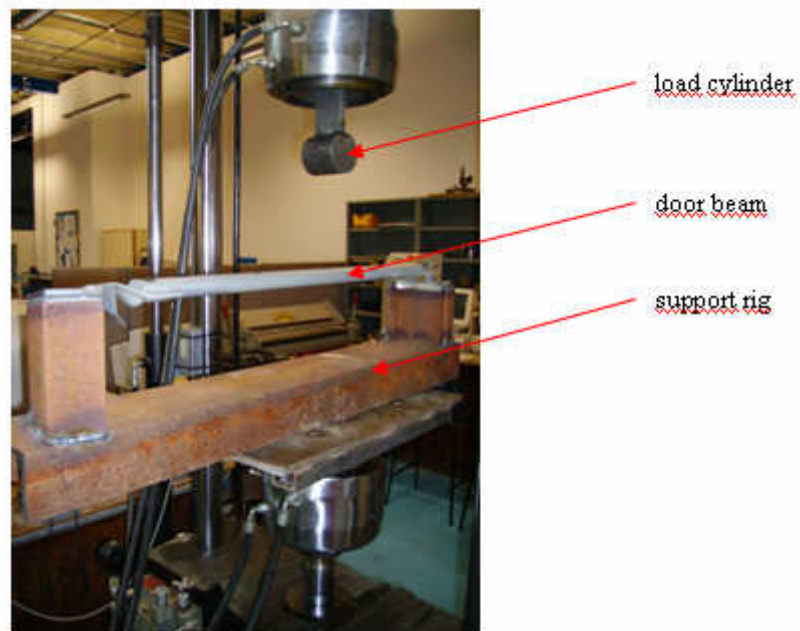
Fig. 9.6: Test setup before lowering the load cylinder

The data relative to Force and displacement, objective of the test, were recorded with a frequency of 10Hz, till the maximum applicable displacement, using the sensors in the cross-head of the test machine.

9.4 Test results

The entire test was performed with the Cranfield University facilities under the supervision of Barry Walker at the beginning of August 2006.

9.4.1 Force vs Deflection

The data relative to Force and displacement collected during the simulation were analysed in Excel and are plotted here:
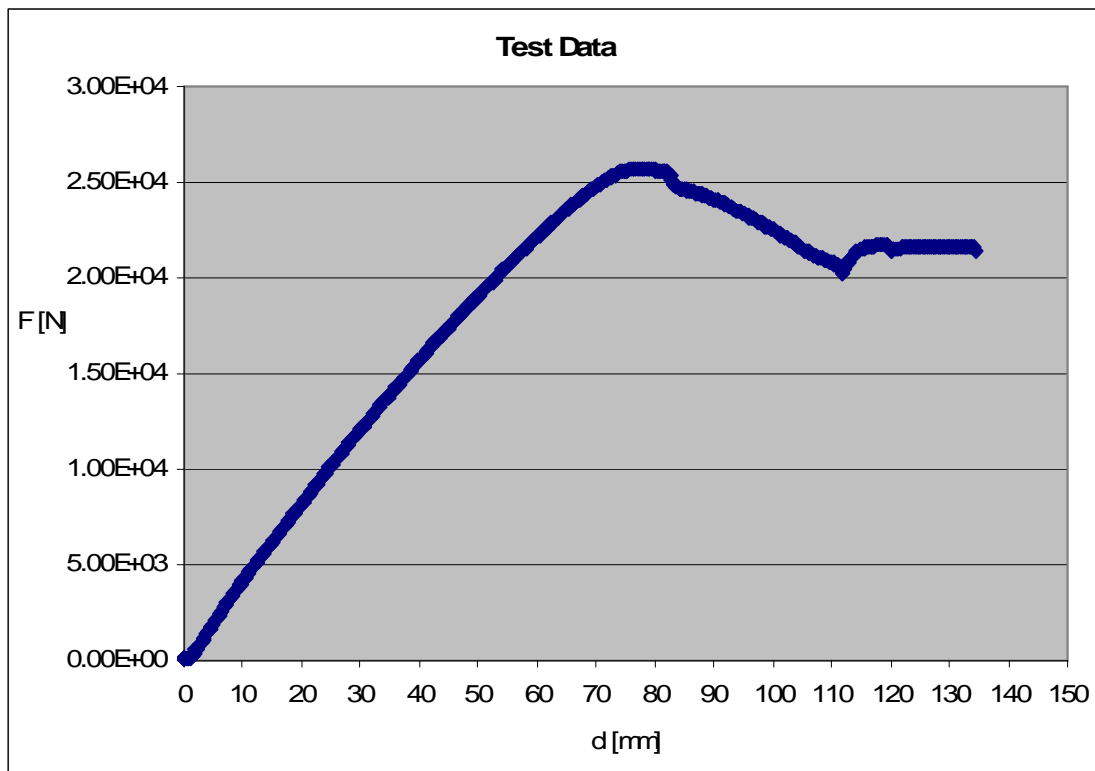
Fig. 9.7: Force-displacement curve obtained during the bending test.

9.5 Deformations and collapse mode

Main phases of the collapse sequence in the laboratory test:
1. Initial deformation of the pipe
2. Deformation of the small-bracket.
3. Large rotation of the small-bracket, Fig.9.8
4. Tearing of material at the base of the small-bracket, Fig.9.10

Fig. 9.8: beam under maximum load (left) and detail of the small bracket (right) when the test was stopped.

Fig. 9.9: details of the small bracket at the beginning of the bending test

Fig. 9.10: details of the small bracket at the end of the bending test

The last interesting element that is worthwhile to mention is the elastic recovery of almost 29mm of the beam.

This phenomenon is also visible in the pictures of Fig.9.11, the first under load at the maximum displacement of 134mm and the second one for the side-impact-beam unloaded.
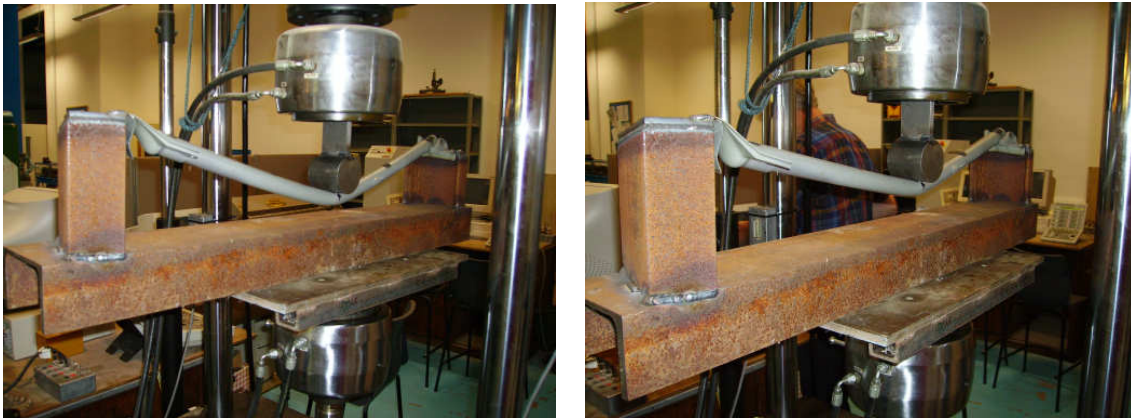
Fig. 9.11: maximum deflection under load (left); deflection for the beam unloaded (right).

10 Description of computer models.

For the reasons explained at the beginning of *chapter 13*, *Bending Test on the isolated side-impact-beam,* the choice was to perform a bending test on the isolated beam, trying to reproduce it with computer simulations. The computer results could then be checked against the experimental results.

10.1 Type of simulation

Simulations of a quasi–static bending test on the isolated side-impact-beam of Nissan Pathfinder / Navara. The intention was to make the simulation model as similar as possible to the laboratory test.

Fig.10.1 bending test procedure

- Simulation procedure: constant velocity applied to a rigid cylinder, to load the side-impact beam in the middle of the beam pipe as shown in Fig.10.1 and Fig.10.2.
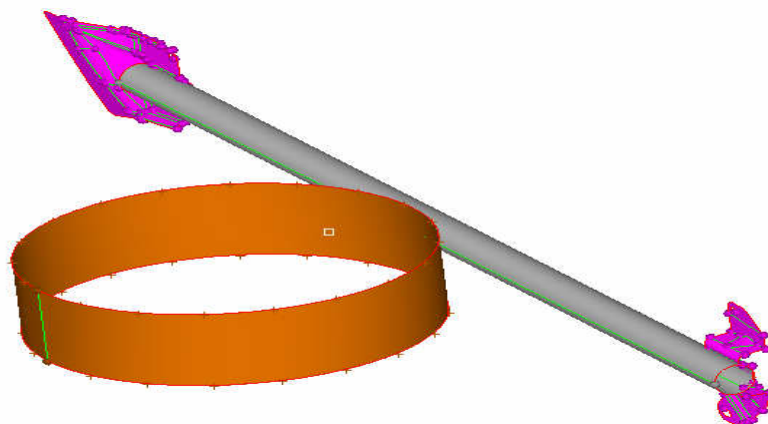
Fig.10.2 simulation of a bending test.

- Velocity applied: 500mm/s.
    Reasons:
    - It is not possible to perform the simulations at the same velocity of the test, because of the excessive CPU time needed to complete them.
    - It is necessary to apply a velocity that keeps the simulation in the field of the quasi-static simulations, where inertial effects can be neglected.

- Dimensions of the rigid cylinder: 300mm diameter.
    Reasons:
    - The simulations were performed before the test, which was conducted in August 2006; for the test the University did not have any resources to machine a steel cylinder of 300mm diameter. Therefore a smaller cylinder was used in the experiments.
    - In the simulations it was decided to use an impactor of the same diameter of the one prescribed for the quasi-static American FMVSS 214: 300mm (see *chapter 3, US Side impact*).

10.2 Type of constraints

As stated in the Ref [33], the defining of the restraints conditions is one of the most difficult and complex during a modelling process. In the following graph it is shown a qualitative assessment of the relative levels of difficulty and uncertainties in defining the geometry, material, loads and restraints.
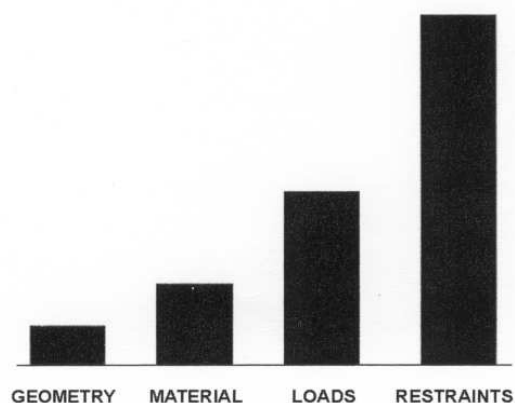
Fig.10.3: qualitative assessment of relative levels of difficulty and uncertainties in defining the geometry, materials, loads and restraints. Ref [33]

In the bending test the sheet metal beam-brackets are welded along their edges on two 12mm thick plates, as shown by the pictures in Fig.10.4

Fig.10.4: 12mm plates at which are welded the side-impact-beam brackets.

These 12mm thick plates are fixed through welds at the test rigs, as we can see in Fig.10.4. To reproduce the same situation described for the test some important choices have been done in the computer models, summarised below.

- **Computer models assumptions**:

  - The 12mm thick plates are considered as two rigid plates, see Fig.10.5

  - The side-impact-beam is attached to these rigid plates, see Fig 10.5

  - The welds between the pipe and the brackets of the side-impact-beam, described in *paragraph 8.4,* are considered as perfect, so any failure parameter have not been set.

  - The welds (existing) between the brackets and the 12mm thick plates (rigid plates in the models) are considered as perfect, so any failure parameter has not been set and a failure is not allowed.

- The constraints are applied to the rigid plates.
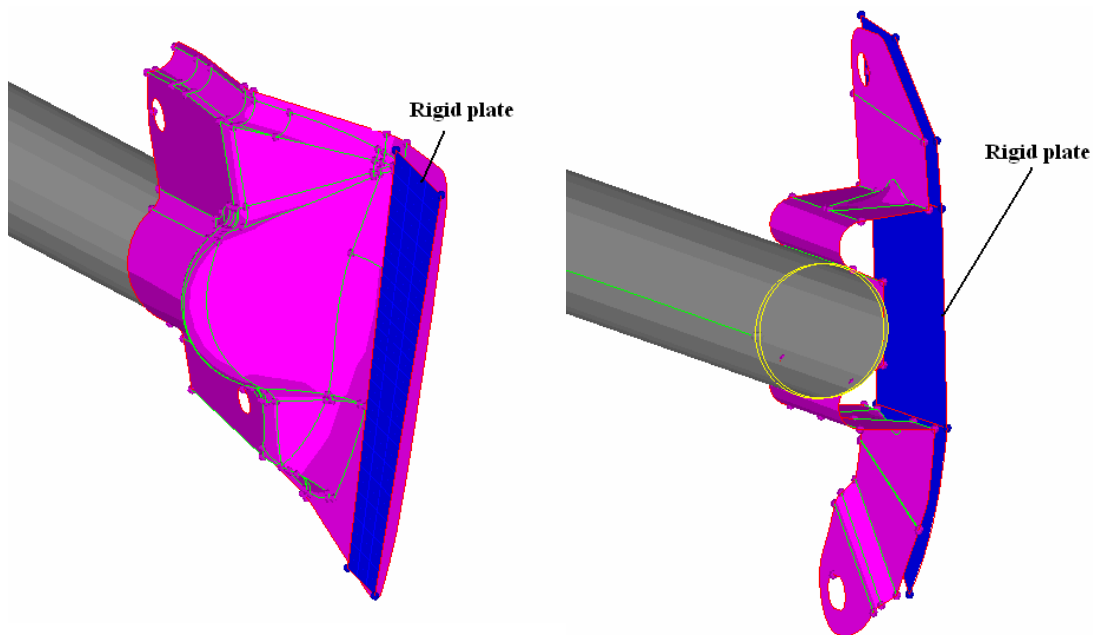
Fig.10.5: rigid plates in the computer models to represent the 12mm thick plates of the bending-test.

As stated above, in the computer models the constraints are applied to the rigid-plates; in particular two different situations have been considered:

- **CaseF**: Rotations and translations of the rigid plates not allowed
   Reasons:
   - In the bending test performed with the university machines the test rigs were designed prevent any rotation or translation of the 12mm thick plates.

   - The main objective is to reproduce the same conditions existing during the bending laboratory test on the isolated side-impact-beam.

- **CaseB1-CaseB2**: Rotations allowed but translations not allowed of the rigid plates.
   Reasons:
   - To understand how the type of constraint affects the models.

   - This second type of constraints seems much more similar to what happens on the car, where rotations are likely allowed, see *chapter 4*, *Collapse mechanism of a simple-model of a car made with beam-elements*. In fact, if the beam is laterally loaded, what happens is a pivot of the whole beam, brackets included, around the A and B pillars of the car.

♦ Two different pivot lines considered on the rigid-plate on which the small bracket is attached
  • **CaseB1,** see left image of Fig.10.6
  • **CaseB2,** see right image of Fig.10.6
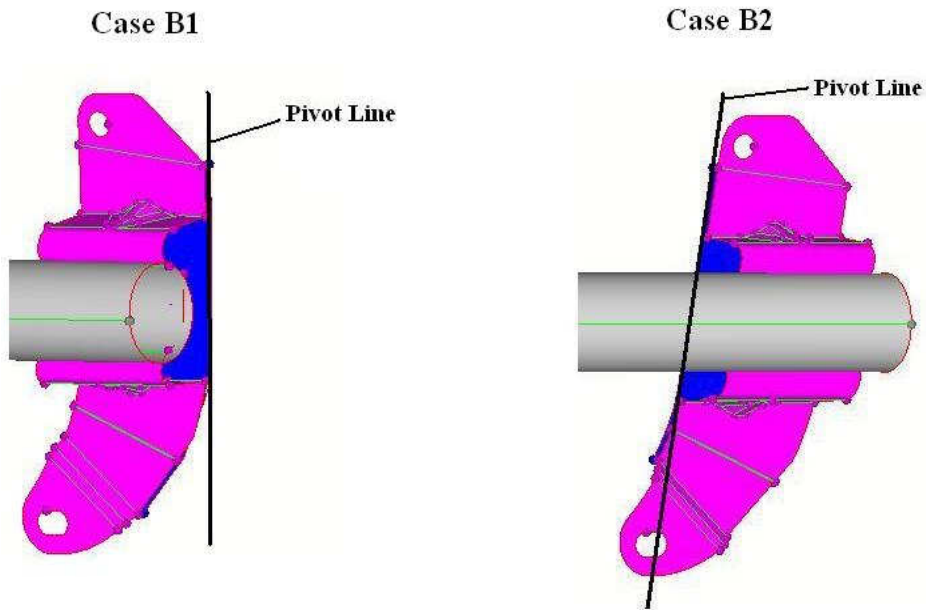
Fig.10.6 different pivot lines considered for the rotation of the rigid-plate at which the small bracket is attached: Case B1 on the left; Case B2 on the right

Reasons for two possible pivot lines:
  ▪ From the picture taken of the side-impact-beam within the door it is difficult to estimate the possible pivot line of the small-bracket, see Fig.10.7

Fig.10.7: detail of the small bracket within the door Nissan Navara /Pathfinder

♦ In **CaseB1** and **CaseB2** the pivot line on the rigid-plate at which the big-bracket is attached has never been changed. So **CaseB1** and **CaseB2** have in common the same position of the pivot line shown in Fig.10.8.

Same pivot line on the rigid-plate of the big-bracket for CaseB1 and Case B2
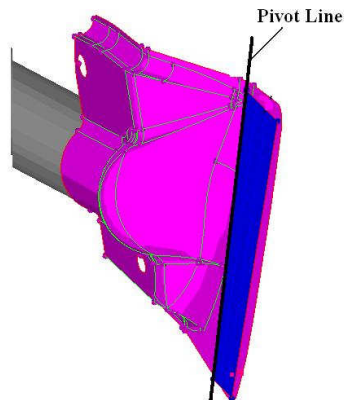
Fig.10.8: the pivot line it has never been changed on the rigid-plate at which the big-bracket is attached.

Reasons for only one possible pivot lines:

- From the picture taken of the side-impact-beam within the door, Fig.10.9, it is possible to notice that part of the big-bracket of the side-impact-beam is embedded between the inner and the outer skin of the door. This fact reinforces the big-support in that zone leading from the author's point of view at only one possible pivot line .

Fig.10.9 particular of the big-bracket of the side-impact-beam within the door of Nissan Pathfinder / Navara.

	Rotation of rigid-plates	Translation of rigid-plates
CaseB1	Yes*	No
CaseB2	Yes*	No
CaseF	No	No
* different pivot line considered for the rigid-plate of the small-bracket, see Fig.14.6		

Tab. 10.1 summarizing table for type of constraints used.

10.3 Type of mesh

In this thesis we considered two different modelling for the small and big brackets of the side-impact-beam, see Fig.10.10:

- **Brackets rigid**
  Reasons:
  - Initial understanding of the side-impact-beam behaviour

  - As explained in *paragraph 9.1*, *Test rigs,* the brackets are welded on two 12mm thick plates. At the beginning of the simulation campaign, without any data from the bending test (performed later, in August 2006) it was considered the possibility that the plates at which the side-impact-beam brackets are welded could increase the stiffness of the brackets, leading me to consider them as rigid.

  - to have an initial indication of what mesh dimensions could be reasonably exploited for the development of this project

- **Brackets deformable**.

Big-bracket of the side-impact-beam
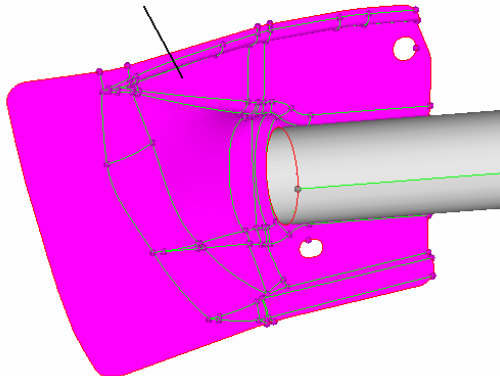
Small-bracket of the side-impact-beam
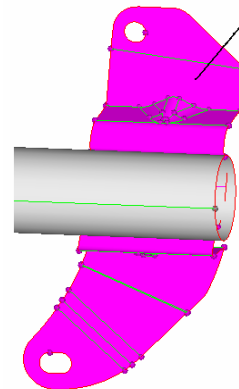
Fig.10.10: brackets of the side-impact-beam.

For each of these two families of simulations a sensitivity analysis was performed varying the mesh dimensions of the pipe:

- Brackets rigid
  - ♦ Mesh of the pipe considered:
    - 2mm
    - 3mm
    - 5mm
    - 8mm
    - 12mm double adaptation (see *paragraph 10.3 part1*)
    - 12mm triple adaptation. (see *paragraph 10.3 part1*)

  - ♦ Mesh for the side-impact-beam brackets:
    - The brackets are rigid bodies.

- Brackets deformable:
  - ♦ Mesh of the pipe considered:
    - 2mm
    - 3mm
    - 5mm
  - ♦ Mesh for the side-impact-beam brackets:
    - 5mm
    - 10mm

Mesh size of the brackets	Mesh size of the pipe
Rigid	2mm
	3mm
	5mm
	8mm
	12mm double adaptation
	12mm triple adaptation
5mm	2mm
	3mm
	5mm
10mm	2mm
	3mm
	5mm

Tab. 10.2 summarizing table for different meshes considered.

10.3.1 Brief explanation of the Adaptive mesh.

In this work it was decided to try adaptive meshing for some simulations.
There are two types of adaptive mesh: the h type, in which the number of elements is increased and the polynomial order of the elemental shape functions doesn't change; the q type, where the number of elements is the same, but the polynomials order is increased. Ls-Dyna includes an h-adaptive mesh for the shell elements.
In the h-adaptive process, the elements are subdivided into smaller elements where more accuracy is needed. The elements involved in what is called a fission process are subdivided into elements with side h/2, where h is the characteristic size of the original elements.[23] The fission process can consist of several levels of adaptation, as shown in the following picture.
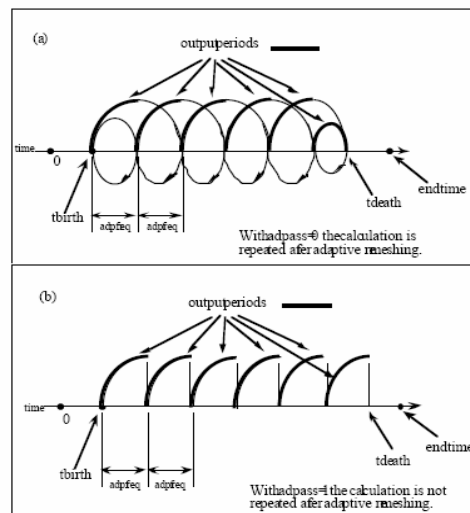
Fig. 10.11: Adaptivity mesh procedure, Ref [23].

The adaptive mesh can be used in Ls-Dyna setting the card *CONTROL ADAPTIVE, where the main parameters used in this work were:

ADPFREQ: time interval between adaptive refinements
ADPTOL: adaptive tolerance error in degrees; if this value is reached the element is split into descendant elements.
ADPOPT: parameter to set different adaptive options; in this thesis the adaptive option is given by the total angle change in degrees relative to the surrounding element for each element to be refined, option 2.
MAXLVL: is the parameter to set the level of refinement: values of 1, 2, 3, 4 allow a maximum of 1, 4, 16, 64 elements, respectively, to be created for each original element.
TBIRTH is the time at which starts the adaptive process
TDEATH is the time at which the adaptive mesh ends.

The values set in the card above for this thesis were:
*CONTROL ADAPTIVE

ADPFREQ, ADPTOL, ADPOPT, MAXLVL, TBIRTH, TDEATH
1.0E-03, 5(2.5), 2(3), 2, 0.0, 0.6

The values in brackets indicate that two different options were evaluated:
for ADPTOL it was established to use an adaptation of the elements every 5 degrees with a double fission of the element (MAXLVL equal to 2) while an adaptation every 2.5 degrees was coupled with a triple fission (MAXLVL equal to 3).
To set all these parameters, in a reasonable and quick way, it was very useful to read the work done by Miranda Carbajal about the use of an adaptive mesh in an automotive crashworthiness problem.[20]
Finally it is worthwhile to underline that the choice to start with a 12mm mesh is based on the fact that this dimension is often used in the automotive crashworthiness field for full scale simulations, as stated by Mahadevan, Liang and Fekete.[22].

10.4 Methodology of evaluation

The simulations performed are evaluated in terms of:

- Force –displacement graph
  - Comparison with other simulation results.
  - Comparison with test results

- Hourglass energy (see *chapter7. 9, Hourglass*)

- The Energy absorbed has not been considered as a parameter of evaluation because the beam is only a part of the complex structure of the car. In a side-impact-test the absorbed Energy refers to the complete car-structure and not only to one of its component parts, because all the car-body is involved in the collapse mechanism, see *chapter 4.*

- The Energy absorbed has been used only in the case of some mesh-sensitivity analysis to estimate the differences in the Force-displacement graph between the meshes used.

- Visual outputs from Ls-Post, see *chapter 6, Software.*

10.5 Summary of type of constraints and meshes considered

	Rotation of rigid-plates	Translation of rigid-plates
CaseB1	Yes*	No
CaseB2	Yes*	No
CaseF	No	No
* different pivot line considered for the rigid-plate of the small-bracket, see Fig.14.6		

Tab.10.3 summarising table for different type of constraints considered

Mesh size of the brackets	Mesh size of the pipe	Type of Constraint
Rigid	2mm	CaseB1
	3mm	CaseB1
	5mm	CaseB1
	8mm	CaseB1
	12mm double adaptation	CaseB1
	12mm triple adaptation	CaseB1
5mm	2mm	
	3mm	
	5mm	
5mm	2mm	
	3mm	
	5mm	
10mm	2mm	
	3mm	
	5mm	

Tab. 10.4 summarizing tables for types of constraint

11 Effects of modelling method on the FE results for isolated beam

Modelling is an iterative process that involves a lot of parameters and inputs; in this thesis the work done is complicated by the fact that the simulations have been performed before having data from the bending test on the isolated side-impact-beam (performed in August 2006). These circumstances have led me to build many different models, spending months and obtaining several results.   In this chapter only the most significant results achieved are shown.

11.1 Models with rigid brackets

The Reasons that led to consider as first instance the side-impact-beam brackets as rigid are explained in *paragraph 10.3, Type of mesh.*
The aim of the following *sub-paragraphs of section 11.1* is to show some sensitivity-analysis results for the models in which the side-impact-beam brackets are considered as rigid. As explained previously, the results are compared in terms of Force – displacement graphs, graphical outputs from Ls-Post processor and Hourglass Energy, see *chapter 7.9, Hourglass.*

> ➢ **Summary of type of constraints, meshes and type of shell-elements considered**

	Rotation of rigid-plates	Translation of rigid-plates
CaseB1	Yes*	No
CaseB2	Yes*	No
CaseF	No	No
* different pivot line considered for the rigid-plate of the small-bracket, see *chapter 14*		

Tab.11.1: summary of types of constraints.

Brackets	Mesh of the pipe	Constraint	Shell-element*	Simulation name
Rigid	2mm	CaseB1	Belytschko-Tsay	2mmB1
	3mm	CaseB1	Belytschko-Tsay	3mmB1
	5mm	CaseB1	Belytschko-Tsay	5mmB1
	5mm	CaseB1	Belytschko-Wong-Chang	5mmB1-Bwc
	5mm	CaseB1	Fully Integrated Belytschko-Tsay	5mmB1-Fully
	8mm	CaseB1	Belytschko-Tsay	8mmB1
	12mm double adaptation	CaseB1	Belytschko-Tsay	12mmD-B1
	12mm triple adaptation	CaseB1	Belytschko-Tsay	12mmT-B1
*see *chapter 7.8, Properties* and Ref. [23]				

Tab.11.2: summary of the simulations performed in this section

11.1.1 Mesh effects on the models

To understand the type of constraints and meshes used in these models and to understand the acronyms in the legend of the graphs the reader has to refer to the Table 11.2, *Summary of type of constraints, meshes and type of shell-elements considered, page. 69* .
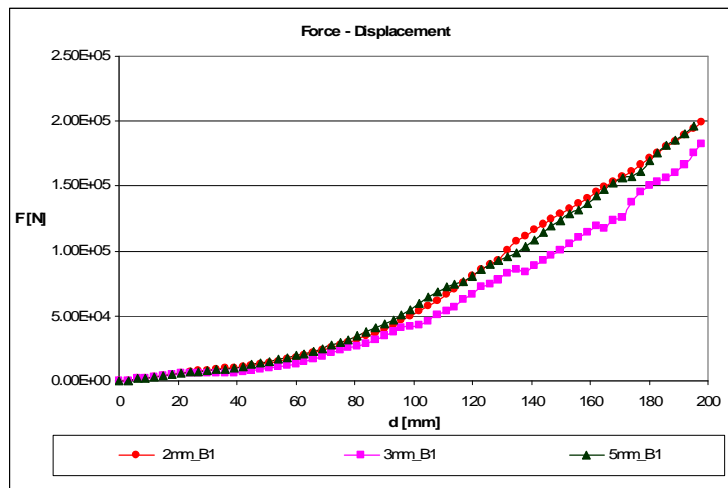
Fig. 11.1: comparison between meshes of 3mm, 2mm and 5mm in the case of rigid-brackets.
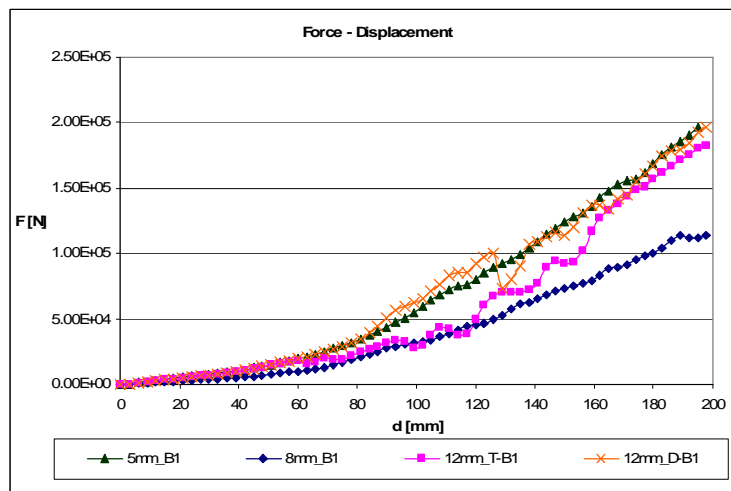
Fig. 11.2: comparison between meshes of 12mm, 8mm and 5mm in the case of rigid-brackets.

Evident aspects of the results achieved:
- The 2mm and 5mm mesh show Force-displacement graphs very similar, see Fig.11.1.

- The other analysed meshes, 12mm, 8mm and 3mm show a trend that is different respect with the 2mm and 5mm meshes.
- The 3mm is the mesh, of the ones considered, that is able to be much closer to the 2mm and 5mm in terms of Force-displacement graph.

Concerning modelling aspects on the results achieved:

- **Inaccurate representation of the initial geometry:**
    - The coarser meshes, 12mm and 8mm, share in common an inaccurate representation of the initial geometry: the pipe cross section, in both cases has not a circular shape but an octagonal one.
    - The inaccuracy in the correct shape representation adversely affects the contact detection, which needs, as explained in Ref [23], an accurate modelling of the contact zones, especially for the type of contact used in this work, *AUTOMATIC_SURFACE_TO_SURFACE.
    - In the central zone of the side-impact-beam when the octagonal pipe starts to be squeezed, there are some faces in contact with the rigid cylinder used to load the beam and some other, really close to the previous ones, which don't touch the impactor (rigid cylinder).
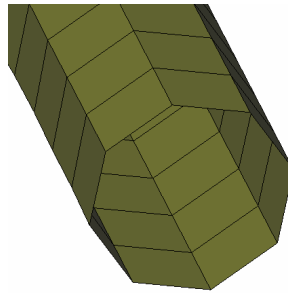
Fig. 11.3 octagonal cross section of the pipe in the case of 12mm and 8mm mesh.

- **It is incorrect to use adaptive meshes only in the central part of the pipe:**
    - From Fig.11.4 it is evident that the model is affected by the sudden changing in the mesh density along the pipe: we pass from a finer mesh in the central part to a coarser mesh of 12mm at the ends of the pipe.
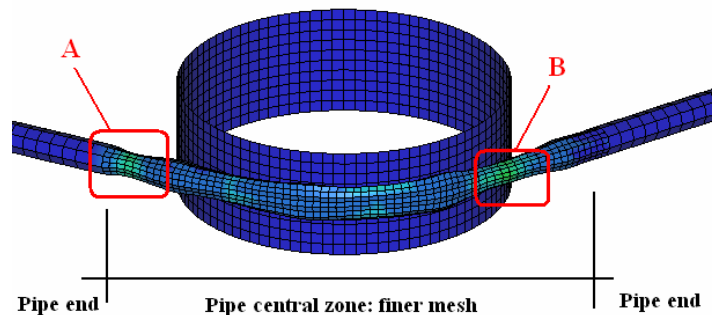
Fig. 11.4 sudden mesh changing along the side-impact-beam pipe

- Fig.11.4 shows that the pipe narrows in the zones named as A and B in Fig.11.4. This not physical behaviour seems to be related to the translation from a softer zone in the middle, where there is a finer mesh, to stiffer zones at the pipe ends, where it is noticeable a coarser mesh.
- **Ratio between Hourglass and Internal Energy:**
  - The Hourglass can be considered as a parameter to have a numerical verification of the models, as explained by Stewart, Gullerud and Heinstein on the paper "Solution verification for explicit transient dynamics problems in the presence of hourglass and contact forces" [37].
  - For the 2mm and 5mm meshes the Hourglass ratio at the simulation end-time (where Force reached its maximum) is not different to what happens for the other meshes considered.

Simulation Name	Hourglass / Internal Energy
2mm_B1	0.7%
3mm_B1	8%
5mm_B1	1%
12mm_D-B1	6.7%
12mm_T-B1	5.7%

Tab.11.3: ratio between Hourglass and Internal energy for different meshes considered.

11.1. 2 Effects of considering different formulations for the shell-elements.

To understand the type of constraints and meshes used in these models and to understand the acronyms in the legend of the graphs the reader has to refer to the Table 11.2, *Summary of type of constraints, meshes and type of shell-elements considered, page. 69* .
The analysis conducted here is in relation to a different formulation chosen for the shell-elements of the mesh.
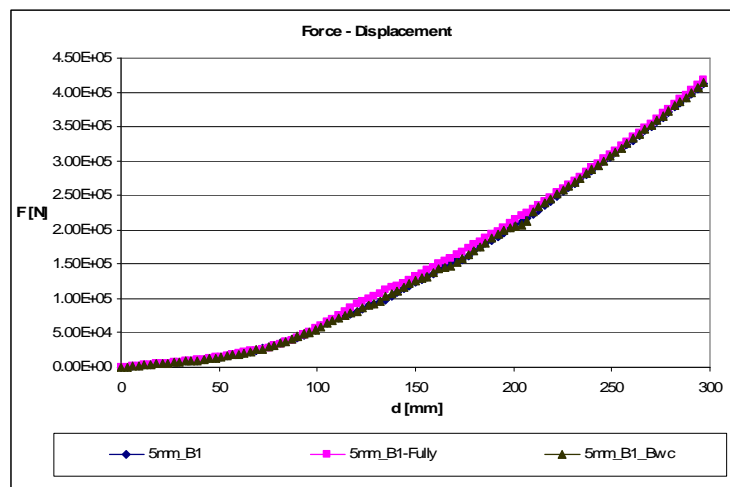
Fig.11.5: sensitivity analysis on formulation of shell-elements used.

From Fig.11.5 it is evident that the type of shell-elements used seems not to affect the Force-displacement graphs obtained.

11.1. 3 CPU-time needed to complete the simulations with rigid brackets

Ls-Dyna is an explicit code whose stability is conditioned by the time-step, strictly dependent on the mesh dimensions, see *paragraph 7.5, Time step.*
To better understand the relation between time and mesh dimension we have compared different CPU-time required in relation to the mesh density and to the formulation chosen for the shell-elements of the model. The simulations have been run using the Linux grid in Cranfield University Computer Centre.

2mm_B1	181097
3mm_B1	30551
5mm_B1	7779
8mm_B1	2279
12mm_D-B1	5069
12mm_T-B1	38305
5mm_B1_Fully	18595
5mm_B1_Bwc	10606
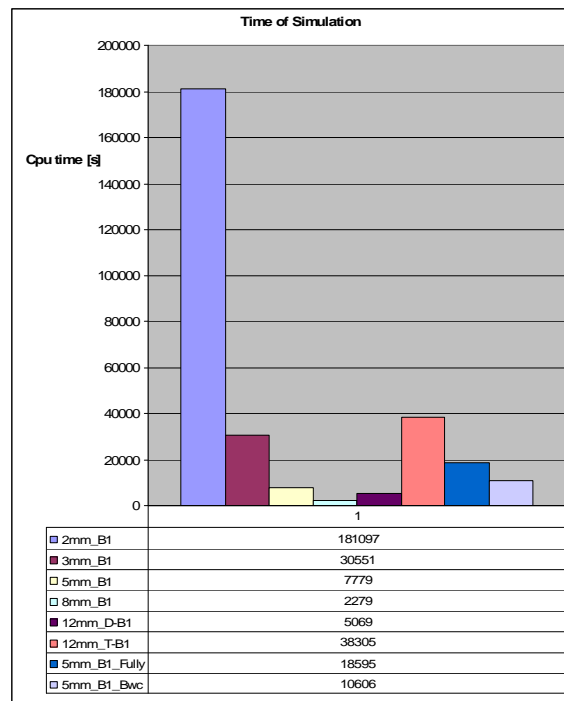
Fig. 11.6: CPU-time needed to complete the simulation.

As it is visible from Fig.11.6, the finer is the mesh the higher is the CPU time, needed to complete the simulation.

11.1.4 Final conclusions for simulations with rigid-brackets.

- For the non physical behaviour and for the problems explained in the *paragraph 11.1.1* it has been decided not to use adaptive meshes in the development of the computer simulations performed in this thesis.
- In the models developed in the following part of the thesis it has been decided to use only the under-integrated Belytschko-Tsay shell-element for its lower computational-time compared with the Belytschko-Wong-Chang formulation and with the Fully integrated Belytschko-Lin-Tsay shell-element.
- Ls-Dyna does not have a curve shell-element, but only planar shell-elements (4-nodes); that's why, to obtain a correct representation of the pipe cross section in the

development of the models, see Fig.11.7, we decided to use only the 5mm mesh, the 3mm mesh and the 2mm mesh to model the pipe.
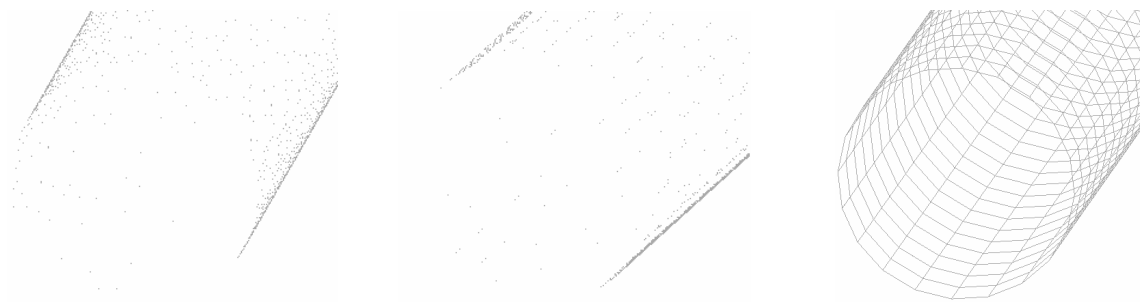
Fig.11.7 different meshes for the pipe: 2mm on the left, 3mm centre, 5mm on the right.

11.2 Models with deformable brackets.

The aim of the following *sub-paragraphs of section 11.2* is to show some sensitivity-analysis results for the models in which the side-impact-beam brackets are considered as deformable to check the material properties used for the brackets. The results are compared in terms of Force – displacement graphs, graphical outputs from Ls-Post processor and Hourglass Energy, see *chapter 7.9, Hourglass.*

➢ **Summary of type of constraints, meshes and type of shell-elements considered**

	Rotation of rigid-plates	**Translation of rigid-plates**
CaseB1	Yes*	No
CaseB2	Yes*	No
CaseF	No	No
* different pivot line considered for the rigid-plate of the small-bracket, see *chapter 10*		

Tab.11.4: summary of types of constraints.

Mesh of the brackets	**Mesh of the pipe**	**Constraint**	**Shell-element***	**Simulation name**
10mm	2mm	CaseB1	Belytschko-Tsay	C2mmB1
	3mm	CaseB1	Belytschko-Tsay	C3mmB1
	5mm	CaseB1	Belytschko-Tsay	C5mmB1
5mm	2mm	CaseB1	Belytschko-Tsay	R2mmB1
	3mm	CaseB1	Belytschko-Tsay	R3mmB1
	5mm	CaseB1	Belytschko-Tsay	R5mmB1
	5mm	CaseB2	Belytschko-Tsay	R5mmB2
	5mm	CaseF	Belytschko-Tsay	R5mmF
*see *chapter 7.8, Properties* and Ref. [23]				

Tab.11.5: summary of the simulations performed in this section

11.2.1 Mesh effects on the models

In Fig.11.8 three different meshes for the pipe are compared, using the same 10mm mesh for the brackets.

Fig.11.9 is once again a mesh sensitivity analysis between three different meshes for the pipe, keeping a mesh of 5mm for the brackets, which is a finer mesh compared to the case described by Fig.11.8.

To understand the type of constraints and meshes used in these models and to understand the acronyms in the legend of the graphs the reader has to refer to the Table 11.5, *Summary of type of constraints, meshes and type of shell-elements considered, page. 74 .*
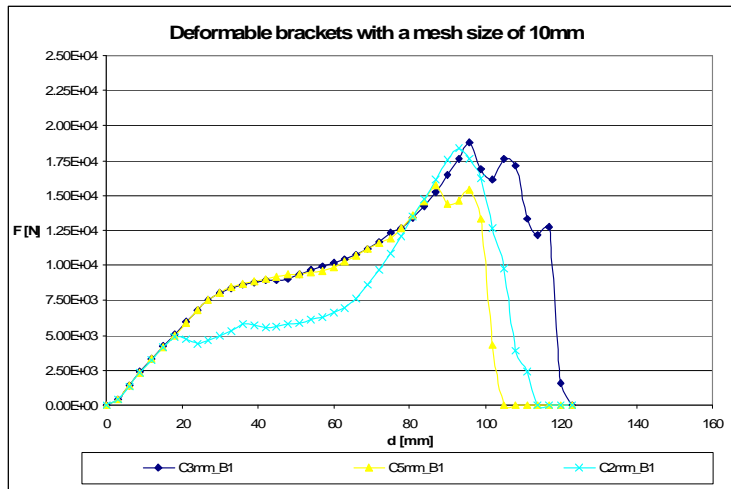
Fig.11.8 sensitivity analysis for the mesh of the pipe considering deformable brackets with a mesh of 10mm.

♦ Comparison of the Force-displacement graphs of Fig. 11.8 in terms of Energy absorbed

Deformable brackets with a mesh size of 10mm		
	Total Energy Absorbed [mJ]	**Comparison with C5mm_B1 %**
C2mm_B1	877370	7% less than C5mm_B1- Energy
C3mm_B1	1228059	15% more than C5mm_B1 - Energy
C5mm_B1	931098	

Tab.11.6: Force-displacement graphs compared in terms of Energy-absorbed.
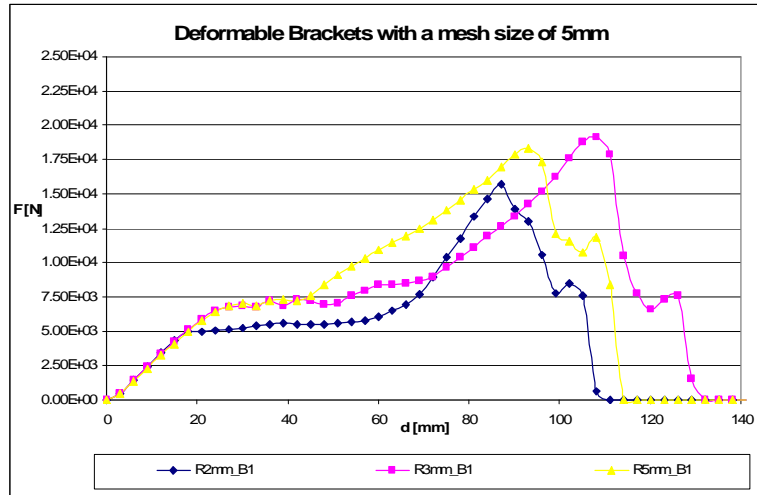
Fig.11.9 sensitivity analysis for the mesh of the pipe considering deformable brackets with a mesh of 5mm.

♦ Comparison of the Force-displacement graphs of Fig. 11.9 in terms of Energy absorbed

Deformable brackets with a mesh size of 5mm

	Total Energy Absorbed [mJ]	Comparison with R5mm_B1 %
R2mm_B1	754110	20% less than 5mm_Energy
R3mm_B1	1141329	5% more than 5mm Energy
R5mm_B1	1083792	

Tab.11.7: Force-displacement graphs compared in terms of Energy-absorbed.

Evident aspects of the results achieved:
- Even if the mesh size of the pipe is changed, in both the situations analysed, the trend of the curves show a similar behaviour, see Fig.11.8, Fig.11.9.
- In the case described by Fig.11.9, the model R3mm_B1(mesh of 3mm on the pipe) shows a Force-displacement graph and an absorbed Energy very close to the model R5mm_B1(5mm mesh for the pipe).

11.2.2 Collapse mechanism for constraints of the type CaseB1*.

*see *Table 11.5*

The curves in Fig.11.8, Fig.11.9 reach different Force and displacement values, but show a similar behaviour, following these four phases:
1. Deformation of the brackets (initial tract of the curves with the same slope)
2. Rotation of the rigid-plates at which the brackets are attached, see *paragraph 10.2, Type of constraints,* (phase characterised by the flat tract of the Force-displacement graphs, see Fig.11.9, Fig.11.8)
3. Pulling force along the beam (after the flat tract of the curves, where the slope changes)
4. Separation in the small-bracket zone of the side-impact-beam, due to a tearing of the material:
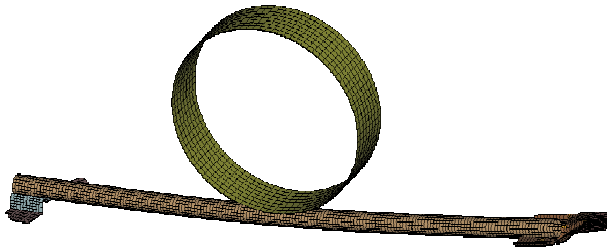
Fig. 11.10: initial deformation of the pipe.
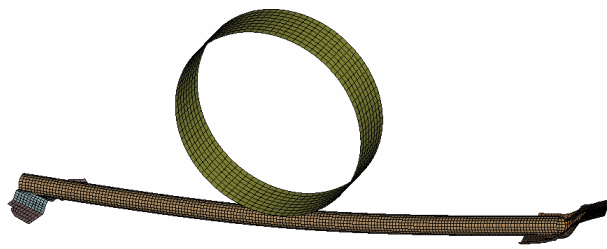
Fig. 11.11: deformation and rotation of the brackets.
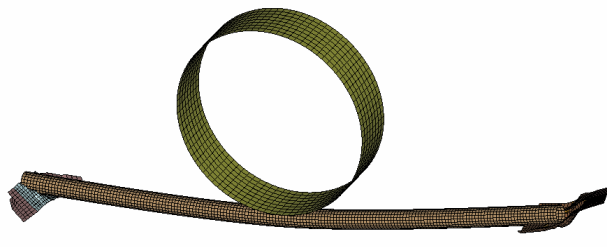
Fig. 11.12: maximum rotation of the small -bracket.
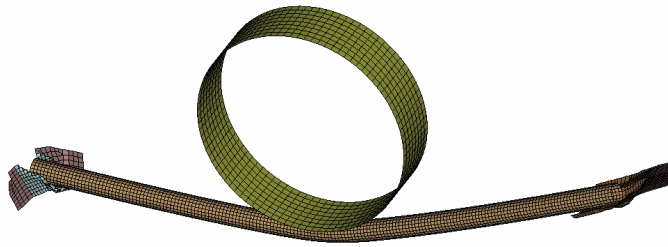
Fig. 11.13: high tension force along the pipe and pulling of the small-bracket.

84

11.2.3 Sensitivity analysis on different types of constraints.

The reasons for this type of analysis are due to the following aims:

♦ To investigate the effects of different types of constraints on the models.
♦ At the beginning of the computer-modelling-process we did not know what type of test rigs it would be possible to manufacture in relation to the economical resources and to the University devices available.

As indicated in *chapter 10 , Computer models description,* on the real car the side-impact-beam probably rotates around the A and the B-pillars of the car; in the bending-test, instead, not to exceed the budget available the final choice (known only later in August) was to consider the brackets as welded on to 12mm thick plates totally fixed in translation and rotation, *see chapter 9, Bending-Test on the isolated side-impact-beam .*
To understand the type of constraints and meshes used in these models and to understand the acronyms in the legend of the graphs the reader has to refer to the Table 11.5, *Summary of type of constraints, meshes and type of shell-elements considered, page.74.*
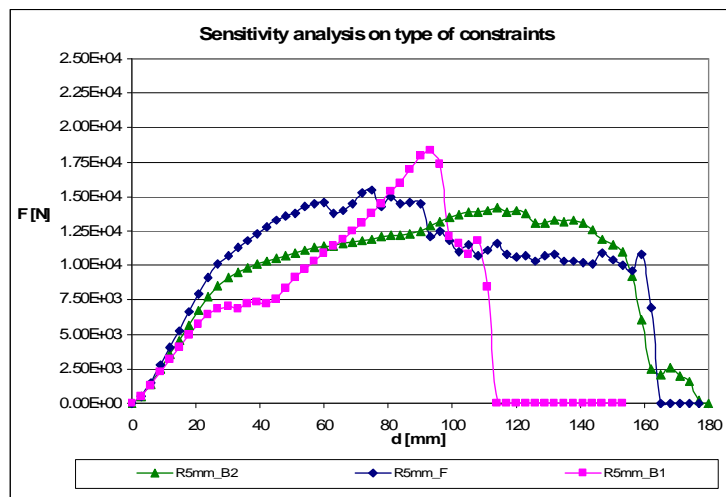
Fig.11.14: sensitivity analysis on type of constraints.

The models are very sensitive to the type of constraints used; in particular, a great difference is noticeable in the simulations in which the rotation of the rigid-plates (at which the brackets are attached) is allowed (indicated respectively as R5mm_B1 and R5mm_B2, see *Tab11.5 and paragraph 10.2, Type of constraints*).
The graph of Fig.11.14 shows that for constraints of the type CaseB2 (pivot line on the rigid-plate of the small-bracket shifted, *see paragraph 10.2, Type of constraints),* a longer rotation of the rigid-plate is allowed (flat tract of the curve), leading to a delay in the final drop to zero of the Force-displacement graph.
In the CaseB1 (pivot line on the rigid-plate of the small-bracket not shifted, *see chapter 10*) the peak of Force reached is higher, indicating that in this situation the pulling force along the pipe is the predominant aspect with respect with the rotation of the rigid-plate (flat tract of the curve), determining a tearing of the material in the small-bracket zone, as described in *paragraph 11.2.2.*
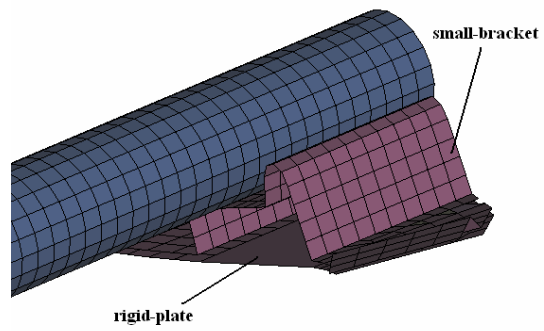
Fig. 11.15 detail of the small-brackets attached at the rigid-plate.
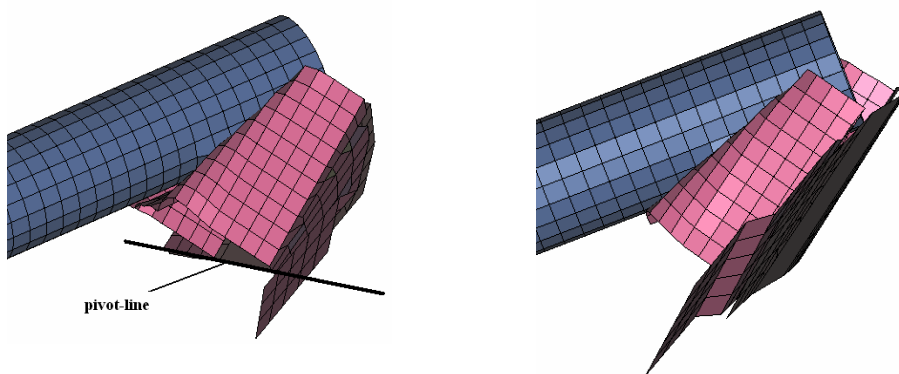
Fig.11.16: collapse sequence of the small-bracket for constraints of the type CaseB2.
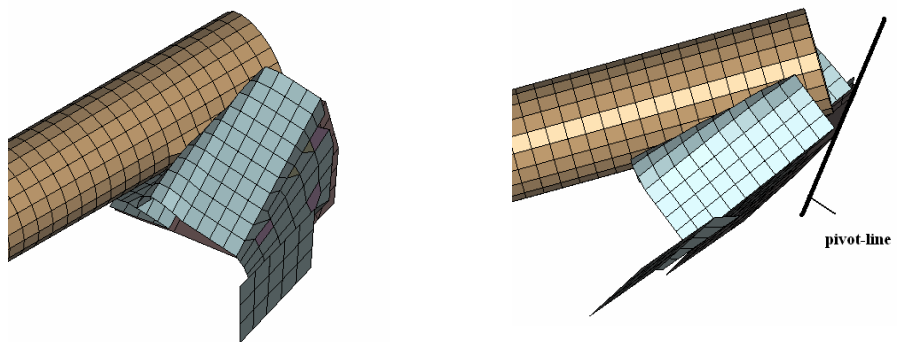
Fig.11.17: collapse sequence of the small-bracket for constraints of the type CaseB1.

11.3 Conclusions

➢ Although the models with rigid-brackets are a great approximation, (in reality the brackets of the side-impact-beam are deformable), it has been useful to perform this kind of simulations to exclude any mesh of the pipe initially considered as the adaptive ones and the 8mm.

➢ The analysis conducted with the rigid-brackets has also allowed us to realise that the under-integrated Belytschko-Tsay shell-element is suited for the models developed.

➢ Until data of the bending-test are available, in terms of Force-displacement graph and conditions at which the bending-test has been performed, it is not possible to chose the type of constraint and the mesh that best represent the bending-test.

12 Comparison between bending test and simulations

12.1 Collapse mechanism of the side-impact-beam during the bending-test

Main phases of the collapse sequence in the laboratory test:
5. Initial deformation of the pipe
6. Deformation of the small-bracket
7. Large rotation of the small-bracket
8. Tearing of material at the base of the small-bracket, Fig.12.1

Fig. 12.1: tearing of material at the basis of the small-bracket.

Other important aspects observed:
- No failure or damage of the welds between the pipe and the brackets.
- Small rotation of the big-bracket compared with the one on the small-bracket, Fig.12.2.

Fig.12.2: small rotation of the big-bracket

- Force-displacement graph of Fig.12.3
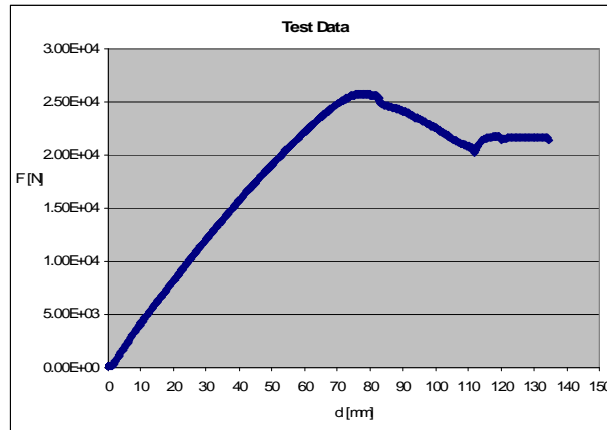
Fig.12.3 Force-displacement graph obtained in the bending-test

12.2 Choice of the simulation which is best representative of the bending-test

12. 2.1 Type of constraints

In the bending-test, as described in *chapter 9, Bending-test on the isolated side-impact-beam,* the brackets have been welded along their edges on two 12mm plates; these plates are totally fixed in rotation and translation, *see Fig.9.2.*
From these two aspects it is evident that if we want to represent correctly the type of constraints used in the bending-test it is necessary to consider the rigid-plates of the simulations (representative of the 12mm thick plates of the test-rigs) as totally fixed in rotation and translation, CaseF in the models, see *chapter 10, Computer models description.*

12. 2.2 Mesh of the brackets

Two meshes have been considered for the brackets: a coarser mesh of 10mm and a finer mesh of 5mm, *see Tab 11.5.*
Observing the images from Ls-post, Fig.12.4, it seems that the coarser10mm mesh, (indicated with the letter C in the graphs of *chapter 11*) shows a tearing of material on the small-bracket starting in a zone that is different from the one observed during the bending-test, Fig.12.1. The finer mesh of 5mm, instead, represents correctly the tearing phenomenon evident at the base of the small-bracket, Fig.12.5.
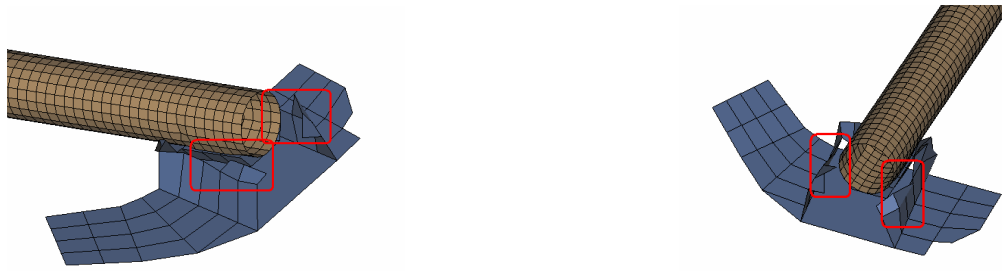
Fig.12.4: tearing phenomenon on the small-bracket for a mesh of 10mm of the brackets
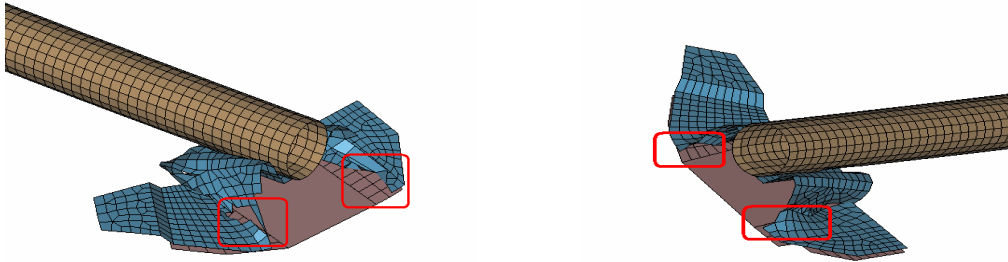
Fig.12.5 tearing phenomenon starting at the base of the small-bracket with mesh of 5mm of the bracket.

12.2.3 Mesh of the pipe.

At the end of *chapter 11, Effects of modelling method on FE results for isolated beam*, it has been decided to consider three different meshes for the pipe because of their capability to correctly represent the geometry. In Fig.12.6 there is a comparison between the three meshes considered using a 5mm mesh for the brackets, see *paragraph 12.2.2*, and the same type of constraint used in the bending-test (rigid-plates fixed in rotation and translation), see *paragraph 12.2.1.* To understand the acronyms in the legend of the graph the reader has to refer to Table 10.5 of *Summary of type of constraints, meshes and type of shell-elements considered.*
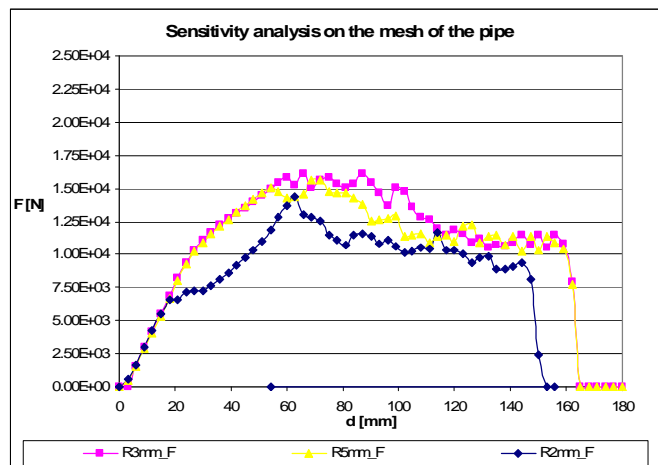

Fig.12.6: different meshes for the pipe.

12.3 Test – best simulation similarities.

The simulations indicated in Fig.12.6 as R5mm_F and R5mm_F have the same mechanism of collapse of the bending-test and show a similar Force-displacement graph. However, in the development of the thesis it has been decided to consider the model R5mm_F as best representative of the bending-test, because it allows to save computational time respect with the model R3mm_F, for the reasons explained in *paragraph 10.3.1, CPU time.*,
The reasons that lead to this choice are here summarised:

- Both the test and model R5mm_F show the same behaviour, determined by an accentuated rotation of the small support which causes a separation and consequently a failure, starting from the points located at the basis of the small support.

- In the simulation the welds between the pipe and the beam supports are considered as perfect(a failure parameter has not been considered), behaviour confirmed by the test in which no separation or evident damage were suffered by these welds.

- In the zone of the big support no separation was noticed, but only a moderate rotation, visible either in the test and in the FE model.

12.4 Test – best simulation differences

The most evident difference between the test and the model R5mm_F is noticeable by a match between the two Force–displacement graphs obtained.
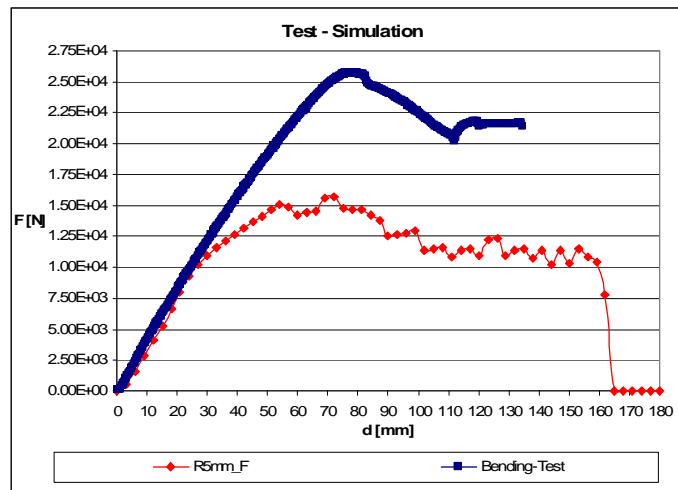
Fig. 12.7: Force – displacement graphs for test and best-simulation.

Even if as illustrated previously the simulation is able to reproduce the collapse mode of the test, it is not able to predict the same Force values, which seem to be higher.

Concerned by the great differences shown by the Force – displacement graph, I tried to identify the possible problems that could affect the model:

- Different dimensions of the impactor used in the simulation and in the test, respectively 300mm and 75mm of diameter. In the bending-test it was necessary to use an impactor with reduced dimensions because it was not possible for the resources available to machine a cylinder of 300mm of diameter.

- The test was performed at a speed of 3mm/s, while in all the simulations, to shorten reasonably the time, the speed was set to 500mm/s, almost 200 times bigger.   This could lead to problems related to strain-rate, in fact, it is widely accepted that most materials behave differently when strain-rate changes: the strength increase with increasing strain-rate showing absolute independency between the absolute increase in yield and the static yield strength Ref[40], Ref [41]. As stated by Ref[43] at $10^{-1}s^{-1}$ strain rate sensitivity becomes pronounced and at 10^2s^{-1} the material resistance to impact changes.
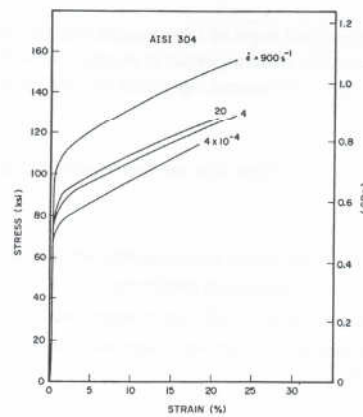
Fig. 12.8: effect of strain rate on AISI 304, from Ref[39].

As suggested by Ref[42] when a single component of a vehicle is tested in isolation the effects of strain rate have to be taken in account to obtain better results; effect that could be neglected without affecting the goodness of the results for a full car-crash simulation.

- The third concerning aspect is due to the material model used in Ls-Dyna. The choice of using a bilinear elastic-plastic model with linear hardening, type 3 in Ls-Dyna, was made because of the absence of characterisation curves of the materials in question. Furthermore the only information available to approximate the materials curves, as explained in the chapter *Materials,* were only relative to a possible range of variability or to the minimum requirements needed by Nissan. For the pipe, for example, the only data we know are relative to minimum performances required: ultimate stress of 1470MPa and 10.8% elongation at break.

12.5 Model tuning

▪ It was demonstrated, by changing the diameter, that the dimensions of the impactor do not affect the results achieved, see Fig.12.9, Fig.12.10, Fig.12.11.
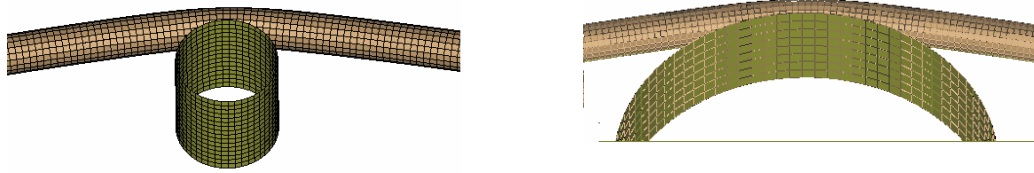
Fig.12.9: different impactor used in the simulations, 75mm on the left, 300mm on the right.
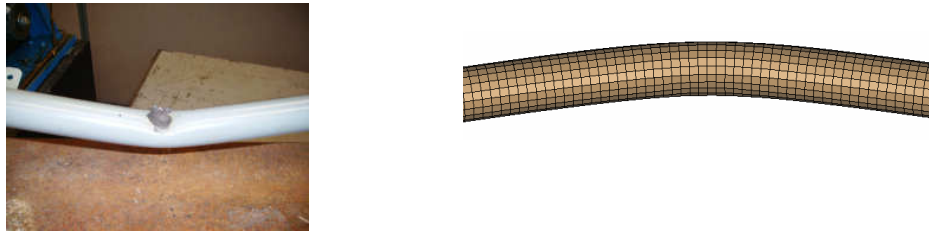
Fig.12.10: deformation of the pipe in the bending-test, impactor of 75mm (image on the left); deformation of the pipe in the simulation, using an impactor of 300mm (image on right).

Name of the simulation*	Diameter of the impactor
R5mm_F	300mm
R5mm_F_Impactor75mm	75mm
*see also *Table 11.5*	

Tab.12.1 diameter of the impactor
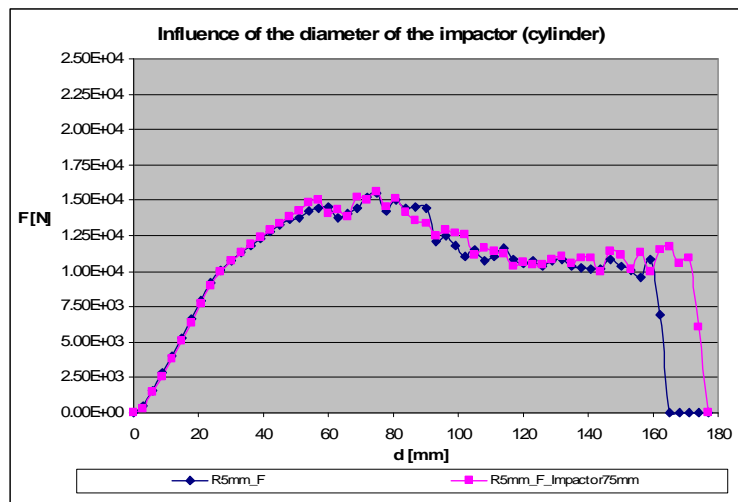
Fig.12.11: influence on the model of the diameter of the impactor used (rigid-cylinder).

- It is difficult to investigate the second point underlined in *paragraph 12.4* because it is necessary to introduce a material model that is able to consider the strain rate-effects. Moreover, to consider the strain-rate dependency it is necessary to characterise the material in question at different velocities, to set the correct parameters needed for the more complex formulation of the material model. In this thesis it has been chosen to perform quasi-static simulations at 500 mm/s.

- To face the third possible problem some characteristics of the materials used to investigate their influence have been changed. Because on the pipe no separation was noticed during the test, the ultimate strain after which in the simulation the elements are eroded was kept only for the supports. In particular in the following graph is demonstrated the influence of increasing the ultimate strain, from the minimum value required by Nissan of 21%, to 30%.
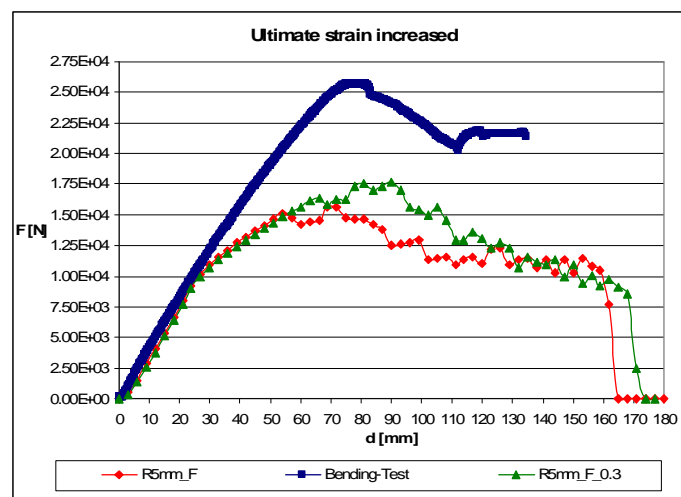
Fig. 12.12: effect of a different ultimate strain.

The material characteristics have been changed on the model, see Tab.12.2, influencing the results achieved, as demonstrated by Fig.12.13.

	Supports			Pipe	
Model name	σ yielding [MPa]	σ ultimate	ε ultimate	σ yielding	σ ultimate
R5mm_F	430	750	21%	869	1470
R5mm_F-S	430	750	21%	1300	1700
R5mm_F-S1	1000	1315	21%	1300	1700

Tab. 12.2: different parameters set for the materials model
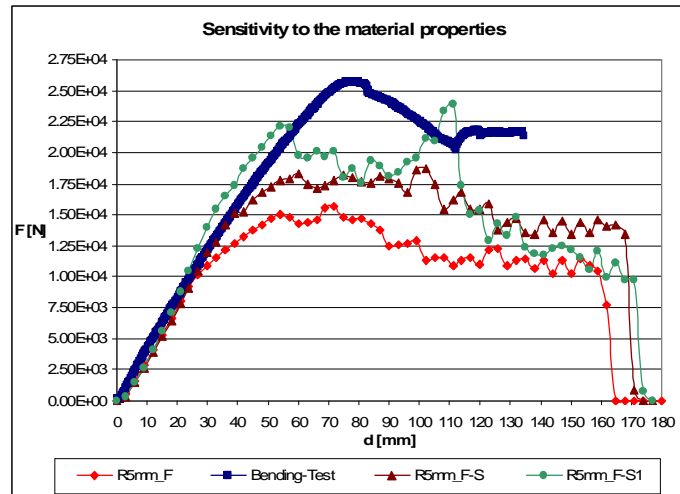
Fig. 16.13: Force-displacement graph for different materials parameters set in the model.

From Fig.16.13 it is quite evident that the characteristics of the materials have a great influence on the Force-displacement graphs, leading to very different results, especially in terms of maximum Forces reached. The more the material properties are increased the higher is the maximum load sustained by the beam.

12.6 Conclusions

- The finer mesh of 5mm of the brackets is the best representative of the collapse mechanism of the tubular side-impact-beam

- The 5mm mesh of the pipe is able to correctly represent the geometry of the pipe and to reproduce the same mechanism of collapse of the side-impact-beam.

- It was correct not to complicate the computer models considering a failure parameter for the welds existing between the pipe and the brackets and between the brackets and the 12mm-thick plates. In fact, failure or damages of the welds have not been noticed during the bending-test on the isolated side-impact-beam.

- Even if the strain-rate effects seem not to play an important role, as suggested by Ref[42], especially for the analysis conducted on single components of a vehicle it could be useful to include strain-rate dependency to improve the model.

- The model shows (as expected) a great sensitivity to material properties; it is important to have precise data relative to the characterisation of the materials used.

- The stress and strain limits of the test specimen are probably greater to the minimum required by Nissan.

95

- The aim of this part of the thesis has been only partially satisfied, in fact:
  - The model spotted as the best simulation reproduces the same collapse mechanism of the tubular side-impact-beam observed during the bending-test.
  - The Force-displacement graph of the best model does not reach the same peak of Forces of the Force-displacement graph obtained from the bending-test.

13 Initial study for press-formed side-impact-beams

The work developed in this part of the thesis is an analysis design, with the aim of substituting the existing tubular side-impact-beam previously described with a press-formed one. In this chapter in particular some ideas and indications for the new design are presented.

13.1 Intended approach

- Preliminary analysis of Nissan requirements and restrictions relative to the new design.
- "Tear down approach" to know how some of Nissan's competitors are actually designing their side-impact-beams.
- Choice of possible candidate shapes for the new design.
- Simulation of a bending test of the new side-impact-beam in isolation.
- Comparison between new designs and the old side-impact-beam (test and best simulation) in terms of:
  - Force - displacement graph
  - Weight of the side-impact-beam

13.2 Methodologies adopted

- The new side-impact-beams are compared with the existing tubular side-impact-beam in terms of:
  - Force-displacement graphs
  - Weight
  - Maximum peak of Force reached during the computer-simulation of a bending-test on the isolated beam.

Reasons for the methodologies adopted:
- The side-impact rules analysed in *chapter 3,* do not give limitations or prescriptions for the design of the side-impact-beams.
- It seems not reasonable to compare a beam in isolation in terms of Energy absorbed, because in all the crash-tests the Energy absorbed refers to the complete structure of the car and not only to one of its components.
- It is important to keep under control the weight of the beam because if we are able to use a lower quantity of material we can save weight and reduce the costs.
- One of the main functions of the side-impact-beam is to guide and promote the correct collapse mechanism of the car-structure, see *chapter4, Collapse mechanism of a simple car made of beam elements.* For these reasons it is important to compare the Force-displacement graph of the existing tubular beam with the Force-displacement graphs of the new press-formed design, by analysing the maximum peak of Force reached in the two cases.

13.3 Nissan's requirements

This section summarises the requirements imposed by Nissan's engineers to the new design, which lead to some important limitations:

- The new side-impact-beam has to be made with a press-forming technique; this fact implies that the new beam has to have an open section.

- The new design has to be fixed to the car through the same spot-welds used for the exisdting one; this requirement limits the possibility to think really different shapes and solutions of the side-impact-beam ends.
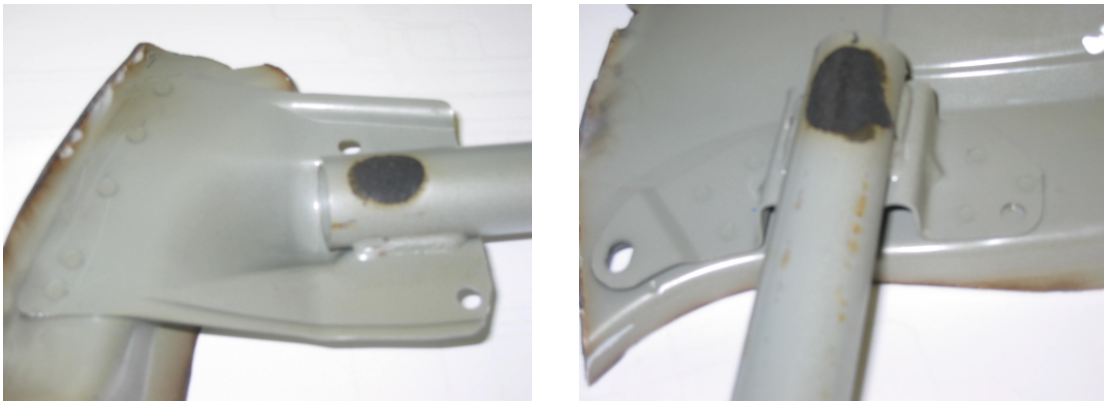
Fig. 13.1: side-impact-beam brackets on Nissan Navara – Pathfinder.

- The side-impact-beam has to have the same length as the old one, 977mm from bracket to bracket, to be fitted in the same position as the previous version.

- The maximum height for the side-impact-beam section must not exceed 100mm, because on the existing small-bracket there are two holes, one on the top and one on the lower flange, that are used for not specified purposes. The requirement was to keep that space free.

100mm
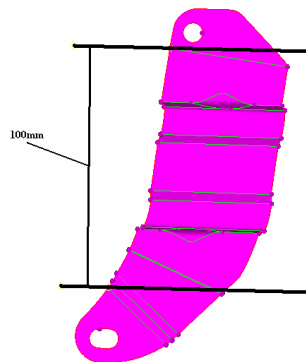
Fig. 13.2: maximum height for the new press-formed design.

- The weight of the new side-impact-beam has to be at least similar to the old one, so Nissan has manifested the intention to use high-strength steel, also of better quality than the one used for the actual design.

13.4 Analysis of press-formed side-impact-beams of other manufacturers

Bearing in mind all the limitations-indications given by Nissan, the first decision was to analyse how some Nissan's competitors are actually designing the side-impact-beams in their cars. Some pictures were taken at several body repairers in Italy and are collected in the *Appendix A*.

The most common solution encountered as suggested also by Richard Schofield of Nissan Technical Centre, is the "top hat" section.

Fig.13.3: (on the left) Bmw X3 and Skoda (on the right) side-impact beams.

BMW X3 Fig.13.3 (on the left):
- Top hat section
  - Total height: 70mm
- Two corrugations
  - Depth of the corrugation: 20mm
  - Width of corrugation: 20mm
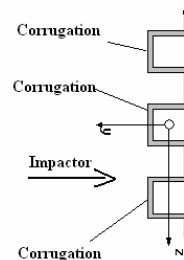
Skoda Fig.13.3 (on the right):
- Top hat section
  - Total height: 80mm
- Two corrugations
  - Depth of the corrugation: 20mm
  - Width of corrugation: 18mm

Fig.13.4: (on the left) Seat Altea side-impact-beam; (on the right) Mini side-impact-beam.

Altea Fig.13.4 (on the left):
- Top hat section
    - Total height: 80mm
- Three corrugations
    - Depth of the corrugation: 20mm
    - Width of corrugation: 20mm

Mini Fig.13.4 (on the right):
- Top hat section
    - Total height: 60mm
- Three corrugations
    - Depth of the corrugation: 15mm
    - Width of corrugation: 15mm

13.5 Crucial decisions for the initial study of the new press-formed design

.
- All the new side-impact-beams for this project designed have the same length of 977mm, as the existing tubular one.
- All the new side-impact-beams designed have in common the same plates, see Fig.13.5, to weld the side-impact-beam to the skin of the door in the same position of the existing one, as required by Nissan. One plate refers to one end of the beam, the other refers to the other extreme of the side-impact-beam.

Fig. 13.5: common plates on the new press-formed side-impact-beams designed

- The central length of the side-impact-beam has been kept common between the various press-formed models designed, as indicates in Fig.13.6. At the initial stage, in fact, we want to spot the best section between the designed ones.
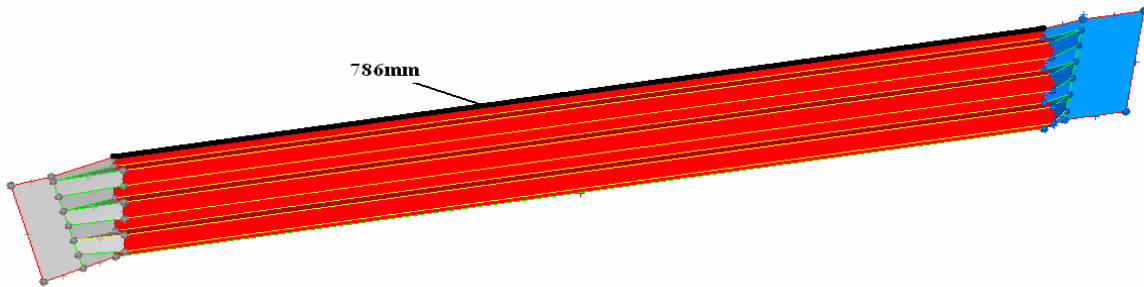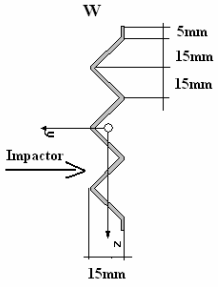
Fig. 13.6: example of new press-formed side-impact-beam designed.

13.6 New sections analysed
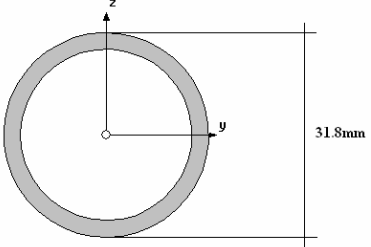
Different sections analysed:

	I_{yy} [mm^4]	I_{zz} [mm^4]	A [mm^2]	Thickness [mm]	Height [mm]
	248482	13976	364	2	90
	327272	44770	484	2	90

	I_{yy} [mm^4]	I_{zz} [mm^4]	A [mm^2]	Thickness [mm]	Height [mm]
	209087	5789	304	2	90
	287877	26721	424	2	90
	247580	14871	420	2	90
	323362	14681	380	2	90

	I_{yy} [mm^4]	I_{zz} [mm^4]	A [mm^2]	Thickness [mm]	Height [mm]
	207681	5602	268	2	90

Tab.13.1: new open-sections analysed.

	I_{yy} [mm^4]	I_{zz} [mm^4]	Thickness [mm]	A [mm^2]
	25615	25615	2.6	238

Tab.13.2: pipe cross-section on the existing side-impact-beam.

13.7 Reasons for the choice of the selected sections.

- Two or three corrugations because:
    - Almost all the side-impact-beams of other manufactures are top-hat sections with two or three corrugations, see *paragraph 13.4 and Appendix A*
    - Only on the new Ford Focus, Fig. A6 of the *Appendix A*, there is only one corrugation, but the beam cross-section is not constant and so complex, probably to avoid buckling problems; at the initial stage of the designing process it has been decided to use simple sections.
- Height of the sections of 90mm:
    - To increase the section properties in terms of second moment of area saving weight. A height of 90mm, in fact, is between the upper limit of 100mm imposed by Nissan and 80mm which is one of the height used by other manufacturers
- The depth of the corrugation has been varied to analyse how it influences the performance of the side-impact-beam.
- The material thickness of 2mm has been chosen to start the analysis, because, as suggested by Nissan, it is a reasonable thickness for the steel sheets used to press-form the side-impact-beam.

13.8 Computer models of the new press-formed side-impact-beams.

13.8.1 Mesh

The work developed in this thesis about the new press-formed side-impact-beams is only at the initial stage of the process; so it is necessary to build some FEA models that could be reliable, giving reasonable and believable results, and not too expensive in term of computational time, to have some answers in a brief period. This last requirement is essential especially at the beginning of the process where it is important to consider a wide range of design parameters and different solutions for the problem. In the later stages of the design process, some configurations will be eliminated. It is only when this has been done, so that the range of designs has been reduced, that it is worth performing more precise FE analysis.

Another element to take into account is the fact that, at the starting point of a new design, the only information available is from the existing tubular side-impact-beam, in terms of test data and FEA results.

Considering all these aspects it was decided to use an average mesh dimension of 5mm for all the new design beams, trying to reproduce the same conditions and assumptions made for the model of the existing tubular side-impact-beam. That mesh type was selected because it seems to respect the requirements illustrated above and it is also the one identified as the best representative of the collapse behaviour of the existing side-impact-beam.

13.8.2 Constraints

The objective is to simulate a bending-test to compare the performances in terms of Force-displacement graph of the existing beam and the new press-formed ones.

Not to affect the results achieved, it is important to apply to the models of the new side-impact-beams the same constraints used for the model of the existing beam. The new press-formed side-impact-beams are attached to two rigid-plates, Fig.13.7, as done for the model of the tubular beam, see *paragraph 10.2, Type of constraints..*

The constraints are applied to the rigid-plates, in particular two different conditions have been considered:

- **CaseBN:** translation not allowed, rotation allowed around the pivot lines of Fig.13.7. this type of constraint seems from the author point of view the most similar situation to the one existing on the complete car during a side-impact.
- **CaseFN:** translation and rotation not allowed.

	Rotation*	Translation
CaseFN	No	No
CaseBN	Yes	No
*pivot lines as indicated in Fig.13.7		

Tab.13.3: type of constraints used.
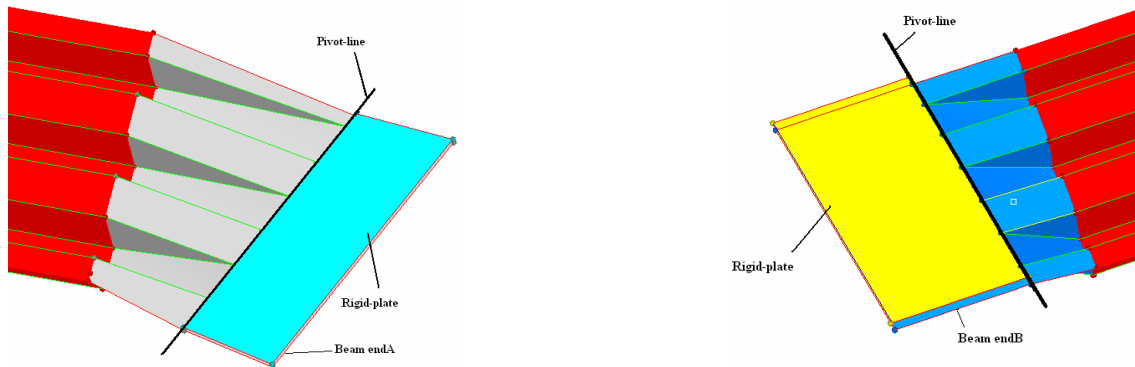
Fig.13.7: rigid-plates at which the constraints are applied on the new press-formed side-impact-beams.

13.8.3 Materials

It was decided to use the material corresponding to the one used in the simulations for the pipe of the existing beam, see Fig.13.7. This choice is made because at the beginning of the analysis the idea is to evaluate and compare the different geometries selected, without introducing other variable parameters.
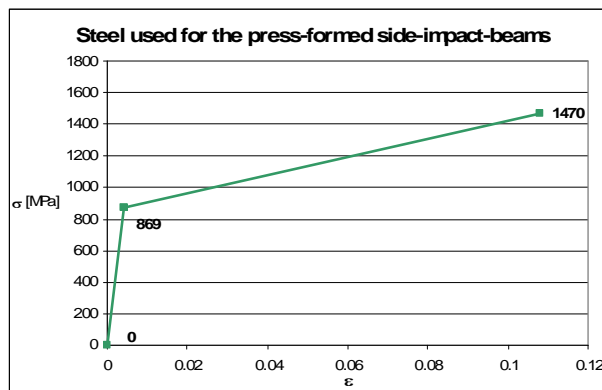
Fig.13.7: material used for the new beam designed, corresponding to the steel used in the computer models of the existing tubular side-impact-beam.

- $\sigma_{ultimate}$ = 1470 MPa (minimum value required by Nissan)
- E = 205000 MPa
- Density = 7.860E-9 tons/mm^3
- Elongation at break = 10,8% (minimum value required by Nissan)
- $\sigma_{yielding}$ = 869 MPa (as AISI 1080)
- E$_{tangential}$ = 5669 MPa.

13.9 Results of the computer models.

Section name*	Type of constraints	Name of the model
A1	CaseBN	A1_BN
A2	CaseBN	A2_BN
A3	CaseBN	A3_BN
W	CaseBN	W_BN
A5	CaseBN	A5_BN
A6	CaseBN	A6_BN
A7	CaseBN	A7_BN
A1	CaseFN	A1_FN
A2	CaseFN	A2_FN
A3	CaseFN	A3_FN
W	CaseFN	W_FN
A5	CaseFN	A5_FN
A6	CaseFN	A6_FN
A7	CaseFN	A7_FN
*see Tab.13.1 for geometrical data of the sections considered		

Tab.13.4: summary of the type of constraints used and name of the computer models

To understand the legend on the graphs of this section the reader has to refer to *Tab.13.4 and to Tab.11.5*. The reader is reminded that the Force-displacement graphs presented in this paragraph are obtained with a thickness of 2mm for all the new-sections considered, see *paragraph 13.7*.

Fig.13.8 and Fig.13.9 show a comparison between the Force-displacement graphs of the new designed side-impact-beams and the best simulation of the existing tubular beam.
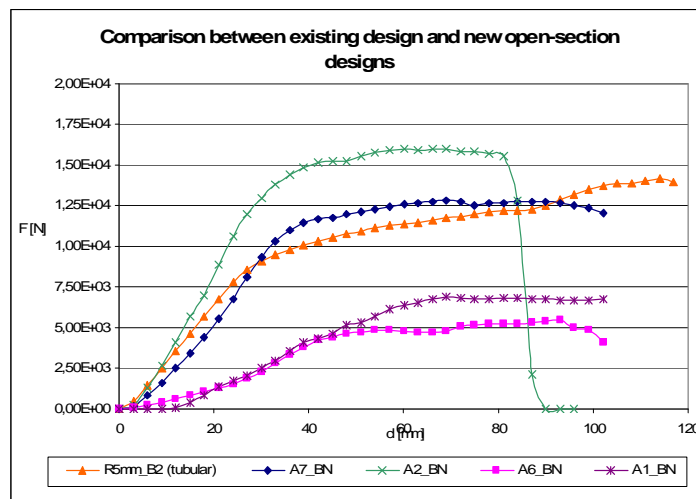
Fig.13.8 comparison between old design and new press-formed beams.

The graphs of Fig.13.8 refer to the models A1, A2, A6, A7, in which the geometry of the beam section differs only for the depth of the corrugations, see Tab13.1.

The benefit (increase of the maximum Force reached) from increasing the depth of the corrugations is evident from the graph.

Also greater initial elastic stiffness (from greater second moment of area) may be seen.
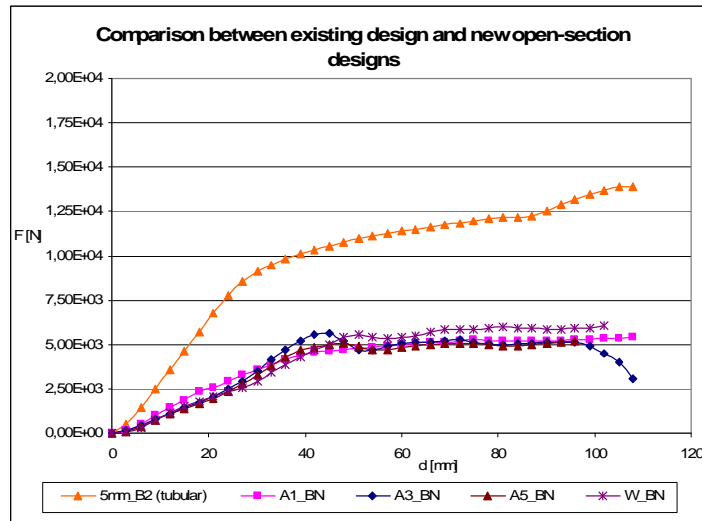
Fig.13.9 comparison between old design and new press-formed beams.

The other sections analysed, in particular the one with two corrugations (indicated as A5) and section W, have poorer performance in terms of Force-displacement graph than the existing tubular side-impact-beam, see Fig.13.9.

In *paragraph 13.2, Methodologies adopted,* it was specified that the comparison between the side-impact beams is made in terms of:

- Force-displacement graphs, to estimate the maximum peak of Force reached by the different models.
- Weight of the different side-impact-beams designed in relation at the weight of the existing one.

In Tab.13.5 the weights of the different beams considered up to this point till now are compared. Once more it is important to underline that all the new open-section designs have a thickness of 2mm.

Name of the section	Weight [Kg]	Percentage respect to weight of the existing beam
A1	2.5	31 % more than the existing beam
A2	3.4	78 % more than the existing beam
A3	3	57 % more than the existing beam
A5	2.5	31 % more than the existing beam
A6	2.2	15 % more than the existing beam
A7	2.8	47 % more than the existing beam
W	2.3	21 % more than the existing beam
Existing-tubular	1.9	0 % more than the existing beam

Tab.13.5: weights of the new-beam designed with a thickness of 2mm.

13.9.1 Considerations on the results achieved

- Only sections A7 and A2 show a Force-displacement graph that is able to reach at least the same peak of Force of the existing side-impact-beam: the other designs do not satisfy the benchmark established as a criterion of evaluation and choice.
- All the sections analysed, with a thickness of 2mm, do not reach the second benchmark required relative to the weight of the side-impact-beam.
- The best performance of sections A7 and A2 are explainable also from Tab.13.6, where the second moment of area of the new-sections is compared to the one of the circular section of the existing side-impact-beam.

Name of the section	I_{zz} [mm^4]	$I_{zz\,(open\text{-}section)}$ / $I_{zz\,(tubular\text{-}section)}$
A1	13976	0.54
A2	44770	1.74
A3	14871	0.58
A5	14681	0.57
A6	5784	0.22
A7	26721	1.04
W	5602	0.21
Existing-tubular	25615	1

Tab.13.6: comparison between the second moment of area of the open-sections and of the tubular one.

- If we want to satisfy the benchmark relative to the weight it is necessary to reduce the thickness of the sections, but this implies also a reduction of the second moment of area, leading to worse performances in terms of Force-displacement graphs.
- To save weight, by reducing the thickness of the section, it is necessary to use steel with higher performances.

From these considerations it emerges that the section that represents the best compromise, between the two benchmarks established, is section A7.
Note especially that it is really possible to reduce the weight by diminishing the thickness, see *Tab.13.7*.
In fact, even if the section A2 has the best Force-displacement graph (over the values reached by the existing side-impact-beam), it has an excessive weight, see *Tab.13.7*.

Section	Thickness [mm]	Weight [Kg]	Percentage respect to weight of the existing beam
A7	1.5	2.1	10 % more than the existing beam
A2	1.5	2.6	37 % more than the existing beam

Tab.13.7: weight of the open-section beams with a thickness of 1.5mm.

The graph in Fig.13.11 refers to the section A7 and it shows how the thickness of the side-impact-beam can be reduced by using a high-strength steel, like AISI 4130, see Fig.13.10. With a thickness of 1mm the weight is 0.4kg lower than that of the existing tubular beam.
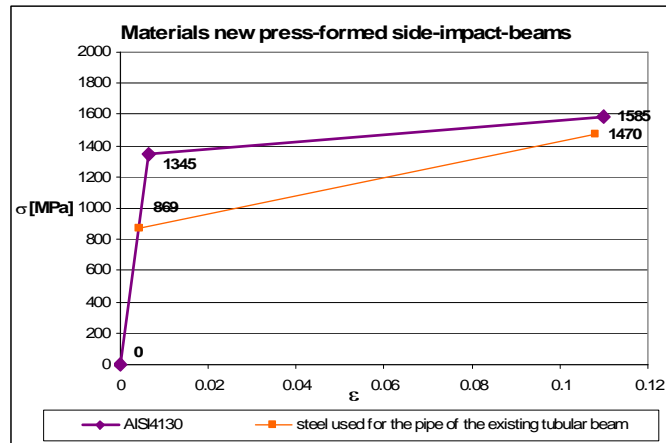
Fig.13.10: different types of steel used for the new press-formed side-impact-beam.

- AISI4130
  - $E_{tangential}$ = 2222 MPa
  - $\sigma_{ultimate}$ = 1585 MPa
  - $\sigma_{yielding}$ = 1346 MPa
  - E = 205000 MPa
  - Density = 7.860E-9 tons/mm^3
  - Elongation at break = 11%

- Steel used for the tubular beam, see *paragraph 13.8.3*

Summary of constraints, thicknesses and materials used:

	Rotation*	**Translation**
CaseFN	No	No
CaseBN	Yes	No
***pivot lines as indicated in Fig.13.7**		

Section name	**Constraint**	**Thickness [mm]**	**Material**	**Name of the model**
A7	CaseFN	1	Same as the pipe of the existing tubular beam	A7_FN-1mm-Pipe
A7	CaseFN	1.5	Same as the pipe of the existing tubular beam	A7_FN-1.5mm-Pipe
A7	CaseFN	1	AISI4130	A7_FN-Pipe

Tab.13.8: simulations performed with constraints of the type CaseFN.

To understand the legend of Fig.13.11 the reader has to refer to the *Tab.13.8*.
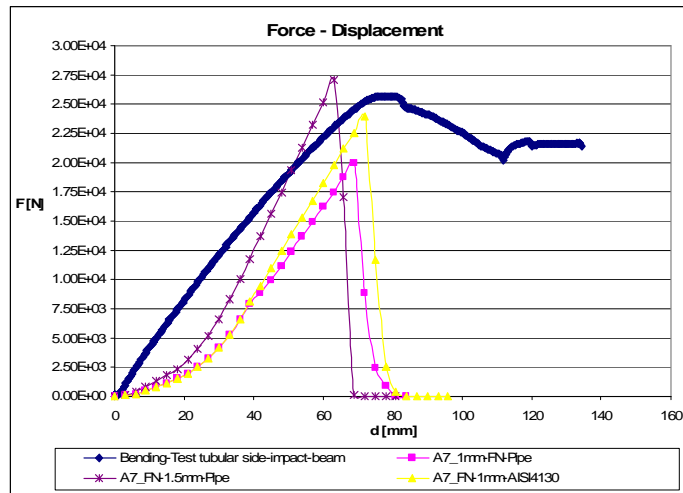
Fig.13.11: bending-test of the tubular existing side-impact-beam compared with the best new press-formed designs.

The graph in Fig.13.11 is also presented to demonstrate how different types of constraints change the Force-displacement graph of the isolated beam. The constraints used here are of the type for CaseFN, see *paragraph 13.8.2*

In Fig.13.11 is also plotted the curve obtained during the bending test for the existing side-impact-beam.
This choice is intended to demonstrate how it is difficult to treat the beams in isolation, because of their very different behaviour during the collapse. On the existing tubular design, because of the geometry of the small-bracket, a large rotation occurs, even if during the bending-test on the isolated beam the rigid-plates (on which the brackets are welded) are fixed in rotation and translation (phenomenon described in *chapter 11*). This behaviour is not present on the new press-formed side-impact-beams, as demonstrated by Fig.13.11, where the maximum peak of Force is followed by the final collapse of the side-impact-beam (drop to zero of the Forces in the graph).

14 Conclusions

- *New press-formed side-impact-beams*

    1. The side-impact-beam is only a part of the side-frame of the car and one of its functions is to promote the correct collapse of the B and A-pillars to which it is attached, see *chapter 4, Collapse mechanism of a simple car made of beam elements.* It looks reasonable to guarantee with the new design a maximum peak Force at least equal to the one obtained during the bending test. It is believed that the necessary Force required to begin the collapse of the other parts of the side-frame of the car has to be equal or less to the maximum peak of Force observed on the isolated side-impact-beam. However without images or data from the complete side-crash, test or simulation, it is not possible to assert anything to validate or to exclude this hypothesis.

    2. To assess the real behaviour of the side-impact-beams and to judge their goodness it is necessary to model the other parts of the car onto which the side-impact-beam is actually spot-welded.

    3. From what was observed in point **2** and for the completely different behaviour between the existing side-impact-beam and the new press-formed designs, at this stage it is only possible to exclude some sections that are clearly not satisfying the requirement because of their excessive weight or for their poor performances.

    4. It seems meaningless to base the choice and the evaluation of the new side-impact-beam on the Energy absorbed, otherwise the effect would be to have a new side-impact-beam made with an extremely high strength steel, capable to reach a very high peak Force, several times bigger than the original beam, probably causing a different collapse mechanism from the one actually existing on the car.

    5. Because, as stated in point **1,** the beam is inserted into a more complex structure, it seems unreasonable to consider what happens at the isolated-beam in the deep-collapse (large displacements on the Force-displacement graph). At that stage the beam shortens and rotates, pulling the other car-components onto which the side-impact-beam is attached. Moreover other parts of the car, like the skin of the door, could limit the deflection of the side-impact-beam with respect to what happens to the side-impact-beam in isolation.

    6. The side-impact-rules, see *chapter3,* and the Energy absorbed refer to the complete structure of the car, so it is difficult to establish and to find criteria to design and treat the side-impact-beam in isolation. Compulsory prescriptions have not been found relative to the single isolated component extracted from the complete car.

7. It is possible that the performance of the existing tubular-beams is superior to the minimum required to pass the certification test. This implies that with a lower performing side-impact-beam the side-impact-test could still be passed in a satisfactory way. But without data or images from the lateral impact this is only an hypothesis it could be interesting to verify, by simulating a side-impact on the complete model of the car.

8. The analysis conducted is only at the initial stage and another important parameter which has not been considered for lack of information is the cost needed to manufacture the press-formed side-impact-beams designed. In fact, in addition to the benchmarks in terms of similarities of weight and maximum peak of Force with the existing design, the other important parameter of choice is the cost.

- *Existing tubular beam*

9. The objective of reproducing with a computer model the bending-test on the isolated existing side-impact-beam has been only partially satisfied, in fact:
  - The model identified as the best simulation reproduces the same collapse mechanism as the tubular side-impact-beam observed during the bending-test.
  - The Force-displacement graph of the best model does not reach the same peak of Forces of the Force-displacement graph obtained from the bending-test.

10. From the observations made in point **9** it is also possible that the side-impact-beam provided by Nissan has properties in terms of characteristics of the materials, superior to the minimum required and indicated in *Appendix E.*

- *Further work*

1. Further work could include simulation of a side-impact including what are the essential structural parts of the car side-frame involved in the collapse mechanism.

2. It has been shown, see Fig.13.11, that to guarantee a peak of Force at least equal to the test results it may be necessary to have an increase in weight or to use a higher performing steel with reduced thickness, to reduce weight with respect to the existing side-impact-beam. One of the next steps could be to find which is the cheapest option between the two, to introduce the cost as third parameter of choice.

References

[1]
Insurance Institute for Highway Safety. Vehicle Compatibility in Crashes. Special issue, October 1999.

[2]
U. Seiffert, L. Wech, Automotive Safety Handbook, Professional Engineering Publishing, 2003.
Warrendale Pa: AE International and co published by Professional Engineering Publishing.

[3]
European Passive Safety Network 2, EPSN2. Task 4.6 State of the art review – Vehicle Structural Crashworthiness, 30 March 2004.

[4]
L.M.M Careme. Occupant Kinematics and Injury Causation in Side Impacts – Fields Accident Experience. SAE SP-851 Side Impact Protection Technologies, SAE 910316, SAE 1991.

[5]
A.K. Zaouk, A.M. Eigen, K.H. Digges. Occupant injury Patterns in Side Crashes. SAE 2001-01-02723, SAE 2001.

[6]
Directive 96/27/EC of the European Parliament and of the Council of 20th May 1996 on the protection of occupants of motor vehicles in event of a side impact and amending Directive 70/156/EEC. Official Journal of the European Communities, L 169, 08/07/1996, p. 001 – 0038.

[7]
Euro NCAP (2006)
Source http://www.euroncap.com/content/test_procedures/side_impact.php
(accessed 19th January 2006)

[8]
J. Campbell, Lecture Notes on Crashworthiness Regulation, Cranfield MSc, Course 2005 – 2006

[9]
U.S. Federal Regulation FMVSS 214.

[10]
P. Astori, M. Anghileri, Lecture Notes on Sicurezza Passiva, Politecnico di Milano, anno accademico 2004 – 2005.

[11]
J.C. Brown, Lecture Notes on Structural Mechanics, Cranfield MSc, Course 2005 – 2006.

[12]
D. Keckman , CRASHD Users' Manual, first revision**.**

[14]
M. Loo, Development of structural crashworthiness to the European side impact test in Ford AUII Falcon. International Journal of Crashworthiness, Vol. 8, No. 2, 2003. Woodhead Publishing

[15]
C. E. Knight. The Finite Element Method in Mechanical Design. Boston: PWS-KENT Publishing Company, 1993.

[16]
I.V. Lau, J.P. Capp, J.A. Obermeyer. A Comparison of Frontal and Side Impact: Crash Dynamics, Countermeasures and Subsystem Tests. In 35th Stapp Car Crash Conference, San Diego, California, P-251, November 18-20 1991. SAE 912896, SAE 1991, p 1899 – 1914. Warrendale

[18]
R.G. Whirley, B.E. Engelmann, Electrical and hybrid vehicle crashworthiness simulation. International Journal of Vehicle Design, Vol.18, No.5, 1997, p. 413 – 432.

[19]
E. Arvelo, Simulation of the Combined Bending/Axial collapse of thin walled top hat beams using DYNA3D, MSc Thesis, Cranfield University, 1998.

[20]
A.M. Carbajal, Investigation into the use of adaptive meshing in crashworthiness analysis, MSc Thesis, Cranfield University, 2003.

[21]
S. Simunovic, P.K.V.V. Nukala, J. Fekete, D. Meuleman, M. Milititsky. Modelling of Strain Rate Effects in Automotive Impact. SAE 2003-01-1383, SAE 2003.

[22]
K. Mahadevan, P. Liang, J. Fekete. Effect of Strain Rate in Full Vehicle Frontal Crash Analysis. SAE 2000-01-0625, SAE 2000.

[23]
Livermore software, DYNA3D User's manual, 1998.

[24]

N. Arndt, R.H. Grzebieta, Lower Extremity Injuries in Side – Impact Vehicle Crashes. International Journal of Crashworthiness, Vol. 8, No. 5, 2003, p. 495 – 512.
Woodhead Publishing

[25]
J.W. Zellner, S.A. Kebschull, R.M. Van Auken, Analysis of Vehicle Tip Stability in Side Impact Tests, SAE 2001-01-1650, SAE 2001.

[26]
B.C. Geigl, H. Hoschopf, H. Steffan, A. Moser, Reconstruction of Occupant Kinematics and Kinetics for Real World Accidents. International Journal of Crashworthiness, Vol. 8, No.1, 2003.
Woodhead Publishing

[27]
M. Lindquist, A. Hall, U. Bjornstig, Real World Car Crash Investigations – A New Approach. International Journal of Crashworthiness, Vol.8, No.5, 2003, p. 375 - 384
Woodhead Publishing

[28]
K. Hughes, Lecture Notes on Simulation for Crashworthiness, Cranfield MSc, Course 2005 – 2006.

[29]
J.C. Brown, A.J. Robertson, S.T. Serpento,. Motor vehicle structures: concepts and fundamentals. Butterworth - Heinemann, 2002
Butterworth – Heinemann

[30]
J.C. Brown, Lecture Notes on Patran / Nastran Training, Cranfield MSc, course 2005 – 2006.

[32]
Altair Engineering, Hypermesh 7.0 Tutorials.

[33]
P. M. Kurowski. Finite Element Analysis for Design Engineers.SAE International Warrendale PA, 2004.

[34]
J. Campbell, Lectures Notes on Introduction to non-linear finite element codes, Cranfield MSc, Course 2005 – 2006

[35]
MatWeb: property data on certified materials.
Source: http://www.matweb.com
(accessed last time on 28th July 2006)

[36]
S. Rao. The Finite Element Method in Engineering (3rd Ed). Butterworth Heinemann, 1999.

[37]
Stewart, Gullerud, Heinstein. Solution verification for explicit transient dynamics problems in the presence of hourglass and contact forces. Computer methods in applied mechanics and engineering, 2006. Elsevier

[38]
J. Brown, Lecture Notes on Introduction to Crashworthiness, Cranfield MSc, Course 2005 – 2006

[39]
R. Vignjevic, Lecture Notes on Simulations for Crashworthiness and Impact, Cranfield MSc, Course 2005 – 2006.

[40]
A. Saxena, D. Chatfield
High Strain Rate Behaviour of Some Hot Cold Rolled Low Carbon Steels.
SAE 76-0209, SAE 1976.

[41]
M. Gamarino, M. Avalle, R. Vadori.
Modelli della Sensibilità allo Strain-Rate e Identificazione dei Parametri Caratteristici di Lamiere d'Acciaio.
Source: http://www.pcm.unifi.it/Lavorisalerno/ART_046.pdf
(accessed last time on 5th August 2006)

[42]
M. Dietenberger, M. Buyuk, C. Kan.
Development of a High Strain-Rate Dependent Vehicle Model.
Source: http://www.dynamore.de/download/af05/papers/B-III-01.pdf
(accessed last time on 5th August 2006)

[43]
P. Cunat
Stainless Steel Properties for Structural Automotive Applications.
Paper presented in the occasion of the Metal Bulletin International Automotive Materials Conference, Cologne 21st 23rd of June 2000.
Source: www.euro-inox.org/pdf/auto/StructuralAutomotiveApp_EN.pdf
(accessed last time on 5th of August 2006)
[44]
R. Cook, D. Malkus, M. Plesha, R. Witt. Concepts and Applications of Finite Element Analysis (4th Ed). University of Wisconsin – Madison , John Wiley and sons, 2002.

[45]
J. Brown, Vehicle body structures assignment for Automotive Product Engineering Course, Cranfield MSc, Course 2005 – 2006

[46]
C. Compton
Injury Severity Codes: A Comparison of Police Injury Codes and Medical Outcome as Determined by NASS CDS Investigations. International Traffic Records Forum, University of Michigan, 3rd August 2005.
Source:www.atsip.org/images/uploads/Session_37_**Injury_Severity**_Codes_Police_vs_NASS_.PPT
(accessed last time: 8th August 2006)

Appendix A – Side-impact-beams pictures of manufacturers in competition with Nissan

Pictures of some current side impact door beams, taken in Italy at different car body repairers.

Fig. A1: Alfa Romeo 147 (left); Seat Altea (right)

Fig. A2: BMW X3 (left); BMW X3 particular (right)

Fig. A3: Jeep Cherokee (left); Mini (right)

Fig. A4: Renault Clio (left); Renault Clio detail (right)

Fig. A5: Lancia Y (left); Lancia Y detail (right)

Fig. A6: Ford New Focus (left); Ford New Focus detail (right)

Fig. A7: Ford New Focus detail2 (left); Fiat Ulysse (right)

Fig. A8: Volkswagen Passat (left);Volkswagen Passat detail (right)

Fig. A9: Skoda (left); Skoda detail (right)

Fig. A10: Fiat Punto first series (left); Fiat Punto second series (right)

Fig. A11: Fiat Punto second series detail 1 (left); Fiat Punto second series detail 2 (right)

121

Appendix B - Simulations performed in Crash-D

Here is shown a typical HINGPROP card of CRASHD [12], Tab.B1, in which it is possible to set different plastic moments at the end of the beams used to build the frame of the car. In the first column the element for which the card is referred is indicated. In the second column it is possible to choose the type of yield criterion used to calculate the collapse and the last columns are used to set different plastic moments at the end of the beams. Setting various plastic moments for each beam element it is possible to strengthen in different manners each part of the car-frame. In this manner it is possible to obtain different sequences of collapse of the complete car, see *chapter 4 an the graphs collected in this appendix.*

HINGPROP

PROP.	YIELD	END1			END2		
NO.	CRIT.	MPX [N mm]	MPY	MPZ	MPX [N mm]	MPY	MPZ
1	3	1850000	2510000	3360000	1850000	2510000	3360000
2	1	1	1630000	1940000	1	1630000	1940000
3	1	1	3000000	2400000	1	3000000	2400000
4	1	1	900000	500000	1	900000	500000
5	1	0	0	0	1	2700000	3600000
6	1	1	2700000	3600000	1	2700000	3600000
7	1	1	519000	340000	1	519000	340000
8	3	505000	1160000	672000	505000	1160000	672000
9	1	1	787000	2350000	1	787000	2350000

Tab.B1: this table refers to the values imposed to obtain the collapse of Fig.B7, see *Ref[12]*

Simulation to understand the phenomenological behaviour

The figures collected in this *Appendix B* show for the different cases analysed the Force – deflection graphs of the loaded node, which correspond to the middle node of the side- impact-beam, see *chapter 4*. In the graphs are indicated with vertical lines the points at which one or more parts of the car body collapses. The collapse is due to a consecutive formation of plastic hinges in the car-frame. Acting on the card HINGPROP by setting different plastic moments it is possible to switch from a mechanism of collapse to another one, changing the load path into the structure, see *chapter 4.* By changing the design of the side frame , differences in collapse sequence are obtained (see Figs B1 to B7). This also alters force vs deflection performance.
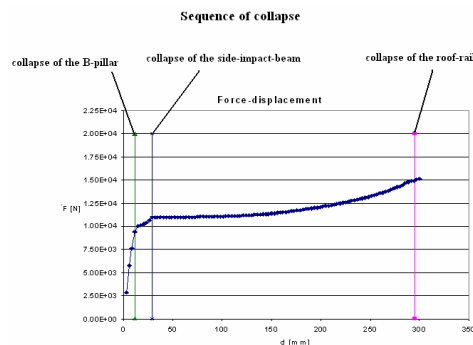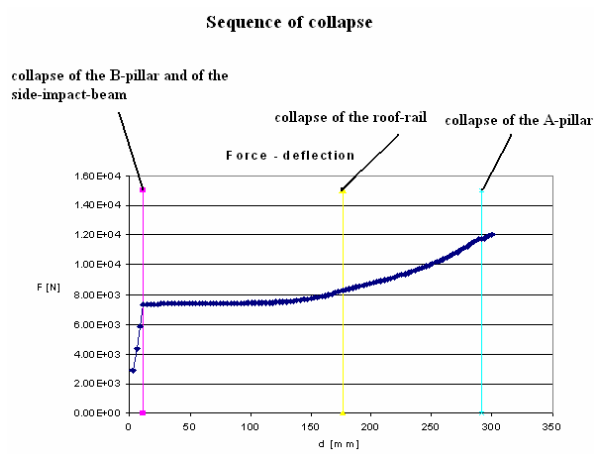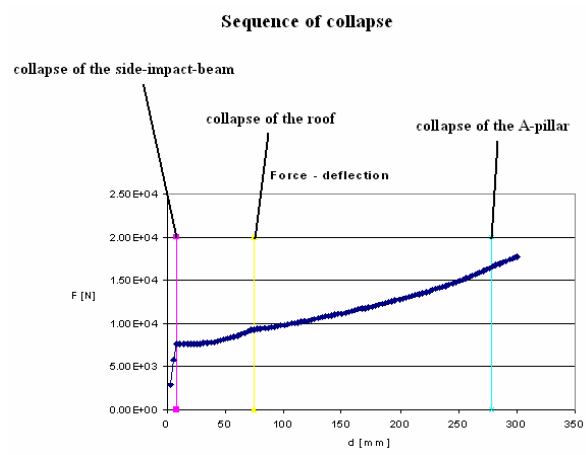

Fig.B1, model 1.

Fig.B2, model 2.

Fig.B3, model 3.
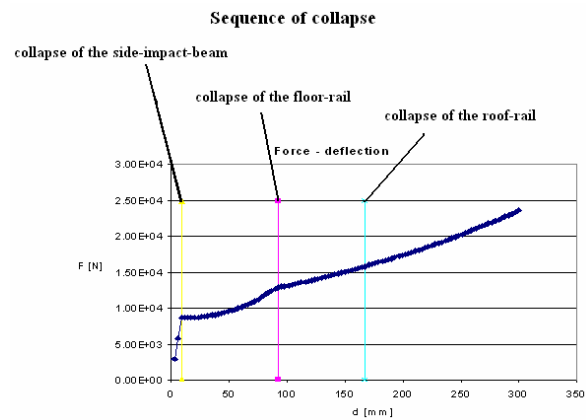
Fig.B4, model 4.
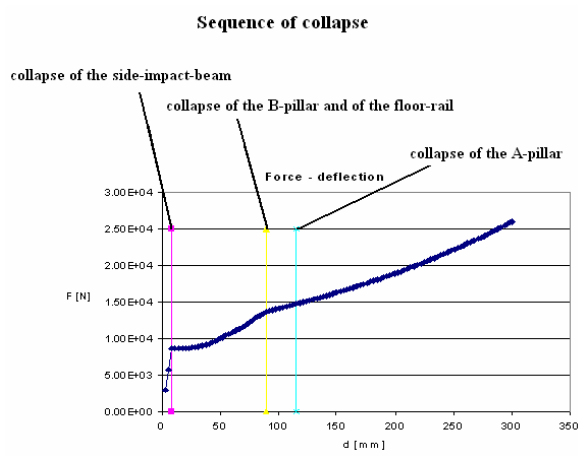
Fig:B5, model 5
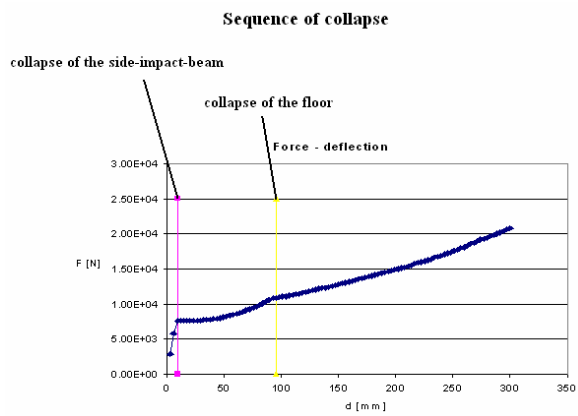
Fig.B6, model 6
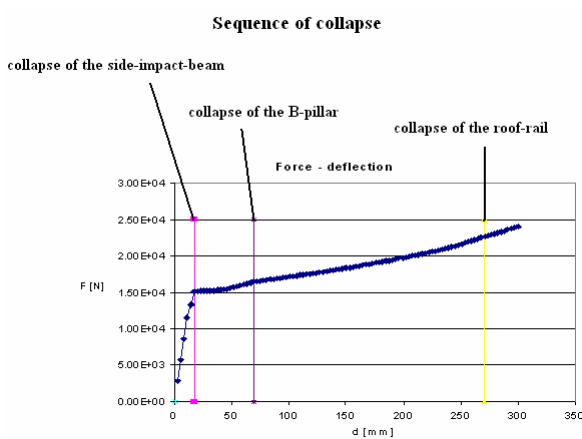
Fig.B7, model 7.

Only in the graph of Fig.B7 it is achieved a mechanism of collapse of the type described in *paragraph 4.4*, that describes it as one of the most desirable.

124

As the whole car-frame is considered and not only one part of it(as done in the rest of the Thesis on the isolated beam), it is interesting to verify whether it is possible to satisfy the first two requirements imposed by the quasi-static test of the American FMVSS214, see *paragraph 3.4*

First two requirements of the quasi-static FMVSS214:

$$P_{initial} = \frac{\int_{0}^{150\,mm} P * d\Delta}{\Delta_{150}} > 1250 \text{ pounds (with seats not installed in the vehicle)}$$

$$P_{int\,ermediate} = \frac{\int_{0}^{300\,mm} P * d\Delta}{\Delta_{300}} > 3500 \text{ pounds (without seats)}$$

In equation 1) and 2) the integral is the Energy absorbed by the car-structure by the indicated displacement of 150mm in the first case and 300mm in the second equation.
$P_{initial}$ and $P_{intermediate}$ are an estimation of the average forces necessary to reach respectively the displacement of 150mm and 300mm.
In the case described by Fig.B7 the first two requirements of the American FMVSS214 could be passed in a satisfactory way:

$P_{initial\ case\ B7}$ = 3596 pounds > 1250 pounds

$P_{intermediate\ case\ B7}$ = 4131 pounds > 3500 pounds.

Appendix C – Test rig sections

Test rigs components:

- C-Channel used as base:

    - Height = 150mm
    - Width = 90mm
    - Flange thickness = 12mm
    - Web thickness = 6.5mm
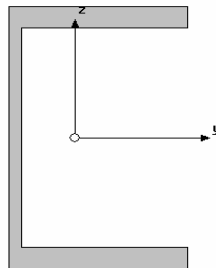
- C-Channels used to raise the beam from the basement:

    - Height = 150mm
    - Width = 75mm
    - Flange thickness = 10mm
    - Web thickness = 5.5mm
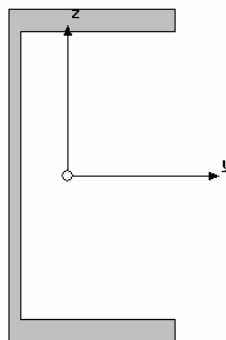
- Plates onto which the beam ends are welded:

    - Length = 150mm
    - Width = 75mm
    - Thickness = 12mm

Appendix D – Hand calculations

In this Appendix we compare the results obtained in this thesis using two different techniques: hand calculation and Ls-Dyna simulation. It is important to underline from the beginning that the aim of the comparison made here is not intended as a validation for the simulations described so far, but it is an other alternative and simple way to treat the problem in analysis. Thus it seems interesting to match the two different techniques used to see how the hand calculations are far from the results displayed by the simulations.

The hand calculations are performed considering the beam as a pipe of the same geometrical properties of the pipe of the side-impact-beam (see also *chapter 8*):

- Thickness = 2.6mm
- 977mm (as the total length of Nissan's beam).
- Area = 238 mm^2
- J = 25615 mm^4 (second moment of Area for bending)

the material of the pipe, in accordance to point 3 of *paragraph 5.1*, is represented with a bilinear elastic-plastic material, see Fig.D1, which has the same Young's modulus E, the same $\sigma_{yielding}$ and the same $\varepsilon_{ultimate}$ of the pipe of the modelled existing side-impact-beam (see also *chapter 8*):

- $\sigma_{yielding}$ = 869 MPa
- E = 205000 MPa
- Density = 7.860E-9 tons/mm^3
- Elongation at break = 10,8%
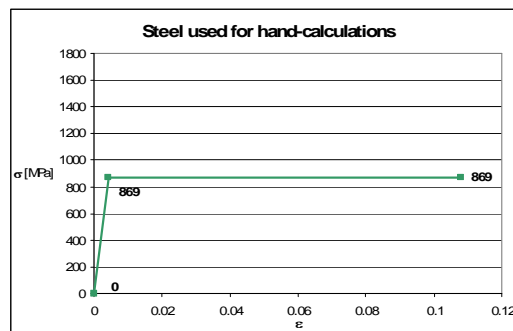
Fig.D1: steel used for hand calculations.

The beam ends for hand calculations, as stated in *paragraph 5.2,* and the side-impact beam (modelled in Ls-Dyna) are fixed in translation but not in rotation, free rotation. In particular for the tubular side-impact-beam it has been considered a constraint of the type B1, see *Tab.10.1, Summary of type of constraints, meshes and type of shell-elements considered*
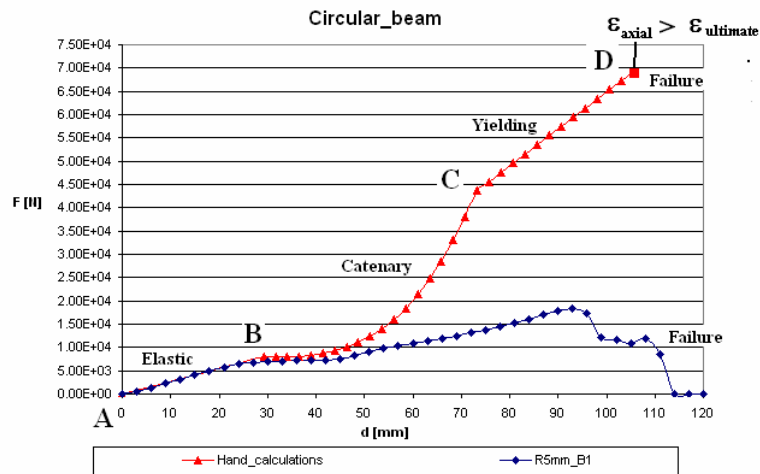
Fig.D2: comparison between hand-calculations and Ls-Dyna model.

Observing the graphs of Fig.D2:

- Elastic range (AB) compares reasonably
- Initial collapse point(B) compares quite well.
- Catenary range (BC) is too high in hand calculations.(possibly due to excessive axial stiffness of the beam because the flexible end brackets were not included in the hand calculation.
- In the axial yielding range (CD):
  - The force in the hand calculation is too high
  - The slope in the hand calculation is too high.

Probably because the end brackets were not included.
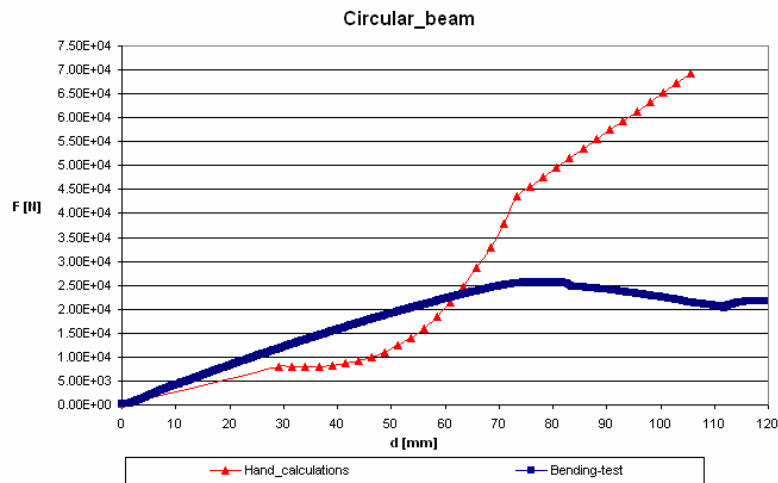
Fig.D4: comparison between hand-calculations and bending-test on existing beam.

128

The graphs in Fig.D4 are very different except for the slope of the elastic range of the curves. This different trend was expected because to perform hand calculations the same steel was used as in the computer-models.

It has been demonstrated to be less performing than the one used for the tube of the tested side-impact-beam.

Appendix E – Nissan papers with material characteristics

DATA NOTE	SHAPE DATA NO.	80181 EB300	PAGE TITLE	SPEC/NOTE BLOCK	PAGE NO.	4 of 4

SPEC/NOTE

NOTE

THE PRINCIPLE OF INDEPENDENCY APPLIES TO THIS DRAWING PER
ISO 8015:85 / NES D0094:00,UNLESS OTHERWISE SPECIFIED.

GENERAL DIMENSIONAL TOLERANCE IS PER
NES D0030 CLASS C.
NES D0016-99 CLASS C.

GENERAL GEOMETRICAL TOLERANCE IS NOT
APPLICABLE.

DEFINITION OF TOLERANCES SHOWN ON THIS DRAWING IS PER.
ISO 8015:85 / NES D0094:00
ISO 1101:83 / NES D0097:00
ISO 5459:81 / NES D0402:00
ISO 5458:98 / NES D0096:00
ISO 10579:93 / NES D0095:00
ISO 2692:88 / NES D0098:00
ISO 1660:87 / NES D0401:00

1. BENDING R4 AT INSIDE AND R5 AT OUTSIDE UNLESS OTHERWISE SPECIFIED.

2. THE MATERIALS MUST CONFORM WITH NES M 0301(SUBSTANCE USE RESTRICTIONS).

3. THE REFERENCE POINT / SURFACE OF THE GEOMETRICAL TOLERANCES SHALL
CONFORM TO THE CAD DESIGN DATA.

4. MATERIAL.
PIPE:TENSILE STRENGTH 1470MPa(150Kg/mm2)MIN.
ELONGATION 10.8%MIN.

THIS PART SHALL BE PER NES STAM 1470 OR,A PIPE BEFORE QUENCHING CAN BE
QUENCHED TO BECOME EQUIVALENT OF STAM 1470.
AFTER INDIVIDUAL PART TEST,NO HARMFUL CRACKS SHALL OCCUR.

STEEL TUBE:DIA.31.8,t2.6 <1>
BRKT-FR:XE360BG,t1.4
BRKT-RR:XE360BG,t1.6
BRKT-A:XSSESG,t0.97

5. THIS ASSY IS ASSEMBLED TO DOOR-FR,INR(80112/3 EB300) THE PANEL SURF MATED WITH
DOOR ASSY-FR INR SHALL BE SMOOTH & FREE FROM BURRS.

6. THIS PART SHALL BE FREE FROM BURRS,WRIKNLES AND CRACKS AFFECTING SERVICEABILITY.

7. SUPPLIER MUST SUBMIT NISSAN BENDING TEST RESULT WHICH IS CONDUCTED ON THE JIG
WITH GUARD ASSY-FR DOOR TAKING INTO ACCOUNT OF MANUFACTURING TOLERANCE.
(LOAD POINT SHOWN ON REF DRAWING.)

8. WELD SHALL BE FREE FROM SUCH DEFECTS AS BURR,UNDERCUT,CRACK,OVERLAP AND PIT.

130

Conversion table (4) from NES steel sheet grade to Renault steel sheet grade

(1) Applicable steels: Hot rolled GA - NES → Cold rolled GI - Renault Standard
(2) Thickness: t=1.6

In the thickness range of t≥1.2, hot rolled steel sheet is available at lower prices than cold rolled steel sheet in Japan.If the hot rolled steel sheet can be manufactured. In Europe, the cold rolled steel sheet is available at lower prices than hot rolled steel sheet. for the thickness of t≤1.8. The conversion from hot rolled steel sheet (NES) to cold rolled steel sheet (Renault Standard) was performed.

[Note]
*1) X: Cold rolled steel sheet (material that allows minor defect)
Z: Cold rolled steel sheet (material that does not allow defect detrimental to uniform painting on the assurance surface)
H: Hot rolled steel sheet.
FF: Cold rolled steel strip with skin pass
G: Galvanizing
*2) Conversion expression: Basically JIS=0.918*ISO+4.84 (agreed with Renault DIMAT). JIS=1.1*ISO is also used.
*3) Under improvement of elongation to N/R common target: SP763-590
*4) Applicable to engine and gearbox only.
*5) The material property values that need to be careful (possible deterioration of performance) in selection of the Renault GI material equivalent to NES-GA material were colored.
*6,7) For conversion grade, select the item with *6 for formability and the item with *7 for strength and rigidity.

NES GA specification

Base metal	NES GA grades	Mechanical Properties (in case of Hot:t=1.6)						
		Tensile strength TS	Rapid deformation strength	Yield point YP	Overall elongation EL(JIS)	n	r̄	BH
Hot rolled mild steel	SP791	≥270		205/325	35/49	-	-	-
	SP792	≥270		195/305	37/51	-	-	-
	SP793	≥270	No regulated	175/275	40/53			-
Hot rolled, hiten	SP791-370	≥370		235/355	33/46	-	-	-
	SP791-440	≥440		295/410	28/41	-	-	-
	SP793-590	≥590	≥730 / No regulated	330/490	23/35	-	-	-

Renault standard GI grade similar to NES GA grade *5

Base metal	Renault standard GI grades *1	Summary	Mechanical Properties (all thickness available)							
			Tensile strength TS	Rapid deformation strength	Yield point YP	Overall elongation EL(ISO)	Reference total elongation Ref: EL(JIS) *2	n	r	BH2_L
Cold-rolled, mild steel	X C G	General grade	290/440		200/330	≥28	≥31	-	-	-
	X/Z E G	Shallow drawing grade	300/360		180/230	≥34	≥36-37	≥0.17	≥1.3	-
	X/Z E G *7	Shallow drawing grade	300/360		180/230	≥34	≥36-37	≥0.17	≥1.3	-
	X/Z ES G *6	Deep drawing grade	280/340		160/200	≥37	≥39-41	≥0.19	≥1.8	-
	X SSES G	Super deep drawing grade	270/350		140/180	≥40	≥42-44	≥0.21	≥2.1	-
	X SSES G	Super-super deep drawing grade	≥270	No regulated	120/160	≥42	≥44-46	≥0.24	≥2.2	-
Cold rolled, hiten	X/Z E220P G	YP220 MPa grade. P added solution reinforced type.	≥340		220/260	≥32	≥34-35	≥0.19	≥1.7	-
	X/Z E235P G	YP235 MPa grade. P added solution reinforced type.	≥355		235/275	≥32	≥34-35	≥0.19	≥1.7	-
	X/Z E260P G	YP260 MPa grade. P added solution reinforced type.	≥370		260/310	≥30	≥32-33	≥0.18	≥1.5	-
	X E220BH G	YP220 MPa grade. P added solution reinforced type with baking effect.	≥340		220/260	≥32	≥34-35	≥0.19	≥1.7	≥40
	Z E260PBH G	YP260 MPa grade. P added solution reinforced type with baking effect.	≥370		260/310	≥30	≥32-33	≥0.18	≥1.7	≥40
	X/Z E280P G	YP280 MPa grade. P added solution reinforced type.	≥385		280/330	≥30	≥32-33	≥0.17	≥1.2	-
	X E280D G	YP280 MPa grade. Deposition reinforced type	375/440		280/330	≥28	≥31	≥0.15	≥0.7	-
	X E280M G	YP280 MPa grade. Manganese steel.	375/440		280/330	≥30	≥32-33	≥0.16	≥1.2	-
	X E320D G	YP320 MPa grade. Deposition reinforced type.	415/480		320/380	≥24	≥26-27	≥0.13	≥0.6	-
	X E360D G	YP360 MPa grade. Deposition reinforced type.	450/530		360/430	≥21	≥23-24	≥0.13	≥0.5	-
	X E360B G *3	YP360 MPa grade. Dual phase type.	600/750		360/430	≥21	≥23-24	≥0.14	≥1.0	-
	X E360BE2 G	YP360 MPa grade. Dual phase type.	600/750		450/530	≥17	≥19-20	≥0.12	≥1.0	-
	FFE440D G *4	YP440 MPa grade. Deposition reinforced.	490/570		420/500	≥17	≥19-20	-	-	-
	X E450B G	YP450 MPa grade. Dual phase type.	≥750		450/550	≥15	≥17-19	-	-	-

↗ indicates the steel used in side impact beam

Appendix F - main cards used in Ls-Dyna

```
*SECTION_SHELL:
```
to define the properties of the shell-elements used to build the models.

```
*CONTROL_HOURGLASS
```
to set a control on the hourglass modes that is different from the default one.

```
*MAT_PLASTIC_KINEMATIC (type 3)
```
to define a bilinear elastic-plastic stress-strain curve with the characteristics of the materials used for the brackets, the pipe and for the new press-formed side-impact-beams.

```
*MAT_RIGID
```
to consider the material of the impactor (cylinder) and the plates at which the brackets are attached as rigid.

```
*CONTACT_AUTOMATIC_SURFACE_TO_SURFACE
```
to define the type of contact existing between the impactor and the central part of the side-impact-beam.

```
*CONTACT_AUTOMATIC_SINGLE_SURFACE
```
to define a contact between all the bodies that are modelled; in particular this card was set to take into account the possible contacts between the different parts of the side-impact-beam or even a contact between the pipe with itself.

```
*CONTACT_SPOTWELD
```
To define the welds between the pipe and the brackets in the simulations with deformable brackets.

```
*CONSTRAINED_EXTRA_NODES
```
To attach the nodes belonging to different rigid bodies; in the case of simulations with rigid-brackets, this card has been used to join together some nodes of the rigid-brackets to some nodes of the rigid-plates.

```
*CONTROL_CONTACT
```
To avoid initial interpenetrations between different parts of the models

To some important people:

Michela…come una gocciolina d'acqua che cade discretamente ed incessantemente mi hai accompagnato per tutto questo tempo…la vera tesi l'hai scritta tu con tutte quelle mail…..nei primi tempi, i più difficili, un "appuntamento" quasi quotidiano….portero' sempre con me questo ricordo…"sei tu la migliore"….le parole non bastano per esprimere qualcosa che e' piu' di gratitudine....

Simply my Sister…
 "ricorda che nella vita, la "vera vita", non è trovare delle risposte, ma farsi delle domande, perché è guardare dietro la collina e chiedersi che cosa c'è dietro che ci fa andare avanti…." (ndr....scoperto solo in Febbraio…..ultima pagina libro Sudoku)

Chiara (Settembre 2005)

Inside me
"vedi di fare il possibile per trasformare anche quest'anno in un periodo di crescita personale, e soprattutto sforzati di conoscere gente e di non startene tutto il giorno in stanza come la tua natura ti porterà sicuramente a fare; fra 10-12 mesi voglio parlare con una persona che questa esperienza ha cambiato in positivo…se sarà così me ne accorgerò subito e te lo dirò con piacere…"

Luca (27 Settembre 2005)

I soliti segreti tra me e Lui
"forse è meglio così: avevo appena ascoltato il cd e…"

Carlo(29 Settembre 2005)

In ritardo…come al solito!!!
"…x ieri sera ci hai beccato, eravamo a porta Venezia! E tu, considerando il fuso, scommetto che sai chi sta giocando a San Siro adesso vero!? Pensa un po' che i ragazzi stanno vincendo con 1 doppietta di Maldini! La vita è davvero curiosa…Mi è disp non averti neanche salutato martedì ma al tuo ritorno mi farò perdonare con una sorpresa (il tuo regalo di compleanno!!)…"

Stefano (2 0ttobre 2005)

Essenziale – no frills
"Buon viaggio balord in bocca al lupo e fatti onore…ci si becca tra 3 settimane. Ciao"

Pero (28 Settembre 2005)

Emozioni
"O doctor come andiamo?Tutto bene?Ambientato?Qui tutto ok sto preparando un esame che per studiare devo tira di bamba è che poi mi brucia la gola…"

Gatto(13 Ottobre 2005)

Destination football
"Ciao, bomber, ho preso addirittura 99!!!stasera festeggiamo insieme. Grazie x l'affetto che mi hai dimostrato, ti stimo moltissimo"

Ghiso(23 Settembre 2005)